Anchor Channels in Composite Concrete Slabs: Experimental and Numerical Investigation

Bogdanić, Anton

UNIrI DIGITALNA KNJIŽNICA

UNIVERSITY OF RIJEKA

FACULTY OF CIVIL ENGINEERING

Anton Bogdanić

ANCHOR CHANNELS IN COMPOSITE CONCRETE SLABS: EXPERIMENTAL AND NUMERICAL INVESTIGATION

DOCTORAL THESIS

Rijeka, 2022

UNIVERSITY OF RIJEKA

FACULTY OF CIVIL ENGINEERING

Anton Bogdanić

ANCHOR CHANNELS IN COMPOSITE CONCRETE SLABS: EXPERIMENTAL AND NUMERICAL INVESTIGATION

DOCTORAL THESIS

Supervisor: Prof. Dr.-Ing. habil. Joško Ožbolt

Rijeka, 2022

Supervisor: Prof. Dr.-Ing. habil. Joško Ožbolt

The doctoral thesis was defended on 27/05/2022 at the University of Rijeka, Faculty of Civil Engineering, in front of the committee members:

1. Prof. dr. sc. Ivica Kožar

2. Prof. dr. sc. Goran Turkalj

3. Izv. prof. dr. sc. Neira Torić Malić

ZAHVALA

Dugujem veliku zahvalnost mom mentoru Prof. Dr.-Ing. habil. Jošku Ožboltu na pomoći i savjetima tijekom doktorskog studija, a posebno sam zahvalan na prilici da nastavimo sa suradnjom u tvrtci Nolasoft. Veliki ste uzor i inspiracija sa svime što ste ostvarili u svom životu!

Zahvaljujem se profesorima Ivici Kožaru, Goranu Turkalju i Neiri Torić Malić što su bili voljni pročitati i ocijeniti ovaj rad.

I would like to express my sincere gratitude to Dr.-Ing. Daniele Casucci for all the suggestions, discussions and time you devoted to this project. Without your help, this would not have been possible!

I am also grateful to Hilti corporation for financial support and idea for this project he authors are grateful to Hilti Corporation, 9494 Schaan, Principality of 421 Liechtenstein, for financial support and especially to Dr. Philipp Grosser for his valuable comments at the beginning of this journey. Thanks also to RI-ISA d.o.o, 51000 Rijeka, Croatia, a member of Permasteelisa Group, for sharing information about the challenges in the design of anchor channels in composite slabs.

Posebno sam zahvalan laborantu Dominiku Štroku na pomoći oko provedbe relativno zahtjevnih eksperimenata koje smo odradili u veselom tonu. Zahvaljujem se i laborantu Dinu Juriševiću te tvrtci GP Krk d.d koja je pripremala uzorke.

Zahvaljujem se i svim zaposlenicima Fakulteta koji su na bilo koji način pomogli ili sudjelovali u ovom procesu, a bilo ih je mnogo. Hvala na svim savjetima, druženjima i preporukama!

Prijatelji boduli, a i svi preko mosta, bez naših druženja i feštica ovaj bi put bilo mnogo teže proći! Mateo, hvala na varenju oslonaca!

Na kraju se moram zahvaliti svojoj obitelji koja mi je uvijek pružala podršku i osiguravala da sigurno idem kroz život. Ne postoje riječi zahvale kojima bih mogao opisati ono što mislim!

ABSTRACT

Anchor channels are a type of cast-in-place fastener that are well suited for supporting curtain walls and other applications in commercial construction because they provide flexibility when connecting structural or nonstructural elements. In modern high-rise buildings, composite slabs consisting of profiled steel decking with an in-situ cast concrete topping are commonly used. In some countries, it is also common to install the attachment point of the curtain wall in a recess of the concrete member often called a "pocket". Therefore, the specific geometry of the composite slab and pockets is a major factor to consider when designing anchor channel connections. However, the influence of complex geometry on the concrete capacity has not been investigated and design is based on engineering judgement. The main aim of this thesis is to investigate the behavior of anchor channels in composite slabs and pockets, for both tension and shear loads. Extensive numerical parametric studies and several experimental campaigns have been carried out to evaluate the difference in the capacity between slabs with complex geometry and equivalent plain concrete slabs under un-cracked conditions. In the numerical studies, the 3D nonlinear FE code based on the microplane model was employed. The numerical models were validated against the corresponding experimental tests and showed excellent agreement. Based on the results, the existing design models valid for plain concrete slabs have been modified and enhanced to improve their predictability, especially in the case of thin members. Moreover, additional modification factors have been proposed to account for the influence of complex geometry on the concrete capacity.

Keywords: anchor channels, composite slabs with profiled steel decking, pockets, modified design models, modification factors, thin members, concrete failure

PROŠIRENI SAŽETAK

Sidreni kanali su tip sustava za pričvršćivanje koji se postavlja na odgovarajuću poziciju prije ugradnje betona. Vrlo su prikladni za oslanjanje ovješenih fasada i drugih primjena u komercijalnoj gradnji zbog prilagodljivosti prilikom povezivanja konstruktivnih ili nekonstruktivnih elemenata. Sidreni kanali se prilikom oslanjanja ovješenih fasada postavljaju po obodu relativno tankih međukatnih ploča, pri čemu nosivost uslijed otkazivanja betona postaje mjerodavna za dimenzioniranje. U modernim višekatnim konstrukcijama često se koriste spregnute ploče od profiliranih trapeznih limova i sloja lijevanog betona na mjestu ugradnje. U nekim zemljama, uobičajeno je da se povezivanje ovješenih fasada vrši unutar udubljenja u betonskoj ploči koje se naziva „džep". Stoga, specifičnu geometriju spregnutih ploča i „džepova" važno je uzeti u obzir prilikom dimenzioniranja spojeva sa sidrenim kanalima. No, utjecaj složene geometrije na nosivost betona nije istražena i proračun je baziran na inženjerskim prosudbama. Osnovni cilj ove disertacije je istražiti ponašanje sidrenih kanala u spregnutim pločama i „džepovima" za vlačna i posmična opterećenja, a naglasak je na oblicima sloma uslijed otkazivanja betona. Provedene su opširne numeričke parametarske analize i nekoliko eksperimentalnih programa kako bi se odredila razlika u nosivosti između ploča sa složenom geometrijom te ekvivalentnih monolitnih betonskih ploča za neraspucani beton. U numeričkim simulacijama korišten je 3D nelinearni program baziran na metodi konačnih elemenata. Osnovna značajka ovog programa je mikroravninski konstitutivni model, a osnovna ideja je praćenje jednoosnih naprezanja i deformacija u unaprijed definiranim smjerovima (mikroravninama). U programu su pukotine modelirane koristeći tzv. pristup razmazanih pukotina, a kako bi se osigurala objektivnost rezultata neovisno o veličini konačnih elemenata primijenjena je tzv. metoda trakastih pukotina. Numerički modeli

su verificirani na osnovu usporedbe s odgovarajućim eksperimentalnim rezultatima, pokazujući izvrsnu podudarnost.

U radu su ponajprije istraženi važeći proračunski modeli u normama za vlačna i posmična opterećenja. Naime, izuzetno je bitno da se referentna nosivost, tj. nosivost u monolitnim betonskim pločama, može čim preciznije odrediti kako bi se mogli primijeniti modifikacijski faktor koji će uzeti u obzir složenu geometriju spregnutih ploča i „džepova". Prilikom istraživanja ponašanja u monolitnim pločama, fokus je stavljen na tanke ploče zbog njihove sve češće primjene u praksi. Na osnovu numeričkih rezultata uočeni su nedostaci kod važećih proračunskih modela i predložene su promjene kako bi se poboljšala njihova točnost. Dodatno su osmišljeni i eksperimenti koji su potvrdili predložene promjene.

Kod primjene sidrenih kanala u spregnutim pločama i „džepovima" varirani su brojni parametri kako bi se istražilo što više mogućih konfiguracija u praksi. Neki od tih parametara su: tip limova, orijentacija limova, debljina ploča, pozicija sidrenih kanala, dimenzije „džepova", itd. Na osnovu brojnih rezultata predloženi su dodatni modifikacijski faktori za određivanje nosivosti sidrenih kanala u spregnutim pločama i „džepovima", posebno za vlačno i posmično opterećenje. Validacija navedenih faktora provedena je pomoću serije pomno osmišljenih eksperimenata.

Osnovni znanstveni doprinos ovog rada očituje se u unaprjeđenu postojećih saznanja i modela za proračun sidrenih kanala u monolitnim betonskim pločama, te potpuno nova saznanja o njihovoj primjeni u spregnutim betonskim pločama i „džepovima". Rezultati ovog rada i prijedlozi za proračun od iznimne su važnosti za primjenu sidrenih kanala kod oslanjanja ovješenih fasada koja je sve raširenija diljem svijeta, a posebno u Europi i SAD-u.

Ključne riječi: sidreni kanali, spregnute ploče s valovitim trapeznim limovima, „džepovi", izmijenjeni proračunski modeli, modifikacijski faktori, tanki elementi, otkazivanje betona

CONTENTS

1

INTRODUCTION

1.1 Background and motivation

Various types of fastening systems for concrete are available on the market today. These systems can be distinguished based on the installation method. Namely, cast-in fasteners are positioned in the formwork before the concrete is poured, whereas post-installed fasteners are installed in the hardened concrete. Another way of differentiating fastening systems is by the load-transfer mechanism [1]. A distinction is made between fasteners that transfer the applied load by mechanical interlock, friction, or bond (see Figure 1.1a). The choice of the appropriate fastener depends on many factors, including the application, installation time, loading situation, etc.

Cast-in anchor channels with channel bolts are becoming increasingly popular for several applications because of their adjustability (installation tolerance), reduced on-site labor requirements compared to post-installed fasteners and large range of resistances that can be achieved. This fastening system consist of a cold-formed or hot-formed steel channel profile equipped with at least two anchors. The anchors can be rounded or I-shaped and can be attached to the channel profile by welding, screwing and riveting. The channel profile is filled with removable foam filler to prevent concrete intrusion during pouring. After removing the formwork, various structural

1

or non-structural elements can be attached to anchor channels with the aid of special channel bolts (T-bolts) that must be prestressed with a defined torque. Special anchor channels with serrated lips are also available on the market, which allow load transfer along the longitudinal axis of the channel. In this case, the channel bolts are manufactured with serrations to ensure an interlocking connection (Figure 1.1b). This fastening system finds its application in the connection of curtain walls, mechanical fixings as well as in elevator shafts, precast facades, stadiums, tunnels, etc.

<div align="center">(a)   (b)</div>
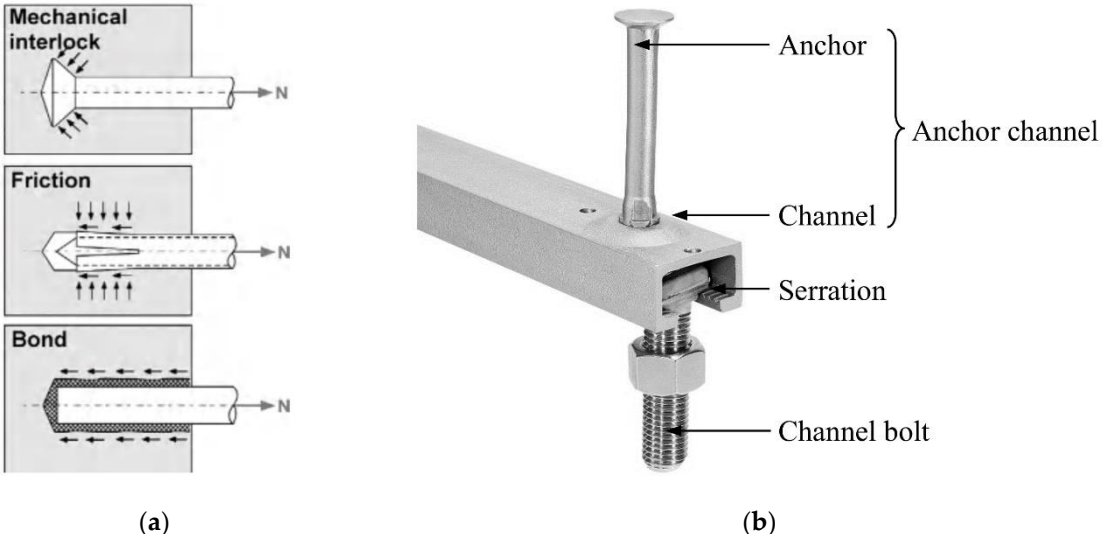
Figure 1.1 (a) Load-transfer mechanisms [1]; (b) Components of fastening system [2]

One of the most common applications of anchor channels is the fastening of brackets supporting curtain wall elements, which are common in modern high-rise buildings. In such an application, anchor channels must cope with challenging conditions, such as thin concrete members, small edge distances, high wind loads, and lightweight concrete as base material. All these factors lead to a significant reduction in the capacity of concrete failure modes, requiring to increase the edge distance, the use of hanger reinforcement or specific solutions that can take the advantage of reinforcement to overcome the limited concrete capacity, such as anchor channels with welded reinforcing bars or other specific solutions (e.g., Hilti HAC EDGE [3]). In general, anchor channels can be installed at the top of the floor slab (ToS) in the vast majority of cases, at the front of the slab (FoS) in some cases, or rarely at the bottom of

the slab (BoS) (Figure 1.2). Since the horizontal, outward component of the load acting on the channel is frequently predominant in high-rise buildings due to wind suction, ToS installation is more critical due to the limited shear concrete edge breakout capacity. Therefore, ToS installation has been studied in detail in the thesis.
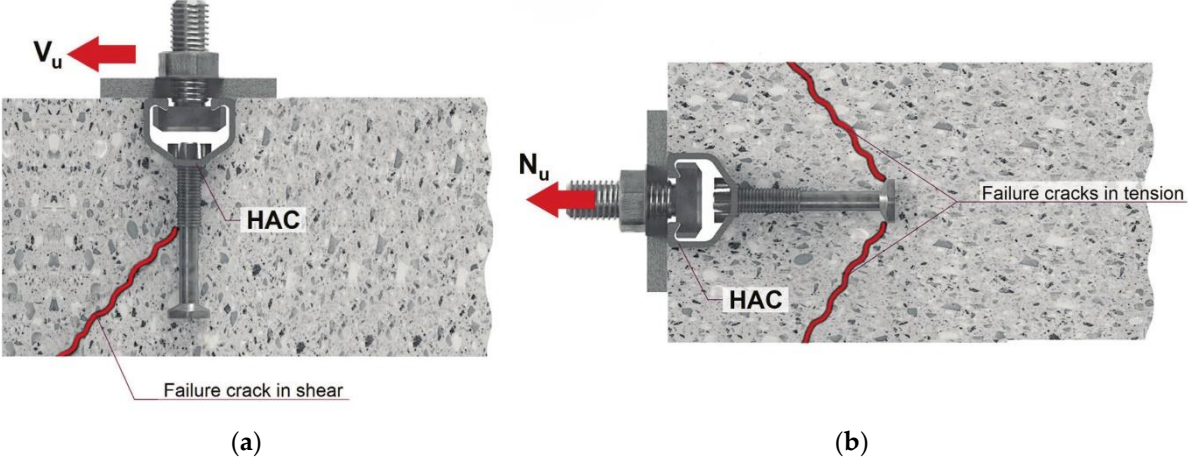
Figure 1.2 Installation of anchor channels in curtain wall applications [3]: (a) ToS; (b) FoS

The design is even more challenging if composite slabs with profiled steel decking are the selected floor system. Composite slabs are commonly used in steel framed buildings. Their main advantages are the speed of construction and the general structural efficiency that can be achieved by reducing weight [4]. In this case, not only does the limited member thickness represent an issue, but also the specific geometry of the composite slabs (see Figure 1.3a). In addition, since the brackets mounted to the top of the slab might occupy a portion of the floor area, anchor channels are often recessed into pockets that reduce the overall thickness of the slab (see Figure 1.3b).

To the best of the author's knowledge, the installation of anchor channels in composite slabs and pockets has not been investigated yet. Consequently, design is mostly based on engineering judgments, which may lead to inaccuracies. This implies that the actual capacity may be overestimated or underestimated depending on the configuration. For instance, given the current absence of data, the concrete edge (shear) capacity should be calculated on the safe side by using the reduced member thickness, neglecting the concrete within the ribs of the steel decking. For pockets, only the

reduced slab thickness in the pocket is considered in the design. Therefore, these topics are not only scientifically interesting, but also extremely relevant for practical applications, especially in countries like the United States.

<table>
<tr><td>(a)</td><td>(b)</td></tr>
</table>
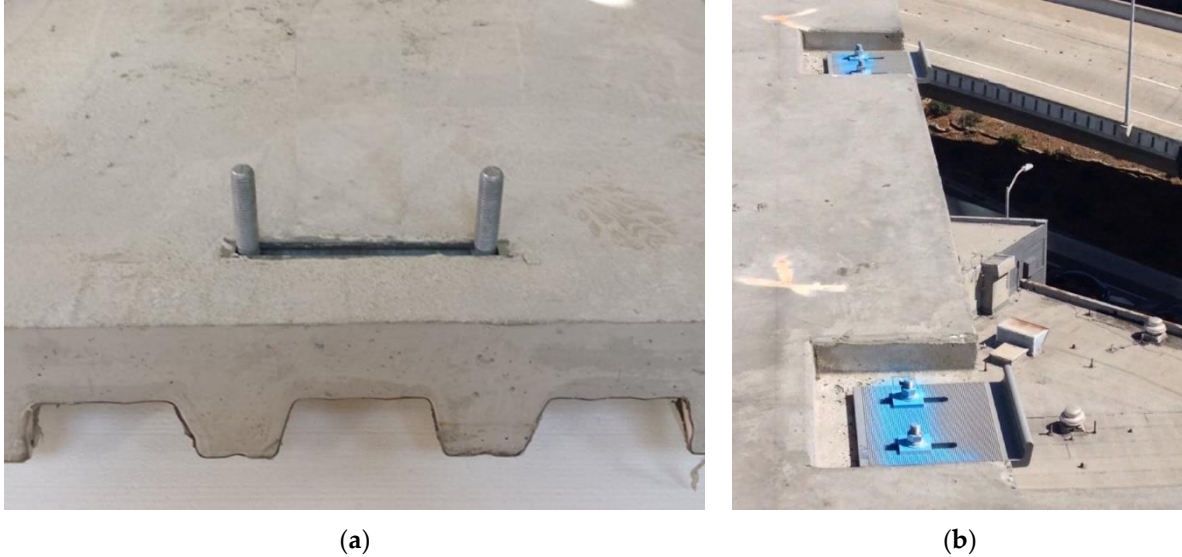
Figure 1.3 Installation in: (a) composite slabs; (b) pockets

1.2   Objectives and hypothesis of the thesis

The overall aim of this thesis is to numerically and experimentally investigate the behavior of anchor channels in composite slabs with the profiles steel decking under tension and shear load and to enhance current design models for improved predictability. Moreover, other relevant topics for curtain wall applications, such as pockets and the influence of surface reinforcement, are considered. Therefore, the research objectives are as follows:

- Investigate typical composite slab geometries, possible applications of anchor channels, and relevant design challenges

- Examine the accuracy and reliability of current design models for anchor channels installed in thin plain (un-cracked) concrete slabs (for tension and shear load)

- Propose modifications of the current design models for plain concrete slabs to provide a sound reference for additional modification factors that account for the influence of composite slabs, pockets, etc.

- Determine the concrete capacity for anchor channels in composite slabs

- Propose a design method for the tensile and shear concrete failure modes for anchor channels in composite slabs

- Investigate the behavior of anchor channels in pockets and to propose an accurate design method

- Discuss the influence of surface reinforcement on the capacity of anchor channels

This thesis is based on the following hypotheses:

- *The capacity of concrete failure modes of an anchor channel under tension or shear is lower for composite slabs than for plain concrete slabs with the same overall thickness. The capacity reduction can be attributed to the complex geometry of composite slabs with the profiled steel decking.*

- *The capacity of anchor channels in pockets can be increased if the pocket geometry and the overall member thickness are considered, and it can generally be improved by proper positioning of the surface reinforcement.*

1.3 Research methodology

In order to achieve the objectives of this thesis, extensive numerical investigations were performed, accompanied by experimental campaigns. The numerical simulations formed the core of the research, whereas supplementary experimental studies were carried out to verify the numerically obtained findings and the proposed recommendations. Indeed, full-scale tests of connections are time-consuming and costly, especially considering the number of parameters and configurations that should be varied. Numerical simulations also provide better insight into the load transfer and failure mechanism. However, it is of great importance that the numerical models are validated against the tests relevant for the study and that the code accounts for all the necessary effects for a material under investigation.

In this study, a 3D nonlinear finite element (FE) code MASA was employed. The code is based on the microplane constitutive law for concrete with relaxed kinematic constraint [5]. The analysis is performed in the framework of the smeared crack approach, whereas the crack band method is used as a regularization technique [6].

The experimental part of this study was carried out in the Construction Laboratory of the Faculty of Civil Engineering in Rijeka, Croatia. The most important devices were two Zwick Roell servo-hydraulic actuators. In addition, displacement transducers type were used to measure displacements, while the concrete properties of tested slabs were determined in the Materials Laboratory using the appropriate devices.

1.4   Thesis outline

The thesis consists of seven chapters and appendices summarizing all numerical results. Below is given a brief description of each chapter:

Chapter 1: In the introduction, the most important details about the fastening system under investigation as well as the motivation for this thesis are presented. Furthermore, insight into the research objectives, hypothesis, and research methodology is also provided.

Chapter 2: Previous studies relevant to this research are presented as part of the literature review. In addition, an overview of current design codes and qualification guidelines is provided.

Chapter 3: The 3D finite element code MASA, which was employed in the numerical simulations, is briefly introduced. As a very important part of this research, the experimental validation of the finite element models for anchor channels in plain concrete slabs and composite slabs is explained in detail. This chapter also delivers the results of the mesh sensitivity analysis and the dependence of the numerical results on the macroscopic material properties of concrete.

Chapter 4: Numerical and experimental investigations of anchor channels in plain concrete slabs are summarized. Emphasis was placed on thin plain concrete slabs in order to obtain the correct reference values for further investigations on slabs with complex geometry (composite slabs and pockets). The design modifications and main conclusions are given at the end of the chapter.

Chapter 5: The numerical and experimental results of the investigation on anchor channels in composite slabs with profiled steel decking are reported. Based on the obtained results, the main conclusions and a design proposal are presented.

Chapter 6: Further relevant topics for the curtain wall application of anchor channel are introduced. The numerical and experimental results for anchor channels in pockets are presented, whereas the influence of surface reinforcement was briefly discussed.

Chapter 7: The final chapter summarizes the thesis and concludes with the main scientific contributions and a proposal for future research.

2

LITERATURE REVIEW

In the last three decades, research on anchor channels has intensified due to their increasing popularity in the construction industry. Initial studies were performed to investigate the behavior of this fastening system installed in thin members reinforced with hairpin reinforcement under combined shear and tension loads [7]. In the following, the most important studies related to the concrete failure modes under monotonic loading are considered [8], [9], [10]. These studies served as the basis for the development of design equations and qualification tests in the current guidelines for the verification of the capacity of anchor channels. The suitability of anchor channels for earthquake loads was studied by means of simulated seismic tests performed in the low cycle range [11]. Initial detailed investigations on the behavior under fatigue loading were carried out in [12], [13], whereas the study of fatigue resistance under combined static and cyclic loads is currently under investigation [14].

The design of anchor channels with channel bolts is rather complicated due to their complex geometry, which may trigger versatile failure modes. For this reason, the current design codes distinguish 18 failure modes, which are further differentiated depending on the direction of loading (Figure 2.1). During the qualification process, the characteristic resistance of each component of an anchor channel system must be determined. Steel verifications are simply a check of the resistance against the acting

loads and are therefore not significant for the scope of this research. In the following, only those concrete failure modes that are relevant for this work are discussed in detail.
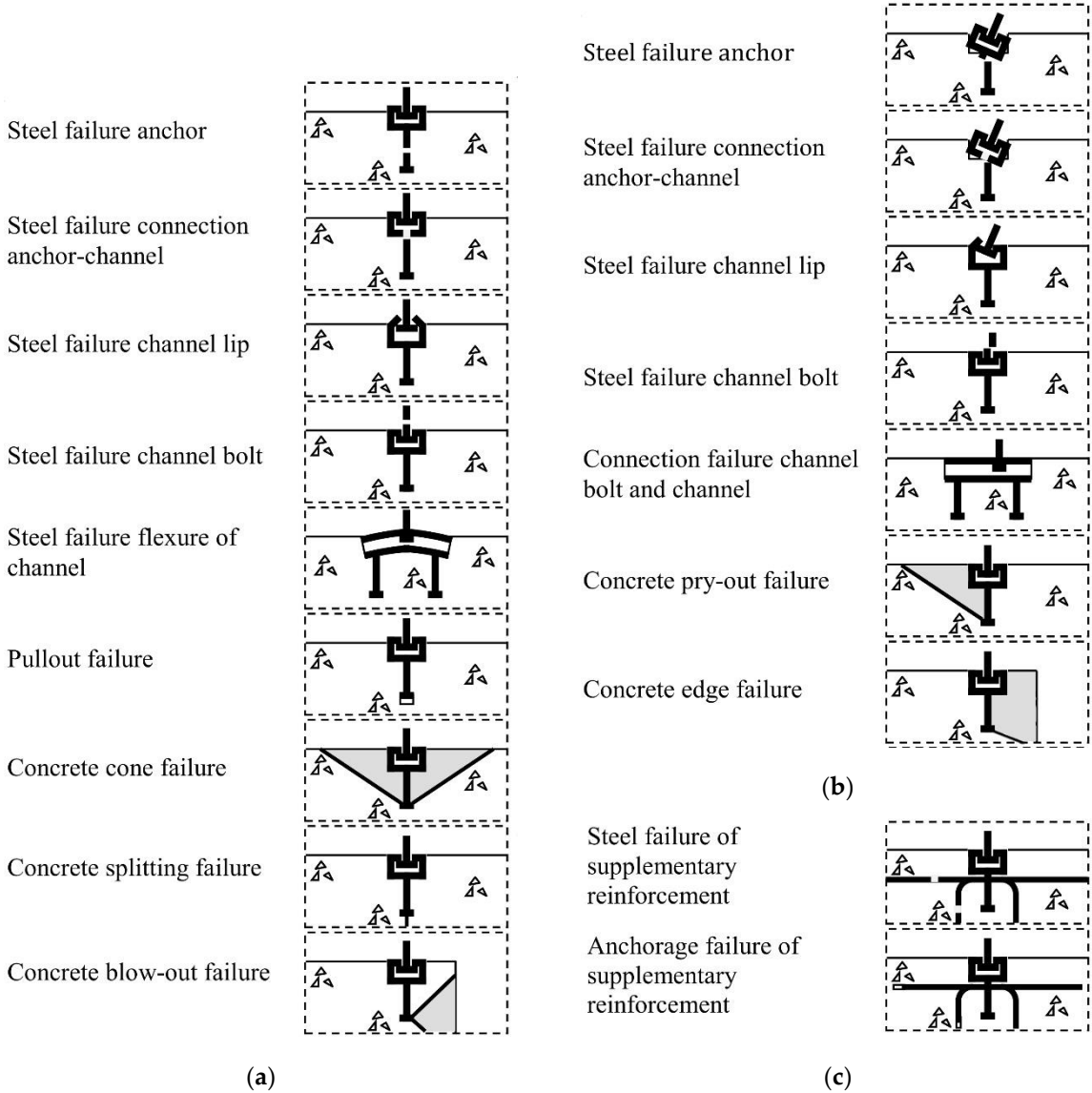
Figure 2.1 Verifications for anchor channels loaded in: (a) tension; (b) shear; (c) tension or shear [15]

2.1 Investigations associated with tension load

Anchor channels subjected to tension can develop four failure modes due to concrete failure. For standard anchor channel on the market, pull-out and blowout failures are rarely decisive. More about these failure modes can be found in relevant studies on headed studs [16], [17]. Concrete cone breakout and concrete splitting are

generally the governing failure modes for installation near the edge, especially for thin members. Therefore, these two failure modes are of particular interest for this study.

2.1.1 Concrete (cone) breakout

Concrete (cone) breakout is characterized by a typical cone-shaped breakout failure pattern. The fastener relies on the concrete tensile capacity to resist the tension load introduced via the anchor head. The slope of the fracture surface is on average about 35°, but may depend on various factors, e.g., stress conditions in the base material, embedment depth, etc. According to this observation, the diameter of the projected surface is approximately three times the embedment depth (h_{ef}), as shown in Figure 2.2a. Consequently, the distance between the neighboring anchors should be larger than $3h_{ef}$ to prevent overlap of the individual failure surfaces [1].

Wohlfahrt [10] conducted an extensive investigation to determine the behavior of anchor channels equipped with two anchors loaded in tension in non-cracked concrete members without supplementary reinforcement. According to Wohlfahrt [10], the failure load can be determined using the well-known CC method [18] as it applies to headed studs. The core of the CC method is the mean failure load of a single anchor subjected to axial tension that may be calculated as follows:

$$N_{u,c}^0 = k' \cdot h_{ef}^{1.5} \cdot f_c^{0.5} \quad [\text{N}]. \tag{2.1}$$

Factor k' represents product-specific ($k' = 16.8$ for headed studs), whereas the capacity is assumed to be proportional to the square root of the concrete (cylinder) compressive strength (f_c), although the capacity may also be influenced by the concrete mix, in particular the type and maximum size of aggregate [1]. The failure load is proportional to $h_{ef}^{1.5}$, which implies that the largest possible size effect predicted by the linear fracture mechanics is assumed. This is due to the fact that the tensile stress in concrete, averaged over the fracture surface at ultimate load, decreases as the size of the fracture area increases [19].

According to the CC method [18], the failure load of a multiple anchors with a spacing of less than $3h_{ef}$, without additional influences, can be calculated as follows:

$$N_{u,c} = \frac{A_{c,N}}{A^0_{c,N}} \cdot N^0_{u,c} \quad [\text{N}]. \tag{2.2}$$

The factor $A_{c,N}/A^0_{c,N}$ considers the geometrical influence of anchor spacing on the failure load, as shown in Figure 2.2b. It is assumed that the failure load increases in proportion to the projected area $A_{c,N}$ of the anchor group under consideration. As can be seen in Figure 2.2a, the projected area $A^0_{c,N}$ stands for the idealized projected area of a single anchor ($A^0_{c,N} = 9h_{ef}^2$). Additional factors that take into account the influence of edge distance, eccentric tension load, or reinforcement could be included in Equation (2.2), but are beyond the scope of this thesis.
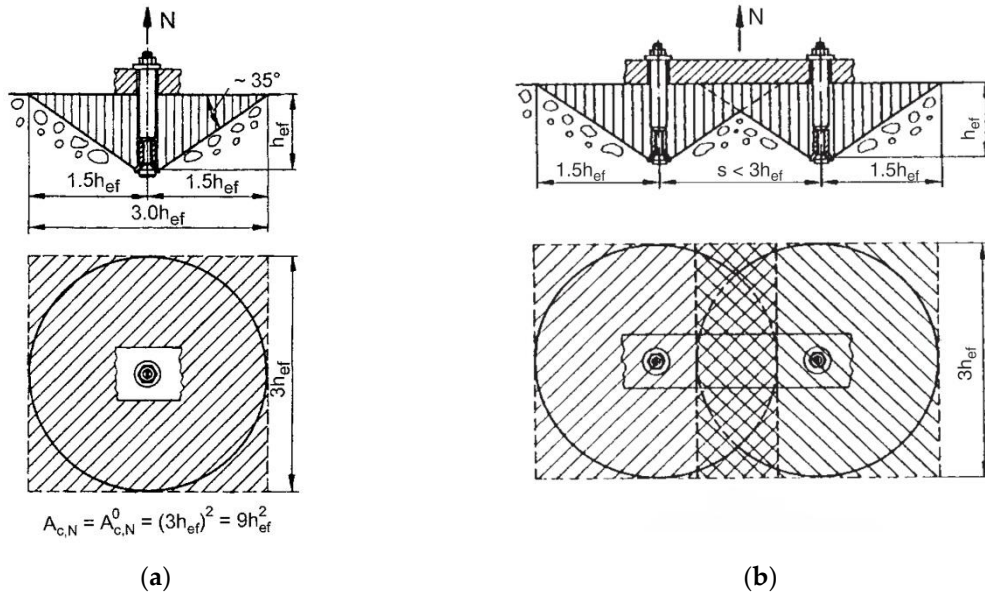
Figure 2.2 CC method: (a) single anchor; (b) anchor group [1]

Subsequent research conducted by Kraus [8] showed that certain modifications to the CC method are necessary. First, the presence of the channel profile in the breakout body may influence the capacity depending on the ratio of the channel height and embedment depth. Therefore, an additional factor should be included in Equation (2.1), i.e., the capacity of a single anchor of an anchor channel should be calculated in accordance with the following expression:

$$N^0_{u,c} = 16.8 \cdot h_{ef}^{1.5} \cdot f_c^{0.5} \cdot \alpha_{ch,N} \quad [\text{N}], \tag{2.3}$$

where:

$$\alpha_{ch,N} = \left(\frac{h_{ef}}{180}\right)^{0.15} \le 1.0 \,. \tag{2.4}$$

Moreover, anchor channels with more than two anchors behave in tension like a continuously supported beam with support points at anchor locations (springs) and partially restrained ends. Moreover, the loads can act at arbitrary position along the channel causing the anchors to carry different loads. This is also the case with the anchor groups. However, if the groups are "compact", a rigid baseplate can be assumed, and in case of eccentricity, a linear distribution between the anchors is assumed and considered with simple factors. In case of anchor channels, the anchors are relatively distant and distributed in one direction, so such an approach would be hardly applicable. Therefore, Kraus [8] decided to perform the concrete verification at the level of the individual anchors. In a first step, the load should be redistributed from the bolts to the anchors. Therefore, a simplified linear triangular distribution over the influence length l_i is assumed, as illustrated in Figure 2.3. The tension in each anchor caused by a tension load $N^{cb}{}_{Ed}$ acting on a channel bolt is calculated as follows:

$$N^a_{Ed,i} = k \cdot A'_i \cdot N^{cb}_{Ed} \quad [\text{N}], \tag{2.5}$$

where A'_i is the ordinate at the position of the anchor i of a triangle with the unit height at the position of the acting load and the base length $2l_i$, and factor k is obtained by the following expression:

$$k = \frac{1}{\sum_1^n A'_i} \,. \tag{2.6}$$

The influence length l_i depends on the moment of inertia of the channel I_y and the anchor spacing s [8]:

$$l_i = 13 \cdot I_y{}^{0.05} \cdot s^{0.5} \ge s \quad [\text{mm}]. \tag{2.7}$$
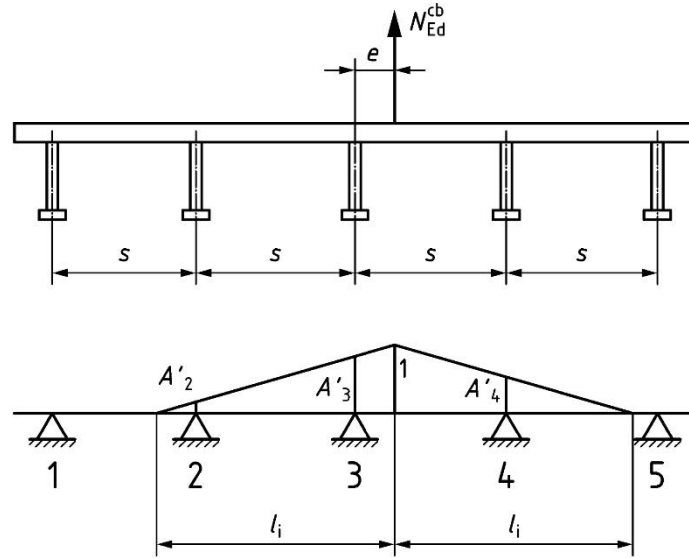
Figure 2.3 Triangular load distribution method [20]

Consequently, the verification is performed for each anchor of an anchor channel, which is opposite to the provisions for headed studs or post-installed anchors, where the global fixture verification is performed. The capacity of one anchor of an anchor channel should be calculated according to the following equation:

$$N_{u,c} = N_{u,c}^0 \cdot \alpha_{s,N} \cdot \alpha_{e,N} \cdot \alpha_{c,N} \cdot \Psi_{re,N} \quad [\text{N}].$$ (2.8)

where:

- $N^0_{u,c}$ – average failure load of one anchor
- $\alpha_{s,N}$ – factor taking into account the influence of neighboring anchors
- $\alpha_{e,N}$ – factor taking into account the influence of edge distance
- $\alpha_{c,N}$ – factor taking into account the influence of corner distance
- $\Psi_{re,N}$ – factor taking into account the effect of a dense reinforcement

As this research was the basis for the current design codes, the modification factors are discussed in detail in chapter 2.3. It should be noted that the influence of member thickness is not accounted for in Equation (2.8).

Further work on the topic of tensile capacity in thin members was performed by Nilforoush [21] for headed studs without the influence of edge distance. Among others, the most relevant topic for this thesis is the influence of member thickness on the concrete breakout capacity for cast-in headed studs. Based on the numerical and

experimental results, a modification factor was proposed to take into account the influence of member thickness on the concrete breakout failure:

$$\Psi_h = \left(\frac{h}{2h_{ef}}\right)^{0.25} \le 1.2 \,. \tag{2.9}$$

In addition, the influence of orthogonal surface reinforcement in un-cracked and pre-cracked concrete members was investigated. It was found that the breakout capacity increases up to approximately 20% if the concrete member is orthogonally reinforced and has a reinforcement content of at least 0.3% in each direction. The favorable influence of surface reinforcement on the anchorage capacity decreases with increasing the thickness of concrete member [21]:

$$\Psi_{Sr} = 1.35 \left(\frac{h_{ef}}{h}\right)^{0.5} \le 1.20 \qquad \text{if } h \le 3h_{ef}$$

$$\Psi_{Sr} = 1.00 \qquad\qquad\qquad \text{if } h > 3h_{ef}. \tag{2.10}$$

In recent years, concrete elements have become thinner and lighter, creating a need for shallow embedment fastening systems. Grosser et al. [22] investigated the effect of the channel profile for shallow embedment depths and suggested a modification of the factor $\alpha_{ch,N}$ which allows an accurate design even for very shallow embedded anchor channels. According to this research, the influence of channel height should be considered as well:

$$\alpha_{ch,N} = 2 - 2.5\frac{h_{ch}}{h_{ef}} \le 1.0 \,. \tag{2.11}$$

2.1.2 Concrete splitting due to loading

Concrete splitting failure due to tension load can be decisive when installing an anchor channel close to an edge or corner, especially in relatively thin concrete members. To the best of the author's knowledge, this failure mode has not been extensively investigated for anchor channels. However, it has already been investigated for other types of fastening systems, such as headed studs, which behave similar to anchor channels. Since the model in the current design codes differs

14

significantly from the models proposed in the following investigations, the main conclusions are mentioned rather than a detailed review of the models.

Asmus [23] extensively investigated headed studs, undercut anchors, and expansion anchors near an edge or corner of a concrete member or in a narrow element. He proposed different calculation methods depending on the load transfer mechanism, but his first proposal was less suitable for design purposes due to its high complexity. Therefore, Asmus [24] later proposed a simplified model valid for different types of typical anchor systems based on the well-known concrete capacity (CC) method [18]:

$$N_{u,c} = N^0_{um,sp} \cdot \frac{A_{csp}}{A^0_{csp}} \cdot \Psi_{h,sp} \cdot \Psi_{s,sp} \quad \text{[N].} \tag{2.12}$$

where A^0_{csp} is the idealized projected area for a single anchor, A_{csp} is the actual projected area for the anchors under consideration (see Figure 2.4 for a single anchor at a corner), $\Psi_{h,sp}$ and $\Psi_{s,sp}$ are modification factors for the influence of member thickness and anchor spacing parallel to the edge, whereas $N^0_{um,sp}$ is the splitting failure load of a single anchor at the edge:

$$N^0_{um,sp} = k_p \cdot c_1^{0.8} \cdot h_{cr,sp}^{0.5} \cdot f_{cc,150}^{0.5} \quad \text{[N].} \tag{2.13}$$

The main feature of his proposal is a product-dependent factor k_p, which takes into account the effect of the load transfer mechanism or of the load bearing area, depending on the fastening system. This factor should be obtained through unconfined tension tests in the corner of a concrete member. In Equation (2.13), c_1 is the edge distance and $f_{cc,150}$ is the concrete compressive strength measured on cubes. The characteristic member thickness $h_{cr,sp}$ is calculated as a sum of embedment depth h_{ef} and the characteristic edge distance $c_{cr,sp}$ as follows:

$$h_{cr,sp} = h_{ef} + c_{cr,sp} = h_{ef} + 1.5c_1 \quad \text{[mm],} \tag{2.14}$$

where the characteristic edge distance $c_{cr,sp}$ can be calculated as $1.5c_1$, which is assumed based on the CC method [18]. Therefore, the characteristic anchor spacing $s_{cr,sp}$ equals $3c_1$.

The splitting capacity is proportional to the ratio A_{csp}/A^0_{csp}, thus directly proportional to the thickness of the concrete member. However, it was found that the splitting failure load is less than directly proportional to the factor $A_{c,sp}/A^0_{c,sp}$, and therefore the factor $\Psi_{h,sp}$ was proposed:

$$\Psi_{h,sp} = \left(\frac{h_{cr,sp}}{h}\right)^{1/2} .$$

(2.15)
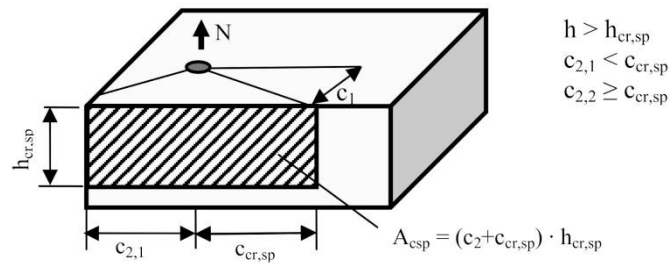
Figure 2.4 Projected splitting failure area A_{csp} of a single anchor at a corner ($A^0_{csp} = s_{cr,sp} \cdot h_{cr,sp}$) [24]

Hüer [25] focused his research mainly on bonded anchors and proposed a design method based on the experimental and numerical results for two possible setups, i.e., confined and unconfined. For unconfined tests, the reaction support of the test rig was located at a distance of at least twice the embedment depth from the anchor, which ensures an unrestricted concrete cone formation. For confined tests, concrete breakout failure was suppressed by introducing the reaction forces into the concrete close to the anchor. In this case, steel failure of the anchor, anchor pull-out, or failure due to formation of splitting cracks in the concrete may occur. It was shown that the maximum load obtained from the confined setup is generally (significantly) greater than that from the unconfined setup, especially when the member thickness is limited. Bending stresses induced by the unconfined setup lead to cracks in the concrete member which, consequently, leads to a decrease in capacity. Therefore, it was concluded that cases where qualification tests for concrete splitting failure were performed under unconfined conditions do not provide reliable information on the actual "global" splitting resistance. Moreover, in thin members, concrete breakout capacity could be additionally affected by the bending stresses introduced by external

16

loads on the fastening elements. The model concrete breakout capacity influenced by bending is basically similar to the model of Asmus:

$$N_{u,cb} = N_{u,cb}^0 \cdot \frac{A_{c,cb}}{A_{c,cb}^0} \cdot \Psi_{h,cb} \cdot \Psi_{g,cb} \quad [\text{N}], \tag{2.16}$$

where $A_{c,cb}^0$ and $A_{c,cb}$ are projected areas (Figure 2.5a), whereas $\Psi_{h,sp}$ and $\Psi_{g,sp}$ are modification factors for the influence of member thickness and group effects. The basic capacity $N_{u,cb}^0$ of a single anchor is calculated as follows:

$$N_{u,cb}^0 = 11.5 \cdot c_1^{1/3} \cdot d^{1/4} \cdot h_{ef} \cdot f_{cm,cube}^{0.5} \quad [\text{N}], \tag{2.17}$$

where c_1 is the edge distance, d is the anchor diameter, h_{ef} is the embedment depth and $f_{cm,cube}$ is the concrete compressive strength measured on cubes. The characteristic member thickness $h_{cr,sp}$ is dependent only on the embedment depth (Figure 2.5b):

$$h_{cr,cb} = 2.25 h_{ef} \quad [\text{mm}], \tag{2.18}$$

and the corresponding modification factor is:

$$\Psi_{h,cb} = \left(\frac{h_{cr,cb}}{h}\right)^{2/3}. \tag{2.19}$$

The characteristic edge distance depends on the edge distance,

$$c_{cr,cb} = 8 c_1^{\;2/3} \quad [\text{mm}], \tag{2.20}$$

whereas the characteristic anchor spacing is twice the characteristic edge distance.
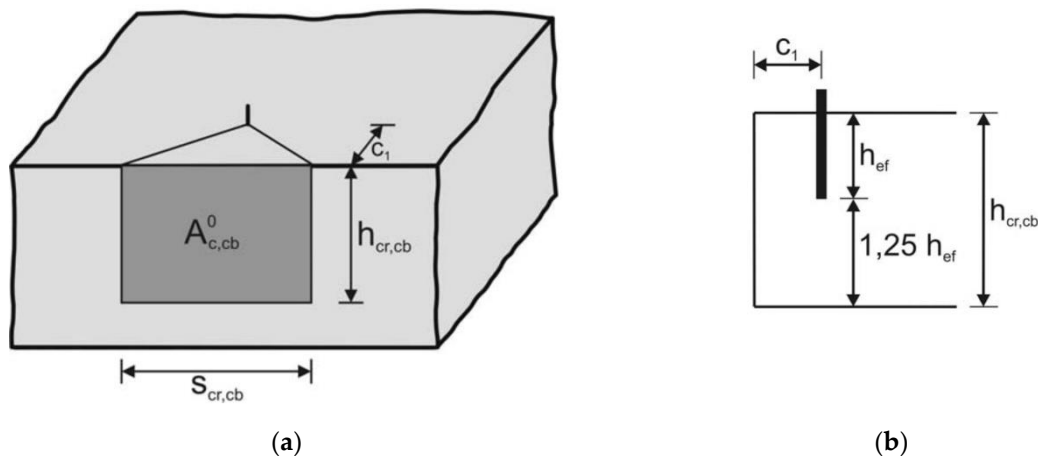
Figure 2.5 (a) Idealized projected area $A_{c,cb}^0$; (b) Characteristic member thickness $h_{cr,cb}$ [25]

The design model for splitting according to EN 1992-4 [26] is based on concrete cone breakout, whereas Asmus [24] and Hüer [25] proposed equations for the splitting verification that are substantially different. Even though a comparison between these models would be possible, it is beyond the scope of this thesis. The reason for this is that the objective is to modify the existing models for anchor channels and not to introduce completely new approaches for the concrete failure modes.

However, since all of these models have the individual modification factor for the influence of member thickness, these factors are compared. An overview of the characteristic member thicknesses and modification factors from the literature is given in Table 2.1. In general, the influence of the member thickness is considered with different exponents, varying between 0.25 [21] and 0.5 [24], as well as different characteristic member thicknesses. According to Nilforoush [21], a characteristic member thickness of approximately 4.15 can be calculated from the upper limit of the modification factor. Even though the considered failure modes are partly different, this appears to be considerably larger than the value provided in [25] or in EN 1992-4 [26] for the splitting failure.

Table 2.1 Comparison between modification factors for the influence of member thickness that can be found in the literature [24], [25], [26]

Author	Characteristic member thickness	Modification factor
Asmus	$h_{cr,sp} = h_{ef} + 1.5c_1$	$\dfrac{A_{c,sp}}{A_{c,sp}^0} \cdot \left(\dfrac{h_{cr,sp}}{h}\right)^{1/2} = \dfrac{h}{h_{cr,sp}} \cdot \left(\dfrac{h_{cr,sp}}{h}\right)^{1/2} = \left(\dfrac{h}{h_{cr,sp}}\right)^{1/2}$
Hüer	$h_{cr,cb} = 2.25 h_{ef}$	$\dfrac{A_{c,cb}}{A_{c,cb}^0} \cdot \left(\dfrac{h_{cr,cb}}{h}\right)^{2/3} = \dfrac{h}{h_{cr,cb}} \cdot \left(\dfrac{h_{cr,cb}}{h}\right)^{2/3} = \left(\dfrac{h}{h_{cr,cb}}\right)^{1/3}$
Nilforoush	$4.15 h_{ef}$[1]	$\left(\dfrac{h}{2h_{ef}}\right)^{0.25} < 1.2$

[1] *Not provided explicitly, calculated from a limit of* 1.2

2.2 Investigations associated with shear load

For shear load, two concrete failure modes are relevant in practical applications, depending on the direction of the loading. These are concrete pryout, which is generally related to the shear load acting away from the edge, and concrete edge breakout, which is associated with the shear load acting towards the edge. However, the governing failure mode depends on the edge distance and the embedment depth, i.e., concrete pryout may develop prior to concrete edge breakout for shallow embedment depths even for the shear load acting towards the edge. The findings gained for concrete pryout of headed studs [27], [28], also apply to anchor channels, although the knowledge has recently been extended by Jebara [29]. He proposed the extended CC method for pryout failure mode, which accounts for single anchor and anchor group as well as for edge and corner influence. This method enhances currently used design provisions which are based on the so-called indirect-tension model [1].

For the installation close to the edge, concrete edge breakout capacity is generally significantly lower than concrete pryout capacity, especially for thin members. Therefore, concrete edge breakout is usually the decisive failure mode in curtain wall applications (ToS installation) due to high horizontal loads caused by wind suction. This failure mode is reviewed in detail.

2.2.1 Concrete edge breakout

The behavior of anchor channels loaded towards the edge was first investigated in detail by Wohlfahrt [10]. According to his study, local failure often occurs, starting at the front face of the channel, before the ultimate load is attained. This is due to the smaller edge distance of the front face of the channel compared to the edge distance of the anchors. Thereafter, the anchors transfer the entire load to the concrete. As a result, the concrete between the anchors is subjected to higher stresses than with headed studs installed at the same spacing, as the channel profile reduces the effective cross section resisting the shear load.

Based on these observations, Wohlfahrt [10], who studied anchor channels with two anchors, proposed the approach analogous to the proposal for headed studs, where the failure load can be evaluated using the CC method [18] in a similar way as for fasteners loaded in tension:

$$V_{u,c} = \frac{A_{c,V}}{A_{c,V}^0} \cdot \Psi_{s,V} \cdot \Psi_{h,V} \cdot \Psi_{ec,V} \cdot V_{u,c}^0 \quad [\text{N}].$$ (2.21)

The basic concrete edge capacity of a single anchor $V^0_{u,c}$ is strongly influenced by the edge distance. Therefore, the ultimate load $V^0_{u,c}$ is proportional to $c_1^{1.5}$, which has the same exponent as the embedment depth h_{ef} in the concrete (cone) breakout equation for tension. The typical breakout pattern and the idealized projected area $A^0_{c,V}$ for anchors under shear loads are shown in Figure 2.6.
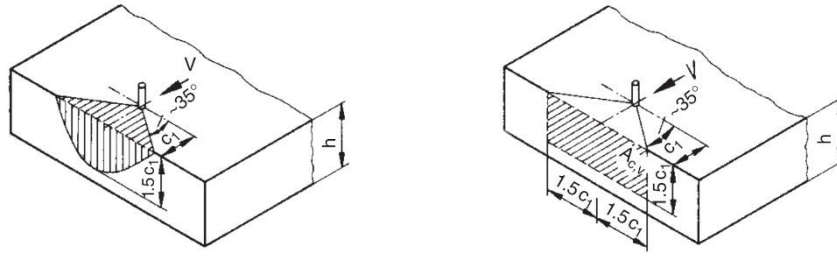
Figure 2.6 CC method adapted for anchors loaded in shear [1]

According to the projected area approach, the failure load should be proportional to the member thickness. However, previous studies on shear loaded headed studs [30], [31] have found that the influence of member thickness should be less than proportional. This is taken into account by an increase factor $\Psi_{h,V}$ when the member thickness is smaller than the characteristic member thickness:

$$\Psi_{h,V} = \left(\frac{1.5c_1}{h}\right)^{1/3} \geq 1.0 \text{ (Zhao et al.)}$$ (2.22)

$$\Psi_{h,V} = \left(\frac{1.5c_1}{h}\right)^{0.5} \geq 1.0 \text{ (Hofmann)},$$ (2.23)

where c_1 is the edge distance and h represents the actual member thickness. It should be mentioned that the minimum member thickness investigated in these studies was 150 mm. Later experimental investigation [32] was performed for thinner members ($h_{min} = 110$ mm), showing that the exponent of 1/3 is a better predictor of the capacity

in thin members. In addition, the ultimate load $V^0_{u,c}$ is influenced by the concrete compressive strength, the anchor diameter and the effective load transfer length, which is equal to the embedment depth for headed studs. The modification factors $\Psi_{s,V}$ and $\Psi_{ec,V}$ in Equation (2.21) take into account the influence of a corner and the influence of eccentric shear load, respectively.

Due to higher stresses in concrete, Wohlfahrt [10] recommended larger characteristic value for anchor spacing ($s_{cr,V} = 5c_1$ compared to $s_{cr,V} = 3c_1$ for headed studs) and for member thickness ($h_{cr,V} = 2.5c_1$ compared to $h_{cr,V} = 1.5c_1$ for headed studs). Therefore, the projected area of the failure surface for a single anchor $A^0_{c,V}$, idealized as a half pyramid of height c_1 and base dimensions $s_{cr,V}$ and $h_{cr,V}$, equals $12.5c_1^2$.

Subsequently, Potthoff et al. [33] showed that Wohlfahrt's proposal is rather conservative for anchor channels equipped with more than two anchors and the influence of arbitrary loading for such anchor channels cannot be considered. Moreover, in contrast to Wohlfahrt [10], it was shown that the shear load is transferred in concrete mainly by the channel profile and only to a smaller extend by the anchors. However, anchors experience high tensile stresses due to the eccentricity between the applied shear load and the resultant of the shear resistance. It was also demonstrated that a model analogous to the model by Kraus [8] for the load redistribution from the bolts to the anchors was sufficiently accurate. Furthermore, in this way, the concrete edge breakout verification could be performed for one anchor of an anchor channel as follows:

$$V_{u,c} = V^0_{u,c} \cdot \alpha_{s,V} \cdot \alpha_{h,V} \cdot \alpha_{c,V} \quad [N]. \tag{2.24}$$

where modification factors $\alpha_{s,V}$, $\alpha_{h,V}$ and $\alpha_{c,V}$ take into account the influence of neighboring anchors, the influence of member thickness and the influence of corner. These factors are further explained in the following chapter 2.3, as this research serves as the basis for the current design codes.

The characteristic ultimate load of a channel segment with one anchor depends on the size of the anchor channel and is given by the following expression:

$$V_{u,c}^0 = k_p \cdot c_1^{1.5} \cdot \sqrt{f_{cc}} \quad [\text{N}]. \tag{2.25}$$

In fact, factor k_p contains all the product specific parameters relevant for the design and according to Potthoff [9] k_p takes the value of 5 for small (≤38/17), 6 for medium (50/30), and 7 for large anchor channels (72/48). As mentioned before, the edge distance is the most influential factor, whereas the concrete compressive strength is taken into account by the square root of concrete cube strength.

The influence of supplementary reinforcement on the concrete edge capacity was studied in detail by Schmid [34]. With supplementary reinforcement, a specimen may exhibit steel failure or anchorage failure, and the minimum of the two is decisive and determines the shear resistance. In floor slabs, especially in non-seismic areas, the reinforcement is usually not in the required quantity or in the correct location, so it does not comply with the design requirements. However, several studies have found that the design codes tend to be quite conservative for many configurations [35], [36]. Recently published work has shown that only employing surface (mesh) reinforcement (Φ6 / 200 mm) leads to a significant increase in capacity of 48% compared to the reference test in plain concrete [36]. This result sounds promising as mesh reinforcement is always available to control cracking or resist spalling, although it was determined for the larger edge distance of 200 mm.

2.3   Qualification guidelines and design rules

The design of anchor channels with channel bolts is based on the design rules that are semi-empirical for some failure modes and therefore require the product-specific factors that should be determined by qualification tests. Moreover, the design is not fully harmonized between Europe and the US [15]. It should be noted that almost all qualification tests are identical in Europe and in the United States, expect for the qualification tests related to the most frequent concrete failure modes under tension (concrete cone breakout) and shear load (concrete edge breakout). The differences are pointed out within chapters Design rules – tension load2.3.1 and 2.3.2.

In Europe, the new EN 1992-4 [26] has recently been issued, finally introducing a design specification at European level for fastening systems in the construction industry. EN 1992-4 [26] has been derived from the revision of the preliminary code CEN/TS 1992-4 [37] which comprises a general first part and four additional parts for headed anchors, anchor channels, mechanical and chemical post-installed fasteners. In addition to the design code, European Organization for Technical Assessment (EOTA) provides the qualification guidelines for the European Assessment Document (EAD). The European Assessment Document EAD 330008-03-0601 [38] is the reference document for anchor channels. After the successful qualification, the product receives the European Technical Assessment (ETA) certificate, which contains all the technical data to perform the design according to EN 1992-4 [26]. It should be mentioned that seismic applications of anchor channels are not covered in Europe so far.

On the other hand, the design rules for anchor channels in the US still need to be included in the design code for structural concrete ACI 318 [39]. Therefore, an additional document was issued by ICC-ES, the Acceptance Criteria AC232 [40]. It comprises supplement clauses for the design of anchor channels and is written as an amendment to ACI 318 [39]. This document also serves as a qualification guideline and the product is documented in the Evaluation (Service) Reports (E(S)R), which may include seismic qualification.

2.3.1 Design rules – tension load

2.3.1.1 Concrete (cone) breakout

The characteristic resistance of one anchor of an anchor channel can be calculated according to the following equation:

$$N_{Rk,c} = N_{Rk,c}^0 \cdot \Psi_{ch,s,N} \cdot \Psi_{ch,e,N} \cdot \Psi_{ch,c,N} \cdot \Psi_{re,N} \quad [N]. \tag{2.26}$$

The basic characteristic resistance $N^0_{Rk,c}$ of a single anchor placed in concrete and not influenced by neighboring anchor or corner effects can be obtained as follows:

$$N_{Rk,c}^0 = k_1 \cdot \sqrt{f_{ck}} \cdot h_{ef}^{1.5} \quad [N], \tag{2.27}$$

where $k_1 = k_{cr,N}$ for cracked concrete and $k_1 = k_{ucr,N}$ for un-cracked concrete. These factors are given in the corresponding ETA. The difference between cracked and un-cracked conditions is considered by a factor of 0.7. It should be mentioned that the value for $k_{ucr,N}$ is obtained as a 75% (5%-fractile – characteristic value) of a constant factor in Equation (2.3) multiplied by the factor $\alpha_{ch,N}$ in Equation (2.4). However, this applies to standard anchor channels, i.e., $h_{ch}/h_{ef} \leq 0.4$ and/or $b_{ch}/h_{ef} \leq 0.7$, where h_{ch} and b_{ch} are the channel height and width, respectively. For anchor channels not falling in these limits, a modification factor of 1.0 and a hypothetical embedment depth $h_{ef}* = h_{ef} - h_{ch}$ must be conservatively assumed in Europe. In the United States, qualification tests may be alternatively carried out in accordance with AC232 [40] for the $0.4 < h_{ch}/h_{ef} \leq 0.5$ and $b_{ch}/h_{ef} \leq 0.7$, which can result in much higher capacity compared to the conservative value in Europe.

The influence of neighboring anchors is taken into account by the modification factor $\Psi_{ch,s,N}$:

$$\Psi_{ch,s,N} = \frac{1}{1 + \sum_{i=1}^{n_{ch,N}} \left[\left(1 - \frac{s_i}{s_{cr,N}} \right)^{1.5} \cdot \frac{N_i}{N_0} \right]} .$$

(2.28)

where:

- N_i – the tension force of an influencing anchor
- N_0 – the tension force of the anchor under consideration
- $n_{ch,N}$ – the number of anchors within the distance $s_{cr,N}$ to both sides of the anchor under consideration
- s_i – the distance between the anchor under consideration and the neighboring anchor
- $s_{cr,N}$ – characteristic anchor spacing

$$s_{cr,N} = 2 \cdot \left(2.8 - 1.3 \frac{h_{ef}}{180} \right) \cdot h_{ef} \geq 3 h_{ef} \quad [\text{mm}].$$

(2.29)

The influence of an edge on the characteristic resistance is taken into account by the modification factor $\Psi_{ch,e,N}$ as follows:

$$\Psi_{ch,e,N} = \left(\frac{c_1}{c_{cr,N}}\right)^{0.5} \leq 1.0 , \tag{2.30}$$

where c_1 is the edge distance and $c_{cr,N}$ is the characteristic edge distance, which is assumed to be half the characteristic anchor spacing $s_{cr,N}$. If an anchor channel is located in a narrow member with two edge distances, the minimum value shall be inserted in Equation (2.32).

Similar expression is valid for the influence of a corner:

$$\Psi_{ch,c,N} = \left(\frac{c_2}{c_{cr,N}}\right)^{0.5} \leq 1.0 , \tag{2.31}$$

where c_2 is the corner distance of the anchor under consideration. If an anchor channel is influenced by two corners, the factor $\Psi_{ch,c,N}$ should be calculated for both corner distances and the product of the obtained values should be inserted in Equation (2.26).

The shell spalling factor $\Psi_{re,N}$ takes into account the effect of a dense reinforcement for embedment depths $h_{ef} \leq 100$ mm.

2.3.1.2 Concrete splitting due to loading

Currently, the design rules for concrete splitting failure of anchor channels differ significantly between Europe (EN 1992-4 [26]) and the United States (ACI 318 [39] with AC232 [40]). In the United States, the verification of concrete splitting failure is included in the concrete breakout verification by means of an additional factor:

$$\Psi_{cp,N} = max\left(\frac{c_{a,min}}{c_{ac}}; \frac{c_{cr,N}}{c_{ac}}\right) \; if \; c_{a,min} \leq c_{ac} , \tag{2.32}$$

where c_{ac} represents the edge distance required to develop full concrete capacity in absence of anchor reinforcement and $c_{cr,N}$ is the characteristic (critical) edge distance for concrete breakout failure. It should be noted that the influence of member thickness is not taken into account.

On the other hand, even if still based on the basic concrete breakout capacity and a similar equation, concrete splitting failure is treated as a distinct failure mode in Europe. According to EN 1992-4 [26], the characteristic resistance of an anchor channel

in case of concrete splitting failure shall be calculated according to the following equation:

$$N_{Rk,sp} = N_{Rk}^0 \cdot \Psi_{ch,s,N} \cdot \Psi_{ch,c,N} \cdot \Psi_{ch,e,N} \cdot \Psi_{re,N} \cdot \Psi_{h,sp} \ [N], \tag{2.33}$$

where the factor $N^0{}_{Rk}$ is the minimum of basic characteristic concrete breakout resistance and characteristic pull-out resistance:

$$N_{Rk}^0 = min\left(N_{Rk,c}^0, N_{Rk,p}\right) \ [N]. \tag{2.34}$$

Modification factors $\Psi_{ch,s,N}$, $\Psi_{ch,c,N}$, $\Psi_{ch,e,N}$, and $\Psi_{re,N}$ in Equation (2.26) should be calculated according to the provisions for concrete breakout failure. However, the characteristic edge distance $c_{cr,N}$ and spacing $s_{cr,N}$ shall be replaced by $c_{cr,sp}$ and $s_{cr,sp}$, respectively. The influence of edge distance should be therefore calculated according to the following equation:

$$\Psi_{ch,e,N} = \left(\frac{c}{c_{cr,sp}}\right)^{1/2} \le 1.0 \ . \tag{2.35}$$

The characteristic edge distance in the case of splitting under load $c_{cr,sp}$ is given in relevant ETA, whereas the characteristic spacing $s_{cr,sp}$ is defined as twice the value of characteristic edge distance for splitting. Although for most fastening systems the characteristic edge distance for splitting $c_{cr,sp}$ should be derived from qualification tests, this is not the case for anchor channels. Indeed, this value should be taken as $3h_{ef}$, i.e. no tests are required [40], [38]. An additional factor $\Psi_{h,sp}$ takes into account the influence of member thickness and is computed as follows:

$$\Psi_{h,sp} = \left(\frac{h}{h_{min}}\right)^{2/3} \le max\left\{1; \left(\frac{h_{ef} + c_{cr,N}}{h_{min}}\right)^{2/3}\right\} \le 2.0 \ , \tag{2.36}$$

where h is the actual member thickness, h_{ef} stands for the effective embedment depth and h_{min} corresponds to the minimum slab thickness allowable by the manufacturer (generally close to the value of h_{ef} [40]). From the upper limitation for $\Psi_{h,sp}$ of 2.0 a characteristic member thickness of $2.83h_{min}$ can be calculated. Moreover, no verification is required if (according to EN 1992-4 [26]):

- The edge distance in all directions is $c \ge 1.2c_{cr,sp}$, and the member thickness is $h \ge h_{min}$ with h_{min} corresponding to $c_{cr,sp}$.

- The characteristic resistances for concrete breakout failure and pull out failure are calculated for cracked concrete and reinforcement resists the splitting forces and limits the crack width to $w_k \leq 0.3$ mm.

2.3.2 Design rules – shear load

2.3.2.1 Concrete edge breakout

The characteristic resistance of one anchor loaded perpendicular to the edge can be calculated according to the following equation:

$$V_{Rk,c} = V_{Rk,c}^0 \cdot \Psi_{ch,s,V} \cdot \Psi_{ch,c,V} \cdot \Psi_{ch,h,V} \cdot \Psi_{ch,90°,V} \cdot \Psi_{re,V} \quad [N]. \tag{2.37}$$

The basic characteristic resistance $V^0{}_{Rk,c}$ of a single anchor not influenced by neighboring anchor, member thickness or corner effects can be obtained as follows:

$$V_{Rk,c}^0 = k_{12} \cdot \sqrt{f_{ck}} \cdot c_1^{4/3} \quad [N]. \tag{2.38}$$

The factor $k_1 = k_{cr,N}$ for cracked concrete and $k_1 = k_{ucr,N}$ for un-cracked concrete. These factors are obtained by qualification tests and are given in the corresponding ETA. In fact, these factors account for the influence of the geometry of anchor channels (e.g., height and width of the channel, embedment depth, anchor diameter, etc.). The maximum value of the factor $k_{cr,N}$ in the qualification guidelines is limited to 7.5, which tends to be conservative for medium and larger anchor channels [41]. If qualification tests are omitted, a significantly lower default values of 4.5 in Europe and 4.0 in the United States should be specified. This represents the only difference between the qualification guidelines in Europe and the United States for shear load.

The influence of neighboring anchors is taken into account by the modification factor $\Psi_{ch,s,N}$ with an identical expression as for the concrete cone breakout:

$$\Psi_{ch,s,N} = \cfrac{1}{1 + \sum_{i=1}^{n_{ch,V}} \left[\left(1 - \cfrac{s_i}{s_{cr,N}} \right)^{1.5} \cdot \cfrac{V_i}{V_0} \right]}, \tag{2.39}$$

where:

- V_i – the shear force of an influencing anchor
- V_0 – the shear force of the anchor under consideration

- $n_{ch,V}$ – the number of anchors within the distance $s_{cr,V}$ to both sides of the anchor under consideration

- s_i – the distance between the anchor under consideration and the neighboring anchor

- $s_{cr,V}$ – characteristic anchor spacing

$$s_{cr,V} = 4c_1 + 2b_{ch} \quad [\text{mm}]. \tag{2.40}$$

The influence of a corner on the characteristic resistance is taken into account by the modification factor $\Psi_{ch,c,V}$ as follows:

$$\Psi_{ch,c,V} = \left(\frac{c_2}{c_{cr,V}}\right)^{0.5} \leq 1.0, \tag{2.41}$$

where c_2 is the corner distance of the considered anchor. If an anchor channel is influenced by two corners, the factor $\Psi_{ch,c,V}$ should be calculated for each corner and the product should be inserted in Equation (2.37).

The influence of member thickness is taken into account by the factor $\Psi_{ch,h,V}$:

$$\Psi_{ch,h,V} = \left(\frac{h}{h_{cr,V}}\right)^{0.5} \leq 1.0, \tag{2.42}$$

where the characteristic member thickness $h_{cr,V}$ should be calculated according to the following expression:

$$h_{cr,V} = 2c_1 + 2h_{ch} \quad [\text{mm}]. \tag{2.43}$$

The influence of shear loads acting parallel to the edge is considered by the modification factor $\Psi_{ch,90°,V}$ with a constant value of 2.5.

The modification factor $\Psi_{re,V}$ considers the type of reinforcement located on the edge:

- $\Psi_{re,V} = 1.0$ for anchor channels in cracked concrete without edge reinforcement or stirrups in both cracked and un-cracked concrete

- $\Psi_{re,V} = 1.4$ for anchor channels in cracked concrete with edge reinforcement and closely spaced stirrups or wire mesh with a spacing $a \leq 100$ mm and $a \leq 2c_1$

Therefore, in case the concrete is properly reinforced, it is assumed that the capacity in cracked concrete can be increased up to the level of un-cracked concrete [42]. No

precise prescriptions on the geometry and the diameter of the reinforcement are given. In addition, according to AC232 [40], the positive influence of longitudinal (edge) reinforcement placed between the anchor channel and the edge can be taken into account by a factor of 1.2. This is the only difference between the design codes in Europe and the United States for this particular failure mode, although this option was provided in the previous EOTA TR 047 [43].

3

FE MODELLING AND EXPERIMENTAL VALIDATION

3.1 FE code MASA

The finite elements analysis of anchor channels was performed with the 3D finite element (FE) code MASA [5]. The FE code is primarily intended for 2D and 3D nonlinear analysis of structures made of quasi-brittle materials such as concrete, although different materials can be simulated with minor modifications (e.g., steel [44], wood [45]). The main feature of this code is the microplane constitutive model, which was presented by Taylor [46] and later extended for modeling of materials that exhibit softening [47], [48], [49]. This material model is formulated in the framework of the macroscopic models, although the tensorial invariance restrictions need not be directly enforced like in phenomenological models for concrete (e.g., plasticity models or damage models). Cracking and damage are modeled in the framework of the smeared crack approach. When the smeared crack approach is used in the local analysis of quasi-brittle materials, a regularization technique should be employed to prevent mesh-dependent results. The specific energy consumption will be dependent on the size of the finite elements because the localization of strains takes place in a row of finite elements. The crack band method [6], one of the simplest regularization techniques, is

employed in the code. More advanced techniques (e.g., nonlocal formulations of the integral or gradient type) can be also employed, but these methods require fine discretization and are therefore computationally demanding for practical applications.

The analysis is performed incrementally, whereby the most effective solution strategy for practical applications appears to be the secant stiffness method. This method forms a tangent stiffness matrix at the start of the analysis and updates the matrix after 25 iterations. Therefore, this strategy is a compromise between constant stiffness and tangent stiffness strategy. For the model preparation (pre-processing) and the evaluation of the numerical results (post-processing), the commercial program FEMAP [50] was used.

3.1.1 Microplane constitutive model for concrete

In the microplane model, the macroscopic response is obtained based on monitoring stresses and strains in different predefined directions (microplanes of various orientations). These microplanes can be thought of as weak planes in the microstructure, such as the contact layers between aggregates in concrete. To provide a unique solution for the softening materials, microplane strains are assumed to be projections of the macroscopic strain tensor ε_{ij} (kinematic constraint) [47].

On the microplane, normal (σ_N, ε_N) and two shear stress-strain components (σ_M, σ_K, ε_M, ε_K) are considered, as shown in Figure 3.1. To realistically model concrete, the normal microplane stress and strain components are decomposed into volumetric and deviatoric parts ($\sigma_N = \sigma_V + \sigma_D$, $\varepsilon_N = \varepsilon_V + \varepsilon_D$). Unlike most microplane formulations for the concrete, kinematic constraint is relaxed to prevent unrealistic model response for dominant tension load and to prevent stress locking phenomena.

Based on the micro-macro work conjugacy of volumetric-deviatoric split and using in advance defined microplane stress-strain constitutive laws (exponential functions), the macroscopic stress tensor is calculated as an integral over unit radius sphere:

$$\sigma_{ij} = \sigma_V \delta_{ij} + \frac{3}{2\pi} \int_S \left[\sigma_D \left(n_i n_j - \frac{\delta_{ij}}{3} \right) + \frac{\sigma_K}{2} \left(k_i n_j + k_j n_i \right) + \frac{\sigma_M}{2} \left(m_i n_j + m_j n_i \right) \right] dS, \qquad (3.1)$$

where S denotes the surface of the unit radius sphere, δ_{ij} is Kronecker delta operator, n_i is unit normal vector component, and k_i and m_i are directions of shear microplane components. The integration is carried out numerically considering 21 microplanes, which was found as a good balance between the accuracy and computational time (see Figure 3.1).
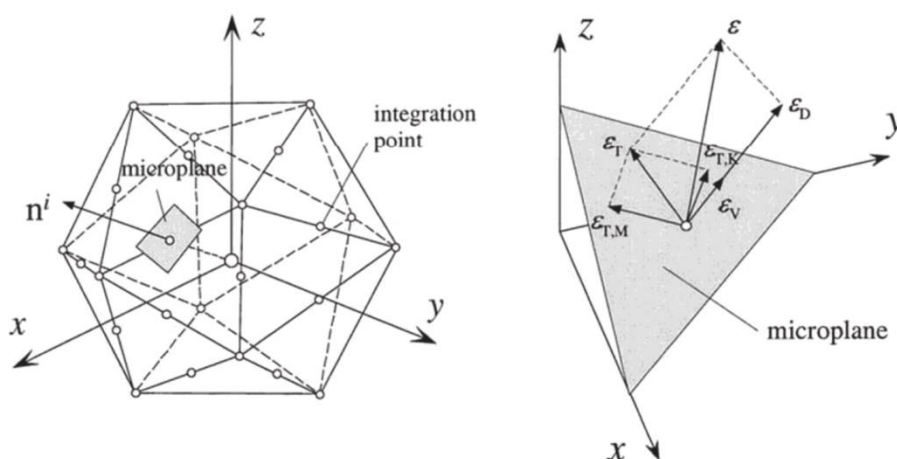
Figure 3.1 Concept of microplane model: spatial discretization of the unit volume sphere by 21 integration points and decomposition of the macroscopic strain vector into microplane normal (i.e., volumetric and deviatoric) and shear strain [5]

The input parameters of the model are macroscopic properties of concrete: Young's modulus, Poisson's number, uniaxial compressive and tensile strengths, fracture energy and element size. Based on these parameters the optimization algorithm is used, which calculates internal microplane parameters that correspond to known (input) macroscopic properties of concrete. For more detail and discussion on the various aspects of the microplane model presented, see [5].

3.1.2 Regularization technique

The crack band method basically assumes that damage (crack) is localized in a row of finite elements. The influence of the element size is eliminated based on the fact that the post-peak (softening) response of the constitutive law (e.g. tension) depends on the fracture energy and the size of the element. The larger the element, the more brittle the

material response should be, so that the specific energy consumption remains constant:

$$G_f = A_f \cdot l_c = \text{constant},$$ (3.2)

where A_f is the area under the uniaxial tensile stress-strain curve and l_c is the crack band width. For the 3D solid elements, the band width is assumed based on the volume of the finite elements, i.e., for the hexahedral elements the band width will be:

$$l_c = \sqrt[3]{V}.$$ (3.3)

Of course, the approach has some limitations, e.g., mesh alignment, extremely small or large elements, or distorted elements can cause difficulties, and the strain localization is then not properly regularized. However, the mesh sensitivity can be minimized if one accounts for these drawbacks. For more detail related to the drawbacks of the crack band method see [51], [52]. It is also worth mentioning that the approach can be enhanced by employing more sophisticated methods to evaluate band width, such as the projection method or the method proposed by Oliver [53]. However, in a number of numerical studies, it has been shown that the above described microplane model together with the crack band approach is able to realistically model cracking of concrete and reinforced concrete structures, e.g. [54], [55], [56].

3.2 Experimental validation

The experimental program summarized in Table 3.1 was conducted as the basis for the validation of the FE simulations. The program consisted of three configurations subjected to shear load and two configurations subjected to tension load. In case of shear load, reference tests were performed in a thick un-cracked plain concrete slab ($h = 300$ mm) where the shear capacity was not affected by the influence of member thickness. Additionally, anchor channels were tested in plain concrete slabs and composite slabs with the same overall thickness of 130 mm to provide information about the capacity reduction due to the presence of voids (complex geometry). In case

of tension load, the same logic was applied as for shear load, i.e., the tested configurations were intended to validate the numerical models for both plain and composite slabs.

Table 3.1 Experimental program aimed for the validation of FE models

Load	Slab type	h [mm]	c_1 [mm]	n_{test} [-]
	Plain (Reference)	300	100	4
Shear	Plain	130	100	4
	Composite	130	100	4
Tension	Plain (Reference)	130	100	4
	Composite	130	100	4

In composite slabs, anchor channels installed perpendicular to the orientation of the profiled steel decking and symmetrically over the flange were subjected to shear load. On the other hand, anchor channels in perimeter beam (parallel orientation) were subjected to tension, with a distance between the anchors and the steel decking of approximately 70 mm (see Figure 3.2a). A profiled steel decking Cofraplus 60 was selected, which has similar geometry to commonly used products such as Ribdeck S60, Metfloor 60, etc.

The selected thickness of 130 mm is frequent in such floor systems owing to the general tendency to build lighter and cost-effective structures. All slabs had the same width and length of 1300 mm and were made of the same batch of a low strength concrete with the maximum aggregate size of 16 mm (see Table 3.2). Slabs were stored in the laboratory 3 days after casting, kept at room temperature and tested at the age of approximately 50 days. As shown in Figure 3.2b, the reinforcement at the top and bottom of the slabs was used for handling purposes and did not affect the test results. Moreover, it not only prevents the whole slab from splitting but guarantees that the test results are not affected by concrete cracks after the previous tests.
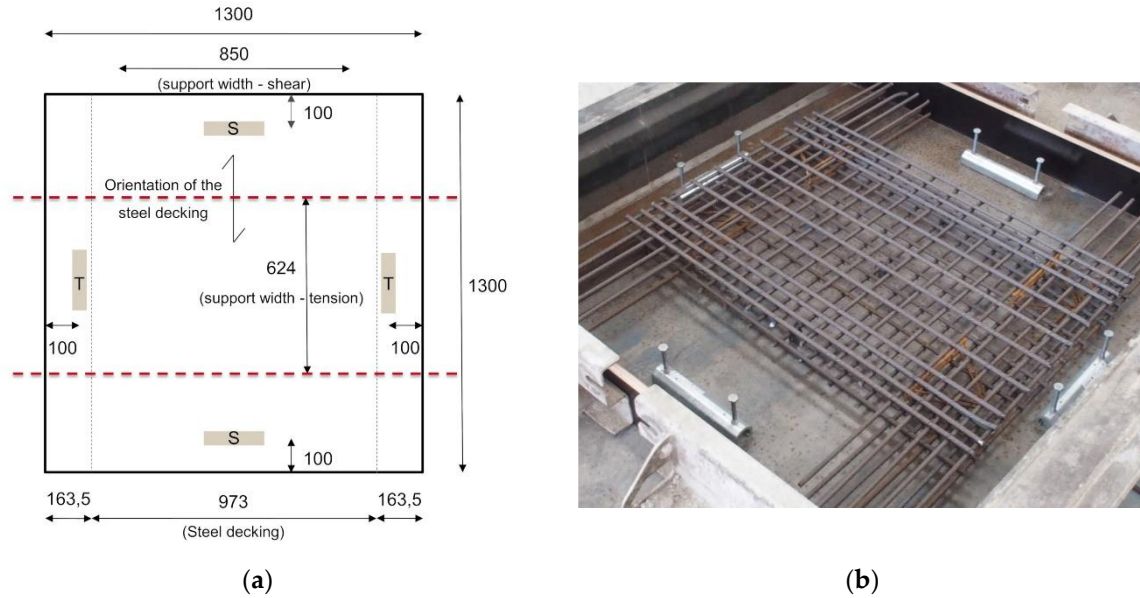
Figure 3.2 (a) Layout of composite slabs in the experimental program (measures in [mm]) (b) Reinforcement arrangement—2 tension and 2 shear tests per slab

Table 3.2 Concrete mix design 1 (crushed aggregate)

Strength class	CEM II/B-M (S-LL) 42.5 N [kg/m³]	Aggregate (D_{max} = 16 mm) [kg/m³]	Water [kg/m³]
C16/20	290	1870	208 (w/c = 0.72)

An anchor channel HAC-60 equipped with two anchors was used for all tests. This anchor channel is geometrically very similar to the HAC-50 used in the numerical simulation and due to the higher steel strength was chosen to avoid steel failures [57]. The original anchors (h_{ef} = 148 mm) were replaced by the shorter anchors (h_{ef} = 106 mm) with equal diameter to enable installation in thin slabs. Based on the dimensions of the selected Cofraplus 60, the anchor spacing of 200 mm was adopted.

The tests were carried out in the laboratory of the Faculty of Civil Engineering in Rijeka, Croatia, using Zwick Roell servo-hydraulic actuators with 250 kN (horizontal actuator) and 500 kN (vertical actuator) load cells. The test setups used for both loading situations are depicted in Figure 3.3. The fixture geometry was manufactured to ensure uniform load distribution on both anchors. The test setups and fixtures complied with the requirements of EAD [38]. The load was applied at a displacement rate of 0.05 mm/s, which was controlled with machine stroke. The displacements were

measured using displacement transducers type LD 320-50 OMEGA. The measurements were sampled with a rate of 100 Hz.

The shear load was applied to two channel bolts (HBC-C M20x80 8.8F) inserted directly over the anchors. To reduce friction, a 1-mm-thick PTFE sheet was placed between fixture, concrete surface, and channel profile. The distance between the support and any loaded anchor should be sufficient ($\geq 2.5c_1$) to enable a complete development of the breakout body. Therefore, the distance of 850 mm was adopted between the supporting beams. The slabs were fastened on the back to the strong floor via steel profile to avoid upward movement during the test.

The same channel bolts placed directly over the anchors were also used for tension tests. In this case, the distance between the anchors and the vertical support was set to $2h_{ef}$ to allow unobstructed formation of the breakout body.

<center>(a)   (b)</center>
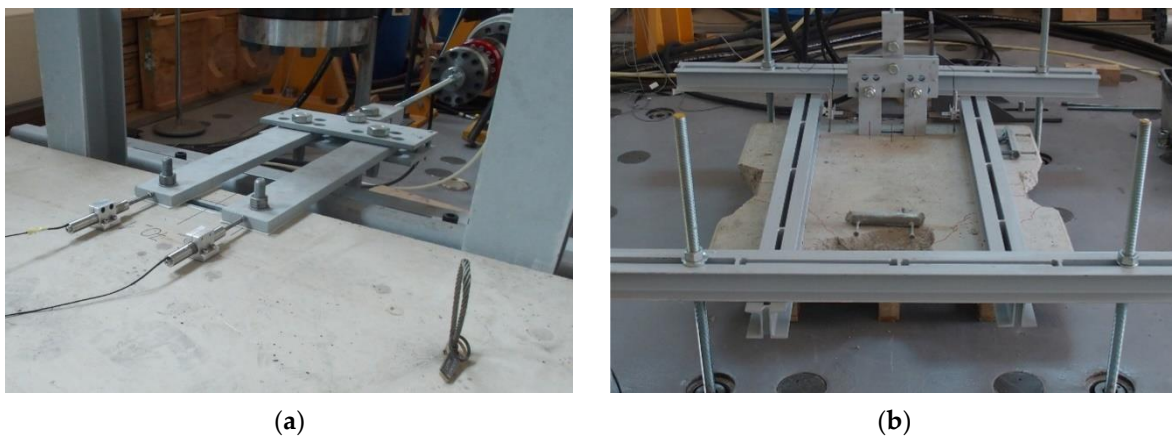
Figure 3.3 Test setups: (a) shear load; (b) tension load

The measured mean cube compressive strength at the time of testing was f_{cc} = 34.62 N/mm² with a corresponding coefficient of variation of CoV = 3.90%, which results in a cylinder strength of f_c = 27.69 N/mm². A total of 5 cubes were tested and stored in the same conditions as the slabs. Six prismatic specimens with a size of 100x100x400 mm were used to determine the fracture energy with the three-point bending test. The specimens were notched in the middle with a depth ratio of 0.5. A mean value of fracture energy of approximately G_f = 55 J/m² (CoV = 4.82%) was derived from the area under the load displacement curve divided by the fractured area [58].

The fracture test was controlled by the high precision displacement transducer Controls 82-P0331/E, which measures the crack mouth opening displacement. To measure vertical displacement of the specimen, the high precision displacement transducer Controls 82-P0331/C was used in combination with the auxiliary testing frame 50-C1200/5. These measured material properties were adopted for the numerical simulations of the experiments.

As the Young's modulus, tensile strength and Poisson's ratio were not experimentally investigated, they were estimated according to CEB-FIP Model Code 90 [59]. However, the tensile strength was slightly increased from the expected value of 2.19 N/mm^2 due to the available results of tension splitting tests carried out for the same concrete mix. Therefore, the following values were used: Young's modulus E_c = 29862 N/mm^2, tensile strength f_t = 2.39 N/mm^2 and Poisson's ratio v_c = 0.18. The behavior of the steel parts of the model was assumed to be linear elastic with a Young's modulus E_s = 210000 N/mm^2 and Poisson's ratio v_s = 0.33, to avoid steel failure prior to concrete edge breakout. In the simulations the load was applied incrementally with a displacement rate of 0.03 mm per increment.

3.2.1 Shear load

The concrete slab was discretized using four-node solid finite elements, whereas anchor channel, channel bolts, steel plate and profiled steel decking were modeled mostly using eight-node elements. The typical FE discretization used in the simulations is illustrated in Figure 3.4. The contact between concrete and steel was modeled using 1D linear contact elements which can take up only compressive forces and in-plane shear forces (friction) [60]. The cross-sectional area of these elements is calculated from the surface of the 3D concrete elements that are connected to the corresponding node of the contact element. The concrete and steel surfaces which are in contact must have the same discretization. Note that the axial (compressive) stiffness of interface elements should be sufficiently high. However, the stiffness should not be too high in order to prevent numerical problems. The stiffness of the

elements was set to 5000 MPa, whereas the friction coefficient of 0.3 was used. However, the friction coefficient has no significant effect on the shear capacity of anchor channels because the applied loads are transferred to the base material mainly through mechanical interlock. These values are based on the calibration of the model and on the values chosen in numerous studies performed with the FE code MASA. It should be noted that stiff connection between the anchor and the channel profile was assumed in the model.

The dimensions of the concrete block were selected such that the boundary conditions and other factors do not influence the shear capacity. The length (x-axis) was based on the edge distance required to allow for an unrestricted breakout body. Therefore, the adopted distance between the anchor and support was $3c_1$. The width (y-axis) should be sufficient to prevent bending of the concrete block, especially for cases with thin members, which could potentially affect the results. Thus, the width was always set larger than $3c_1$.

| (a) | (b) |
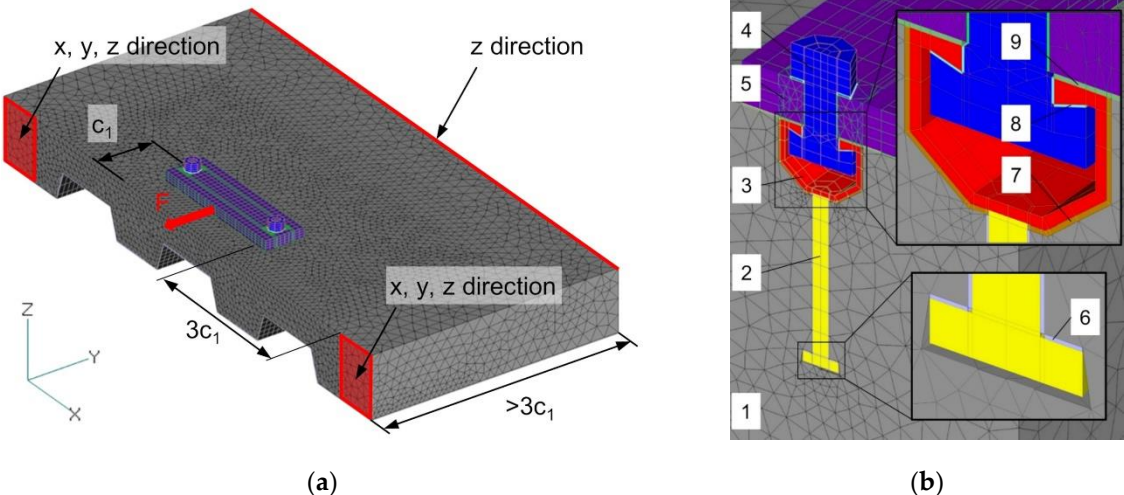
Figure 3.4 (a) Typical FE model with boundary conditions; (b) FE discretization: 1 – concrete slab, 2 – anchor, 3 – channel, 4 – T-bolt with nut, 5 – steel plate, 6 – anchor interface, 7 – channel interface, 8 – T-bolt interface, 9 – PTFE sheet

The boundary conditions were defined through nodal loads and constraints. As shown in Figure 3.4a, nodes on the red surfaces were fixed in all directions, whereas vertical displacements were prevented at the red line on the opposite side of the anchor channel to avoid uplifting of the slab. The anchor channel was loaded at the three

nodes arranged vertically in the middle of the steel plate and simulations were carried out under displacement control. The only difference between the model for composite slabs and the model for plain concrete slabs was the presence of steel decking and the corresponding interface elements with contact bars. The edge trim (or pour stop) of the steel decking in composite slabs was considered as a non-structural element and its contribution was not taken into account.

Table 3.3 summarizes the mean ultimate loads $V_{u,m}$ obtained in the tests, simulation results and their ratios. A correlation between the experiments and the simulations could be observed, i.e., the difference in all three cases is less than 7%.

Table 3.3 Summary of experimental (mean values) and numerical results

Slab type	h [mm]	$V_{u,m}$ [kN]	CoV [%]	$V_{u,m} / V_{u,m,Ref}$ [-]	$V_{u,sim}$ [kN]	$V_{u,m} / V_{u,sim}$ [-]
Plain (Reference)	300	43.47	7.25	1.00	40.50	1.07
Plain	130	29.59	7.80	0.68	28.67	1.03
Composite	130	22.92	8.31	0.53	22.43	1.02

The FE simulations are able to realistically predict not only the ultimate loads, but also the crack pattern. Figure 3.5 shows the comparison between experimentally obtained and numerically predicted crack patterns. The finite elements colored in red correspond to a crack width of approximately 0.1 mm or larger. The influence of complex concrete geometry on the concrete capacity and the influence of member thickness are discussed in detail in chapter 5.1.
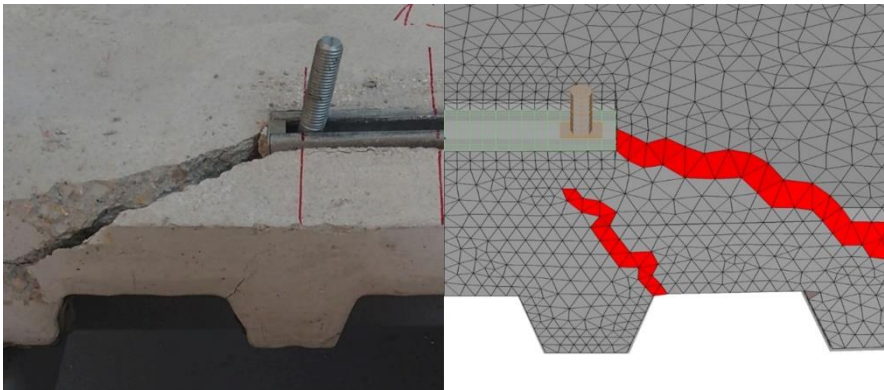
Figure 3.5 Comparison between experimentally and numerically obtained post-peak crack patterns for an anchor channel in composite slab

It is also important to investigate how concrete quality affects the reduction factor due to the presence of the profiled steel decking. Therefore, three concrete qualities (see Table 3.4) were investigated for the 130 mm thick plain and composite slab. The numerical results in Figure 3.6a show that the reduction factor is comparable in all three cases, indicating that the concrete quality has no significant effect. However, it would be useful to investigate this for different cases in the future in more detail, both experimentally and numerically. In addition, a limited parametric study was performed with respect to the material parameters for the plain concrete slab. The macroscopic properties of the medium strength were assumed and the compressive strength, tensile strength and fracture energy were varied separately. The ultimate load is strongly influenced by the tensile strength, while the other parameters have a smaller effect on the load capacity, as shown in Figure 3.6b. These findings are consistent with the similar results for headed anchors [32].

Table 3.4 Macroscopic properties of concrete mixes (mean values)

Abbreviation	f_c [N/mm²]	f_t [N/mm²]	ν [-]	E_c [MPa]	G_f [J/m²]
LS	20	1.57	0.18	27100	50
MS	27.69	2.39	0.18	29862	55
HS	40	3.00	0.18	33350	80

LS – low strength, MS – medium strength, HS – high strength

Furthermore, Figure 3.6a shows the result for the model with considerably larger dimensions of the concrete block than that shown in Figure 3.4 (MS; BC - plain). The dimension of the concrete block behind the channel was doubled and the distance between the anchor and the support was increased to $5c_1$. As can be seen, the load-displacement curve is almost identical to the corresponding configuration in the smaller concrete block, which proves that the dimensions of the concrete block do not affect numerical results.
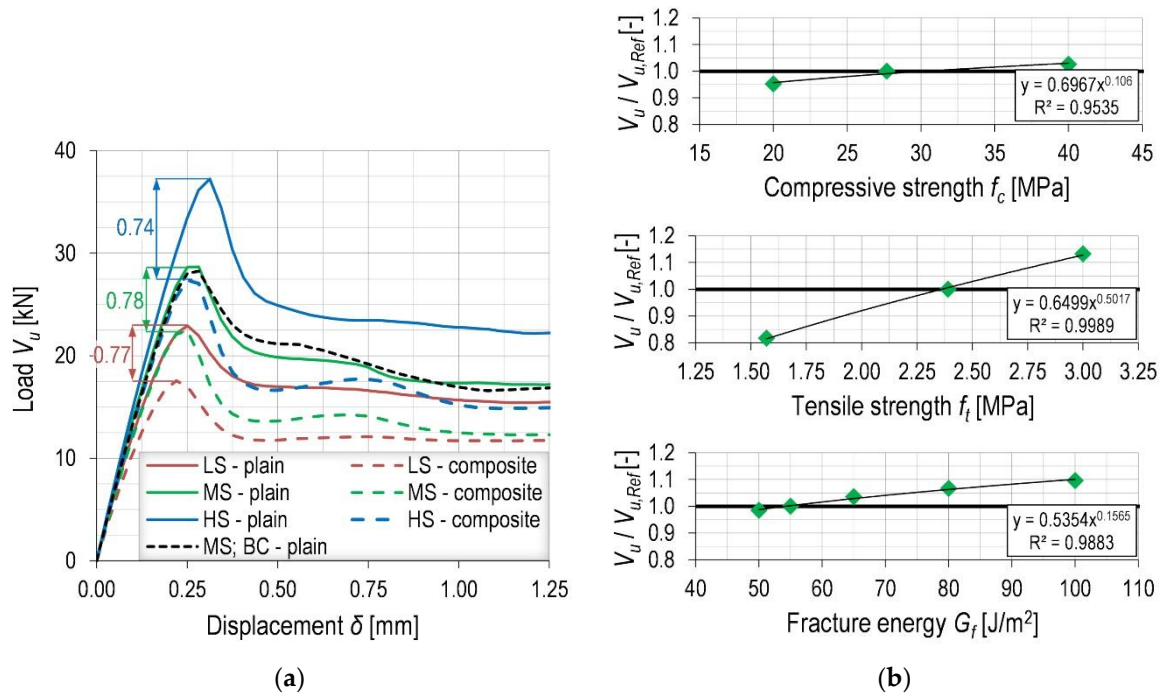
Figure 3.6 (a) Shear capacities for an anchor channel in plain and composite slabs determined for three different concrete mixes and the result for the larger concrete block (MS; BC – plain); (b) Influence of material properties on the ultimate load (reference values: f_c = 27.69 N/mm², f_t = 2.39 N/mm², G_f = 55 J/m²)

To demonstrate the objectivity of the analysis with respect to the FE discretization, the 130 mm thick plain concrete slab was simulated with three different meshes, i.e. fine, medium and coarse. The total number of elements was 100360, 45110 and 15958, respectively. As can be seen from Figure 3.7a, the ultimate loads are almost identical, which is essential for this research. Small differences due to shortcomings of the regularization technique can be observed in the post-peak response. These differences are not very pronounced on either the load-displacement curves or the breakout bodies (see Figure 3.8) and are not relevant for the purpose of the present investigations. In the numerical parametric study, the finite element size was set to approximately 10 mm and gradually increased behind the channel, which would correspond to medium mesh from Figure 3.8.

For comparison, the test results (load-displacement curves) are also shown in Figure 3.7b. In the initial part of the tests, a typical slippage due to the hole clearance can be observed [1]. However, without this disturbance the experimentally measured

stiffness is comparable to the numerical stiffness. Furthermore, in the vast majority of the investigated cases the shape of the load-displacement curves was the same, i.e., with a pronounced peak, after which cracks gradually developed. Therefore, in the following chapters the focus is on the ultimate capacity rather than on the load-displacement curves for anchor channels subjected to shear load. The numerical results of this sensitivity study are summarized in Appendix A.
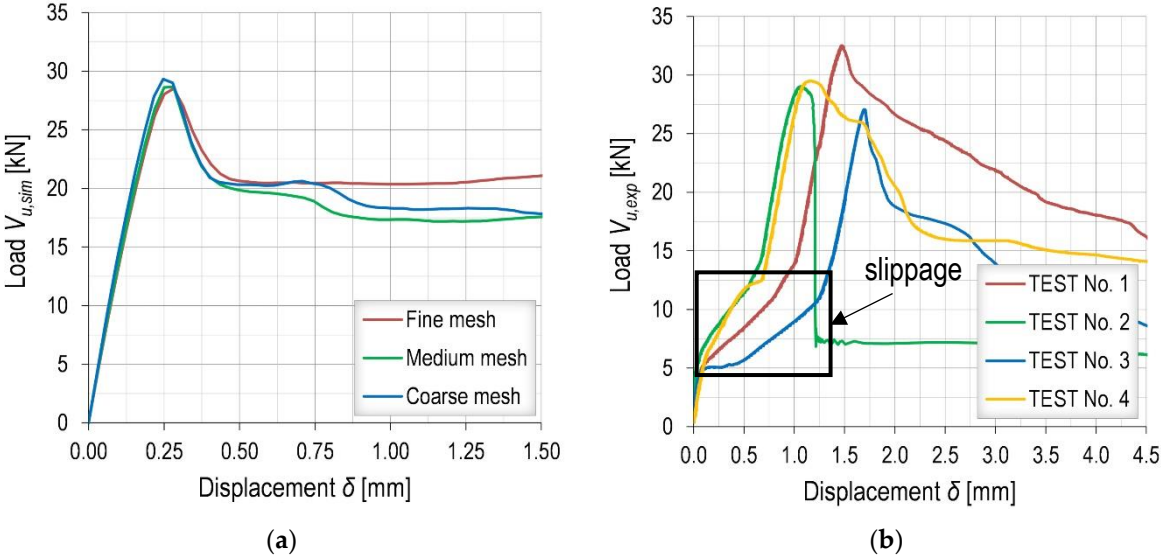
Figure 3.7 Load-displacement curves for HAC-60 in plain concrete slab (h = 130 mm) obtained: (a) numerically for three different meshes; (b) experimentally from 4 tests
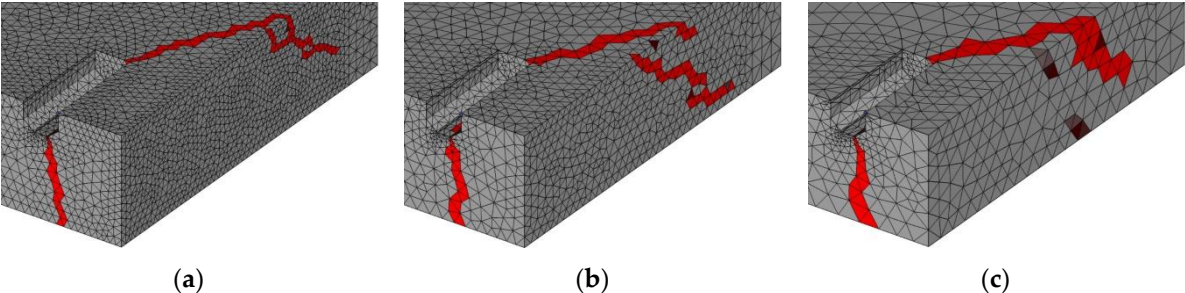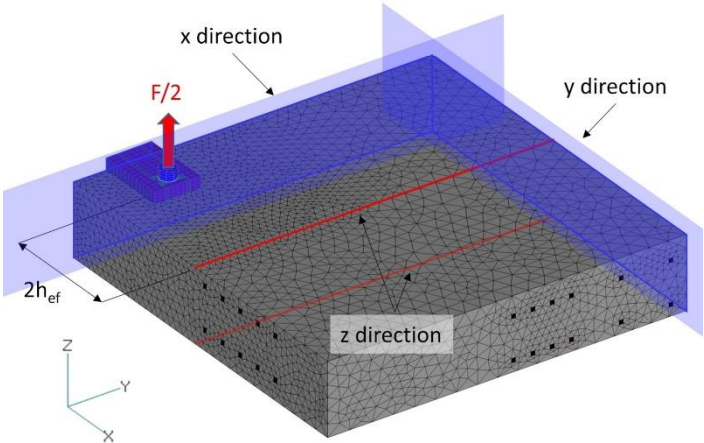

Figure 3.8 Comparison between the obtained breakout patterns for: (a) fine mesh; (b) medium mesh; (c) coarse mesh

3.2.2 Tension load

The numerical model was discretized similar to the model for shear load. Again, steel parts were modeled as linear elastic with a Young's modulus E_s = 210 GPa and Poisson's ratio v_s = 0.33.

The geometry and boundary conditions were taken from the corresponding experiments. The reinforcement was modeled using linear elastic solid finite elements and assuming a perfect bond with concrete. Double symmetry was utilized to reduce the computational cost (Figure 3.9). Experimentally obtained macroscopic concrete parameters were taken in the simulations. The load was applied incrementally with a displacement rate of 0.03 mm per load increment.

Figure 3.9 FE model and boundary conditions.

Table 3.5 shows a comparison between the experimentally obtained mean ultimate loads $N_{u,m}$ and simulation results. The very small discrepancies (less than 6%) indicate that the numerical model is able to realistically predict the ultimate load. Moreover, the experimentally and numerically obtained crack patterns also have comparable shapes, as shown in Figure 3.10, both for the plain concrete slab and composite slab. The finite elements colored in red correspond to a crack width of approximately 0.1 mm or larger.

Table 3.5 Comparison between experimental and numerical results

Slab type	c_1 [mm]	h_{ef} [mm]	h [mm]	$N_{u,m}$ [kN]	σ [kN]	CoV [%]	$N_{u,sim}$ [kN]	$N_{u,sim}/N_{u,m}$ [-]
Plain (Reference)	100	106	130	79.00	0.90	1.14	74.48	0.94
Composite	100	106	130	52.22	2.95	5.66	51.08	0.98
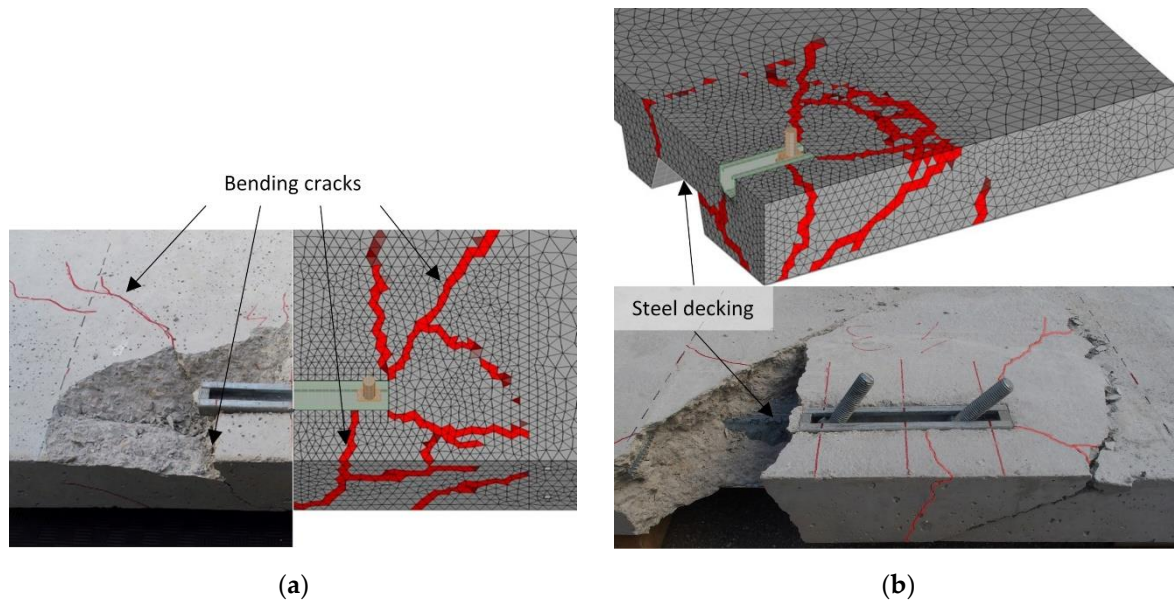
Figure 3.10 Comparison between experimental and numerical breakout patterns for: (a) plain concrete slab; (b) composite slab

To further demonstrate the predictability of the numerical model, additional experiments were simulated, which are discussed in detail in chapter 4.2.4. Anchor channels equipped with short anchors (h_{ef} = 65 mm) were investigated in plain concrete slabs with different thicknesses. For the outcome of this thesis, it is extremely important that the finite element model can reproduce the ultimate loads of such a shallow embedment depth in very thin concrete members. The concrete mix presented in Table 3.2 was used and the obtained mean concrete compressive strength measured on four cores was $f_{c,core}$ = 29.14 N/mm² (f_c = 24.54 N/mm²) with CoV = 6.04. As shown in Table 3.6, the numerical model is quite accurate in terms of peak loads, although the result for very thin members (h = 70 mm) is overestimated by 9%. This can be attributed to the large scatter in the experimental results, which is not surprising for such a shallow embedment depth and member thickness [41].

Numerically and experimentally obtained load-displacement curves are plotted in Figure 3.11. The numerical results replicate the experimental results reasonably well, although a slightly stiffer response can be observed. This effect is already known in the literature [61] and was explained by the local effects, e.g. local crushing of concrete around the anchor head, that cannot be properly accounted for in macroscopic

analyses. However, this discrepancy is not of great importance to the outcome of the investigation. In general, the behavior of anchor channels in thin slabs is strongly influenced by bending stresses. A significant change in stiffness can be observed on the load-displacement curves. This change corresponds to the formation of bending cracks prior to the ultimate load at the positions indicated in Figure 3.10a.

(a)   (b)
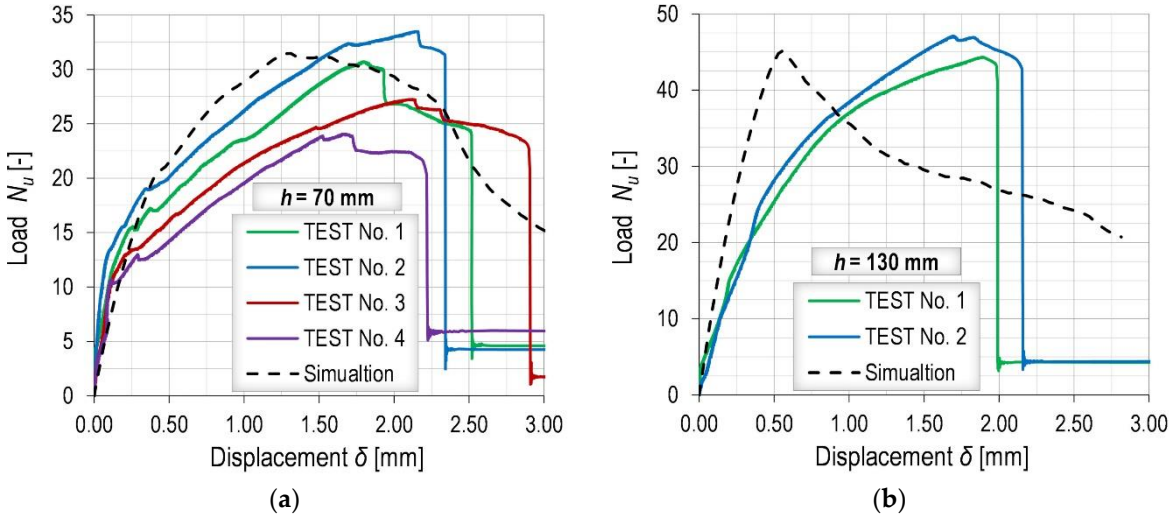
Figure 3.11 Comparison between experimental and numerical LD curves obtained for: (a) member thickness $h = 70$ mm; (b) member thickness $h = 130$ mm

Table 3.6 Comparison between experimental and numerical results – anchor channels with shallow anchors in plain concrete slabs

c_1	h_{ef}	h	$N_{u,m}$	n_{test}	σ	CoV	$N_{u,sim}$	$N_{u,sim}/N_{u,m}$
[mm]	[mm]	[mm]	[kN]	[-]	[kN]	[%]	[kN]	[-]
100	65	70	28.89	4	4.10	14.20	31.46	1.09
100	65	130	45.72	2	1.97	4.31	45.16	0.99

3.3   General information about the numerical parametric studies

Unless otherwise stated, the macroscopic properties of concrete summarized in Table 3.7 were used in all numerical parametric studies. Steel was assumed to be linear elastic with a Young's modulus $E_s = 210000$ N/mm² and Poisson's ratio $v_s = 0.33$, since the failure of concrete was the object of interest. In general, composite slabs are only lightly reinforced with surface mesh reinforcement to control cracking. According to

EN 1994-1-1 [20], the minimum cross-sectional area of the reinforcement should be as follows:

- 0.2% of the cross-sectional area of the concrete above the ribs for unpropped construction.

- 0.4% of the cross-sectional area of the concrete above the ribs for propped construction.

Therefore, the amount of reinforcement usually present in slabs cannot even be considered according to the current code provisions and the influence of reinforcement was not considered in the numerical parametric studies. However, a possible positive influence of surface reinforcement is briefly discussed in chapter 6.2 as an interesting topic for future research.

Table 3.7 Macroscopic properties of concrete in numerical simulations

f_c [N/mm²]	f_t [N/mm²]	ν [-]	E_c [MPa]	G_f [J/m²]
20	1.57	0.18	27100	50

4

ANCHOR CHANNELS IN PLAIN CONCRETE SLABS

4.1 Shear load

4.1.1 Numerical parametric study

In the current code provisions, more precisely Equation (2.43), the characteristic member thickness depends on the edge distance c_1 and the channel height h_{ch}. Therefore, the focus in this part of the study was on the variation of these two parameters, along with the member thickness. As can be seen from the simulation program in Table 4.1, the edge distance $c_1 = 100$ mm was first kept constant and anchor channels with different dimensions were investigated. Three generic channel profiles (small, medium, large) were considered with varying channel height, channel width, anchor diameter and channel wall thickness (Figure 4.1). The investigated channel heights were selected in the range typical for standard products, i.e., between 17 and 48 mm. In all three cases, embedment depths were chosen so that the length of the anchor remained approximately the same (approx. 30 mm). Such shallow embedment depths were selected due to the target of the present research and the general trend in the construction industry to build ever-thinner concrete components.
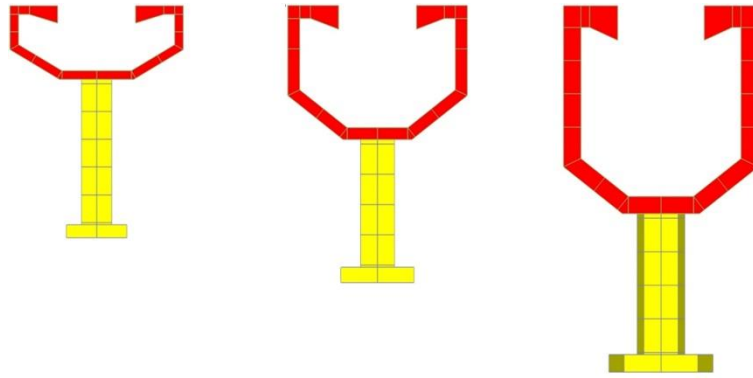
Figure 4.1 Investigated channel profiles (dimensions are given in Table 4.1)

In addition, the influence of member thickness was investigated for larger edge distances of 200 and 300 mm. As shown in Table 4.1, the medium size channel profile was simulated, and the maximum member thicknesses were chosen to exceed the characteristic member thickness according to the current code provisions.

**Table 4.1** Simulation program – influence of member thickness

c_1	h	h_{ch}	b_{ch}	h_{ef}	d	t	s
[mm]	[mm]	[mm]	[mm]	[mm]	[mm]	[mm]	[mm]
100	70, 100, 130, 160, 210, 300	17	40	50	8	2.00	300
100	70, 100, 130, 160, 210, 300	31	42	60	9	2.75	300
100	100, 130, 160, 210, 300, 350	48	45	80	11	4.00	300
200	70, 100, 130, 160, 230, 350, 500	31	42	60	9	2.75	250
300	70, 100, 130, 160, 240, 330, 420, 500, 700	31	42	60	9	2.75	250

4.1.2 Evaluation of numerical results for the influence of member thickness

The numerical results are provided in terms of the factor $\Psi_{ch,h,V}$, defined as the ratio between the ultimate load for the investigated case V_u and the reference capacity of thick concrete member $V_{u,Ref}$. Figure 4.2a shows $\Psi_{ch,h,V}$ for the investigated edge distances as a function of the normalized slab thickness $h/h_{cr,V}$ compared with the current provisions. Comparing the curve for edge distance $c_1 = 100$ mm (green) to the curve representing the code (black), it can be seen that the numerically obtained relative capacities are greater than the code values at a range of approximately $0.5 \leq h/h_{cr,V} \leq 1.0$. However, the numerically obtained factor $\Psi_{ch,h,V}$ has a steeper slope than the black line (current code) for the ratio $h/h_{cr,V} \leq 0.5$. Consequently, the capacity

according to the code may overestimate the actual concrete edge breakout capacity in the case of very thin slabs. The shape of the curves obtained for the edge distances $c_1 = 200$ mm and $c_1 = 300$ mm (in blue and red, respectively), were almost identical to $c_1 = 100$ mm.

The fact that the capacities are underestimated for larger member thicknesses ($0.5 \leq h/h_{cr,V} \leq 1.0$) can be attributed to an overestimation of the characteristic member thickness by the current code provisions. As shown in Figure 4.2a, the factor $\Psi_{ch,h,V}$ remains close to one for $h/h_{cr,V}$ greater than approximately 0.75 for the edge distance $c_1 = 200$ mm and approximately 0.6 for the edge distance $c_1 = 300$ mm. This fact could also be observed from the sizes of the breakout bodies, which were fully developed in members thinner than the characteristic member thicknesses according to the code. As an example, an anchor channel in a member with $h = 420$ mm ($c_1 = 300$ mm) has 96% of the capacity of the thick member ($h = 700$ mm). The failure mode for this configuration is shown in Figure 4.3a, where finite elements colored in red correspond to a crack width of approximately 0.1 mm or larger. The breakout body is almost fully developed, i.e., the crack intersected the bottom surface of the slab very close to the edge. Moreover, the results obtained for limited member thicknesses ranging from 70 to 130 mm are shown in Figure 4.2b in terms of relative capacities $V_u/V_{u,Ref\,(h\,=\,130\,mm)}$, and the trend was very similar for all three investigated edge distances. The relative capacities of anchor channels installed in very thin slabs ($h = 70$ mm) were approximately 55% of the capacities in slabs with a thickness of $h = 130$ mm, whereas the expected value according to the code provisions was 73%. In addition, it can be seen that the capacity changes almost proportionally to the member thickness, although the observation is based on three points. In general, the capacities in very thin members cannot be explained well by the current design model.
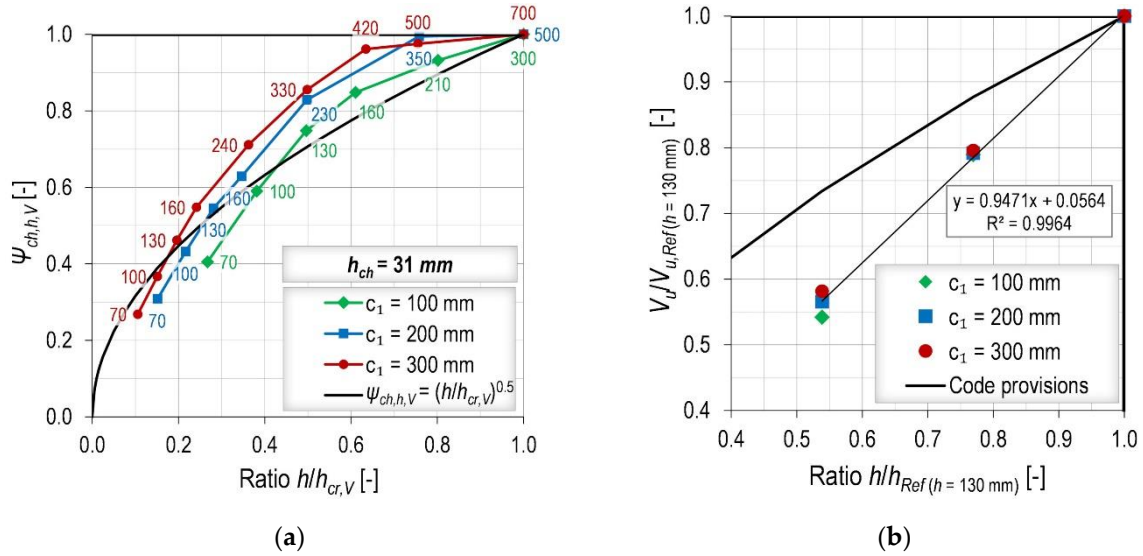
Figure 4.2 (a) Numerically obtained curves of $\Psi_{ch,h,V}$ compared to the current code provisions for different edge distances (data labels represent the member thickness); (b) Capacity reduction for thicknesses less than 130 mm: the trend line based on numerical results showing proportionality between the capacity and member thickness

The results of different channel profiles for the edge distance $c_1 = 100$ mm are shown in Figure 4.3b. The three curves representing the three different channel profiles with different channel heights are almost equivalent, meaning that the influence of the channel profile is accurately accounted for in the expression for the characteristic member thickness by the channel height multiplied by a factor of 2. This influence was not investigated for larger edge distances, since the channel height becomes insignificant compared to the edge distance. As a result, the only way to adjust the characteristic member thickness is the modification of the pre-factor and exponent of the edge distance in Equation (2.43).

The numerical result presented in this chapter are summarized in Appendix B.

(**a**)	(**b**)
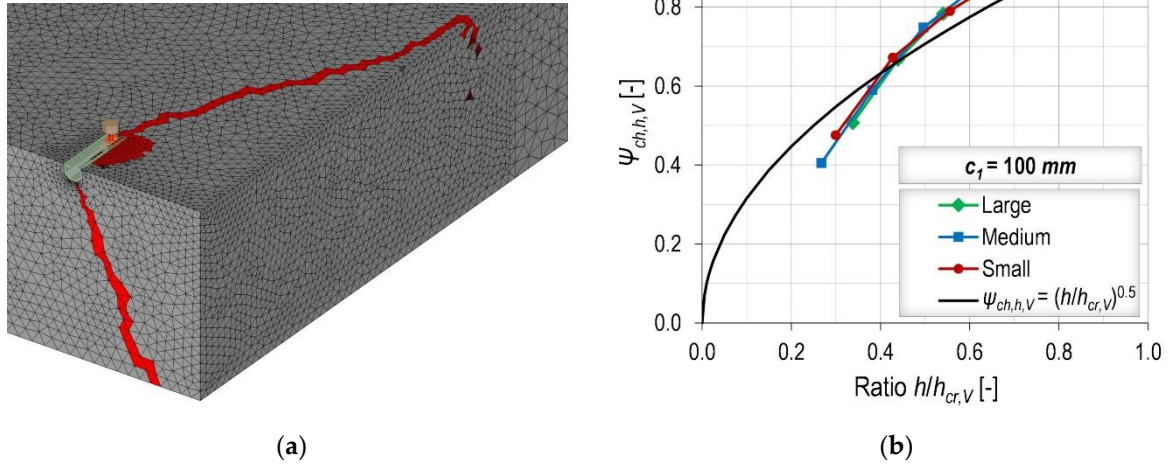
Figure 4.3 (a) Post-peak crack pattern - $h = 420$ mm and $c_1 = 300$ mm; (b) $\Psi_{ch,h,V}$ compared to the current code provisions for different channel profiles

4.1.3   Design modifications for the influence of the slab thickness

Based on the obtained numerical results the following formula for the influence of the slab thickness on the characteristic member thickness is proposed:

$$h_{cr,V} = 8.25c_1^{2/3} + 2h_{ch}\,. \tag{4.1}$$

In the current code, the edge distance is considered to be proportional to the characteristic member thickness, however, according to the numerical results the influence of edge distance is smaller and could be better represented with an exponent of 2/3 and an additional constant factor. This modification allows a more accurate prediction of the characteristic value, especially for larger edge distances.

To solve the problem of overestimated capacities for very thin members, the current expression in Equation (2.42) applies in the range $0.5 < h/h_{cr,V} \leq 1.0$, while for the smaller $h/h_{cr,V}$ ratios a linear reduction should be considered:

$$
\begin{aligned}
\Psi_{ch,h,V} &= \left(\frac{h}{h_{cr,V}}\right)^{0.5} \leq 1.0 \quad && \text{if } \frac{h}{h_{cr,V}} > 0.5 \\[2mm]
\Psi_{ch,h,V} &= \sqrt{2}\,\frac{h}{h_{cr,V}} && \text{if } \frac{h}{h_{cr,V}} \leq 0.5\,.
\end{aligned}
\tag{4.2}
$$

As can be seen from Figure 4.4, the proposed modifications improve the accuracy of the prediction. Namely, the average simulation-to-prediction ratio is 1.01 with a standard deviation of 0.04 as opposed to the current model with a standard deviation of 0.11. In general, this method increases the complexity of the current model, however, it is not possible to improve the accuracy by simply changing the exponent.

(a)   (b)
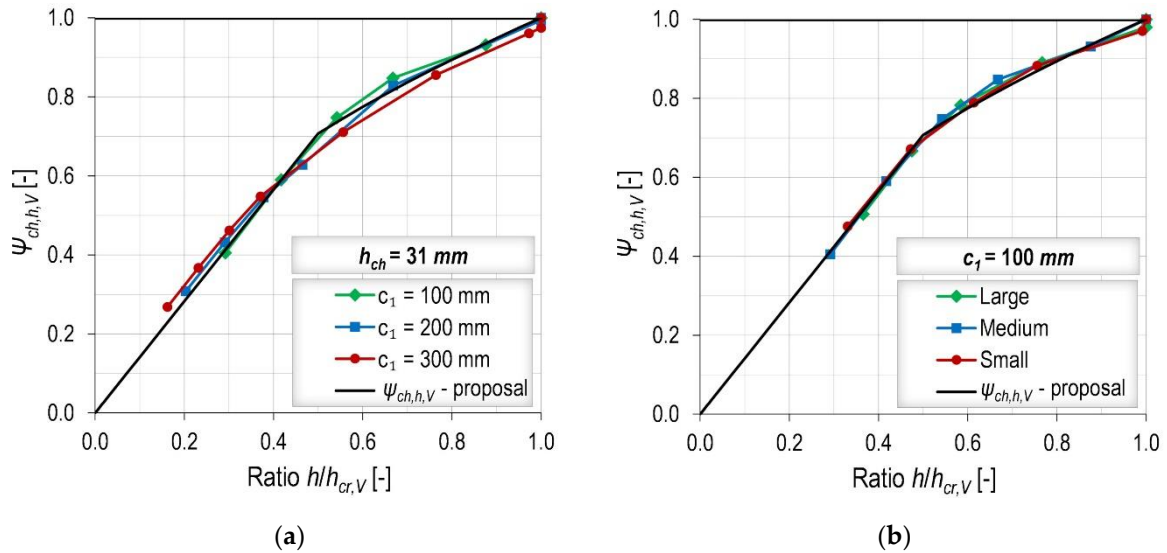
Figure 4.4 Numerical results compared to the modified design proposal for: (a) different edge distances; (b) different channel profiles

4.1.4   Experimental results

Once the analytical expressions were derived, additional experiments were performed to validate the proposed modification factors that consider the influence of member thickness and installation in pockets. All experiments were conducted in accordance with the anchor channel EAD 330008-03-0601 [38], which means that the same procedure as explained in chapter 3.2.1 was followed. The measured ultimate loads are normalized to the concrete cylinder compressive strength $f_c = 20$ MPa using the well-known expression based on the square root of the compressive strength [1], to allow direct comparison.

First, unreinforced concrete slabs with anchor channels at the edge distance $c_1 = 100$ mm were produced with 3 different thicknesses, $h = 70$, 100 and 130 mm. The main purpose was to investigate the influence of member thickness for cases with thin

slabs. A medium size anchor channel (HAC-60) with anchor spacing $s = 200$ mm and embedment depth $h_{ef} = 65$ mm was used. Due to very limited thicknesses, the width and the length of the slabs were set to 1700 mm to prevent splitting. Four tests were conducted for each slab thickness, and the concrete mix specified in Table 3.2 was used. The slabs were tested approximately 90 days after casting and stored in the laboratory at room temperature. The cored cylinders (100x100 mm) were taken out from slabs and the obtained concrete compressive strength was $f_{c,core} = 29.14$ N/mm² ($n = 4$; $CoV = 6.04\%$), resulting in a cylinder compressive strength of $f_c = 24.54$ N/mm².

Table 4.2 summarizes the results and compares them to the current code provisions. Per the table, the experimental results for the member thickness $h = 130$ mm are in excellent agreement with the capacities calculated according to the code provisions. This is consistent with the previous experimental investigations for the same edge distance in this work and in the literature [62]. In chapter 3.2.1, a ratio between the thin ($h = 130$ mm) and thick member ($h = 300$ mm) of 0.68 was observed, whereas the expected value according to the current codes was 0.69. Furthermore, Bede et al. [62] also proved the effectiveness of the current factor for the larger ratio $h/h_{cr,V}$ of 0.76 with the obtained reduction of approximately 15%. However, with decreasing member thickness the code provisions tend to overestimate the concrete edge breakout capacity. A considerable difference between the experimentally obtained and calculated capacity can be observed for the member thickness $h = 70$ mm, where the obtained maximum load was only 69% of the capacity according to the current code provisions. The discrepancy between the test results and code provisions can be explained by the fact that the behavior of anchor channel has not been investigated in detail for such thin members and therefore it is not considered properly in the current code provisions. For example, the vast majority of numerical and experimental results in [9] were obtained for concrete members thicker than 120 mm.

As it can be observed from Table 4.2, the design with the proposed modifications performs better than the code when it comes to thin concrete members, with the ratios

$V_{u,m}/V_{u,proposal}$ closer to 1.0 than the $V_{u,m}/V_{u,code}$. In the case of thin slabs ($h = 70$ mm), the ratio $V_{u,m}/V_{u,proposal}$ of 0.88 can probably be attributed to the larger scatter of the test results, whereas the results for thicker members are in excellent agreement. In general, Figure 4.5a, where the test results are compared with the proposal and the current code provisions, shows that a linear reduction for the ratio $h/h_{cr,V} \leq 0.5$ would be ideal in order to correctly predict the influence of member thickness.

(a)   (b)
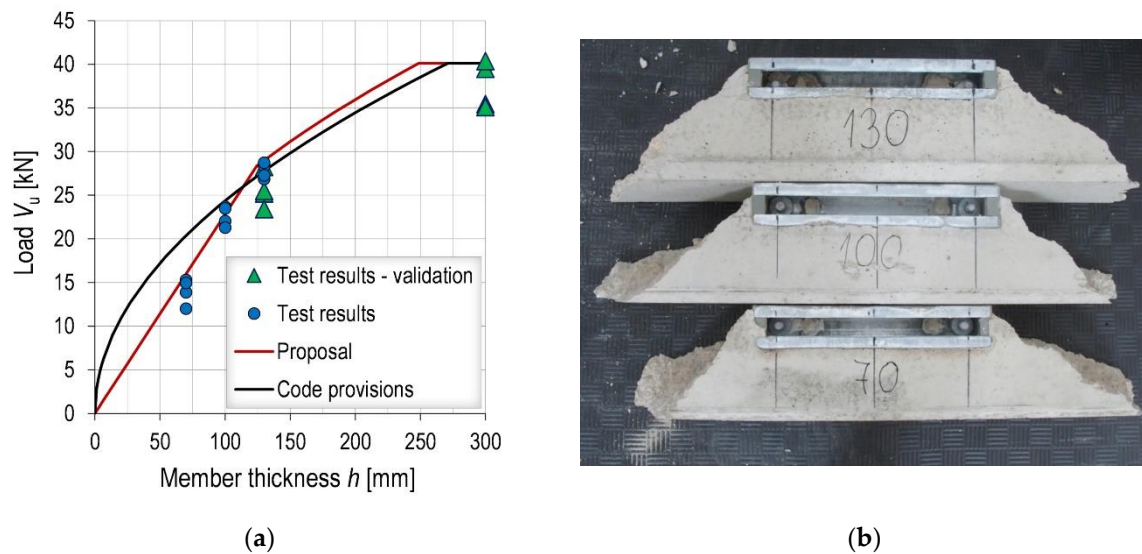
Figure 4.5 (a) Test results compared with the proposal and the current code provisions; (b) Top view of the breakout bodies for investigated member thicknesses (from above) of 130, 100 and 70 mm

Table 4.2 Test results compared with the proposal and the current code provisions ($f_c = 20$ N/mm²)

| h | $V_{u,m}$ | σ | CoV | $V_{u,proposal}$ | $V_{u,m}/V_{u,proposal}$ | $V_{u,code}$ | $V_{u,m}/V_{u,code}$ |
[mm]	[kN]	[kN]	[%]	[kN]	[-]	[kN]	[-]
130	27.80	0.98	3.17	28.99	0.96	27.72	1.00
100	22.62	1.28	5.09	22.75	0.99	24.31	0.93
70	14.03	1.65	10.63	15.93	0.88	20.34	0.69

As the member thickness decreases, the failure surface changes its inclination and for a certain member thickness the crack develops perpendicular to the lower surface of the slab. Such a behavior has also been observed for headed anchors subjected to shear load [32]. The failure surface was already vertical for the member thickness $h = 130$ mm. Looking at the breakout bodies for the investigated member thicknesses from

above, the dimensions are comparable (Figure 4.5b). Therefore, the fracture surfaces only differ in height.

Furthermore, since the proposal for the characteristic member thickness for large edge distances gives smaller values than the current code provisions, an extreme case with $c_1 = 300$ mm was tested at Hilti laboratory in Schaan, Liechtenstein. Namely, a large channel profile (HAC-C 52/34) with an anchor spacing $s = 250$ mm was tested in a concrete member with the thickness $h = 600$ mm, which according to the current code provisions is not sufficient to develop an unrestricted breakout. In this case, the concrete mix from Table 4.3 was used and the slabs were tested one month after casting. A compressive strength of $f_{cc} = 24.55$ N/mm^2 ($f_c = 19.64$ N/mm^2) was obtained on 6 cubes stored under the same conditions as investigated slabs. The mean ultimate load was 171.13 kN ($f_c = 20$ N/mm^2) with a relatively small coefficient of variation of 2.24%.

Table 4.3 Concrete mix design 2 (round aggregate)

Strength class	CEM II B-L 42.5 N [kg/m^3]	Aggregate ($D_{max} = 16$ mm) [kg/m^3]	Water [kg/m^3]
C20/25	350	1858	217 ($w/c = 0.62$)

According to Equation (2.43), the characteristic member thickness should be $h_{cr,V} = 668$ mm for the given parameters. Interestingly, four tests showed fully developed breakout body with heights ranging from 400 to 450 mm, as shown in Figure 4.6. These values are significantly smaller than the calculated characteristic member thickness but are in very good agreement with the numerical results. Using the proposed expression for the characteristic member thickness it was possible to accurately predict the height of the breakout body as:

$$h_{cr,V} = 8.25 \cdot 300^{2/3} + 2 \cdot 34 = 438 \text{ mm.} \tag{4.3}$$
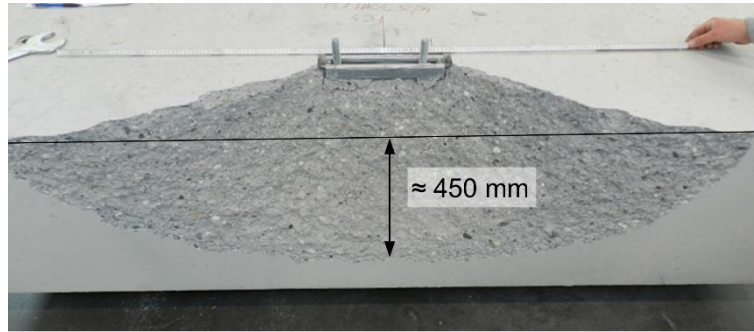
Figure 4.6 Failure surface - $h = 600$ mm and $c_1 = 300$ mm

4.1.5 Concluding remarks

The influence of the member thickness for concrete edge breakout was numerically and experimentally. The importance of this lies in the fact that the correct reference value is needed once more complex topics like composite slabs or pockets are considered. Based on the results, the following can be concluded:

- The current characteristic member thickness for anchor channels is overestimated for large edge distances and leads therefore to conservative resistances. It was found that the edge distance was less than linearly proportional to the characteristic member thickness, so an exponent of 2/3 is suggested. In addition, the influence of channel profile, which is accounted for by the channel height, should be maintained as it is in the expression for the characteristic member thickness.

- The modification factor $\Psi_{ch,h,V}$, which takes into account the influence of member thickness, can lead to overestimated capacities for very thin concrete members. Considering the trend in the construction industry towards slender structures, this issue can be potentially dangerous in practice. Therefore, for ratios $h/h_{cr,V}$ smaller than 0.5, the linear reduction is proposed.

- The proposed modifications of the characteristic member thickness and modification factor $\Psi_{ch,h,V}$ showed considerably better predictability than the current code provisions.

4.2 Tension load

4.2.1 Numerical parametric study

In the numerical parametric study, a slightly different FE model was used than the one used for the verification in chapter 3.2.2, i.e. the boundary conditions were defined so that the model replicates a typical slab for a real-word application, which has significantly larger dimensions than the experimental samples. The edges of the slab were fixed at a certain distance from the anchor (Figure 4.7a). Since bending has a significant effect on the results, the distance between the anchor and the vertical support might affect the behavior and results. However, as shown in Figure 4.7b for two embedment depths, the influence of support spans is not pronounced for distances between 2 and 4 times the embedment depth. For larger values, the bending capacity of the slab is reached before anchorage failure, whereas for smaller values, the formation of the full breakout body is restricted. Double symmetry was utilized for the in-field simulations.
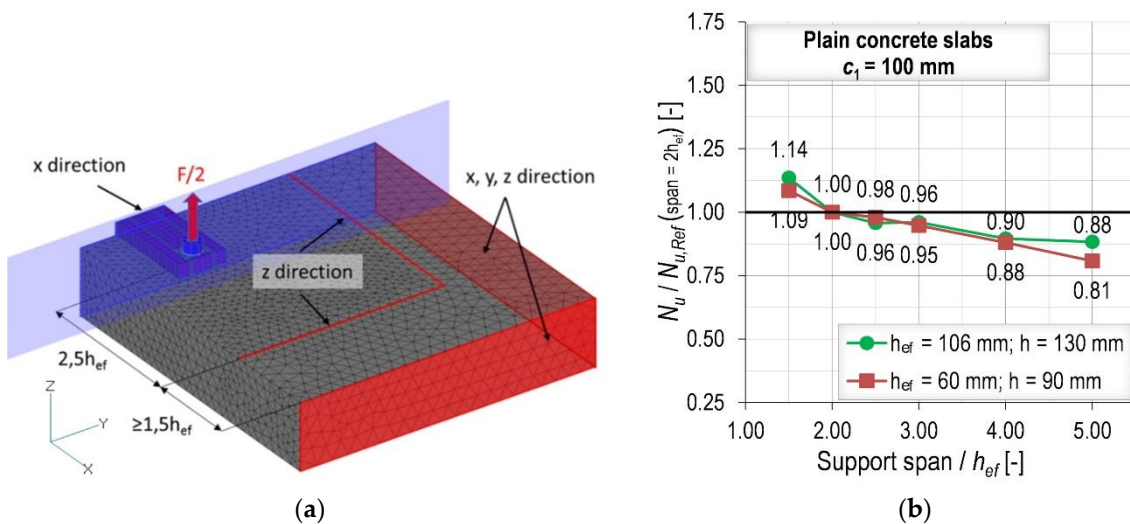
Figure 4.7 (a) FE model used in the numerical parametric study; (b) Influence of support span

The main parameters considered in the parametric study were the member thickness, edge distance and anchor spacing. The simulation program was therefore divided into three parts, each focusing on one of these parameters. In all simulations, a medium size anchor channel commonly used for curtain wall application, the Hilti

HAC-50 anchor channel equipped with two anchors was modeled, varying embedment depth and anchor spacing for the different configurations.

The first part of the program is the one related to the influence of the member thickness. Anchor channels with four embedment depths ranging from h_{ef} = 60 mm to h_{ef} = 175 mm were investigated in plain concrete slabs with different thicknesses. The anchor spacing s = 250 mm was kept constant and in the vast majority of simulations the anchor channel was installed at the edge distance c_1 = 100 mm, which is a common distance in curtain wall applications. To understand the cross correlation with the edge distance, the influence of member thickness was investigated for an additional edge distance c_1 = 200 mm and the embedment depth h_{ef} = 100 mm. Table 4.4 shows the summary of all the performed simulations.

Table 4.4 Simulation program – influence of member thickness

c_1	h_{ef}	h/h_{ef}
[mm]	[mm]	[-]
100	100, 120, 175	1.10
100	60, 100, 120, 175	1.25
100	60, 100, 120, 175	1.50
100	60, 100, 120, 175	1.75
100	60, 100, 120, 175	2.00
100	60, 100	2.50
100	60	3.00
200	100	1.10 – 2.50

In the second part of the program, the influence of edge distance was investigated for three embedment depths h_{ef} = 60, 100 and 175 mm (see Table 4.5), keeping constant the anchor spacing of s = 250 mm. For each embedment depth, two or three different slab thicknesses and several different ratios of edge distance to effective embedment depth c_1/h_{ef} were simulated. As a reference, in-field simulations without the influence of an edge were also performed.

Table 4.5 Simulation program – influence of edge distance

c_1/h_{ef}	h_{ef}	h
[-]	[mm]	[mm]
1.00, 1.67, 2.50, 3.00, 4.00, 6.00, in-field	60	75
1.00, 1.67, 2.50, 3.00, 4.00, in-field	60	130
0.50, 1.00, 1.50, 2.00, 3.00, in-field	100	125
0.50, 1.00, 1.50, 2.00, in-field	100	150
0.50, 1.00, 1.50, 2.00, 3.00, in-field	100	200
0.50, 2.00, in-field	175	193
0.50, 1.50, in-field	175	350

Regarding the third part of the simulation program, the anchor spacing was varied in the range from $s = 100$ mm to $s = 300$ mm, considering different embedment depths. However, for the smallest embedment depth, the anchor spacing was increased up to $s = 840$ mm to get a clear picture of the characteristic spacing (which is much larger than the maximum allowable spacing for common anchor channel systems) and its behavior as a function of member thickness. A summary of the third part of the simulation program is given in Table 4.6.

Table 4.6 Simulation program – influence of anchor spacing

s	c_1	h_{ef}	h
[mm]	[mm]	[mm]	[mm]
150, 200, 250, 300	100	91	130
150, 200, 250, 300	100	106	130
150, 200, 250, 300	100	120	130
100, 200, 250, 300, 500, 720, 840	100	60	75
100, 200, 250, 300, 500	100	60	130
100, 200, 250, 300	100	100	125
100, 200, 250, 300	100	100	200
100, 200, 250, 300	200	100	125

## 4.2.2 Evaluation of numerical results

4.2.2.1 Influence of member thickness

The numerical results shown in Figure 4.8a for the edge distance $c_1 = 100$ mm indicate that as the relative member thickness h/h_{ef} decreases, also the concrete tensile capacity becomes smaller. The effect of the load introduced by a fastener causes larger

bending stresses in thin concrete members, which affect the concrete splitting resistance and load-bearing behavior in general. On the other side, the larger the embedment depth, the smaller the characteristic value of the ratio h/h_{ef} at which the influence of member thickness is not relevant anymore. This observation would be in contrast with the Hüer's findings that the characteristic member thickness should be $h_{cr,cb} = 2.25h_{ef}$ [25]. A possible reason for this difference could be the limited amount of investigated configurations in his work. The current factor $\Psi_{h,sp} = (h/h_{ef})^{2/3}$ of EN 1992-4 [26] is also represented in Figure 4.8a with the dashed curves. It could be observed that the factor provides a reasonably good estimate of the influence of member thickness. Note that in Figure 4.8a the ratio h/h_{ef} (and not h/h_{min}) has been selected as parameter for the horizontal axis, as the h_{ef} is physical dimension and is not selected arbitrarily by the manufacturer as the h_{min}, making it more convenient for comparison purposes.

The numerical results for the edge distances $c_1 = 100$ mm and $c_1 = 200$ mm are shown in Figure 4.8b (only for $h_{ef} = 100$ mm). The capacities without the influence of member thickness were obtained for similar h/h_{ef} ratios for both investigated edge distances. Moreover, the dashed lines in Figure 4.8b also show a comparison with the modification factors from the literature [24], [25], [21] that are introduced in Table 2.1. In all the available design proposals, the exponent related to the ratio h/h_{ef} and the characteristic member thickness indicates the dependence of the ultimate capacity on the slab thickness. The range in which the influence of member thickness becomes relevant is relatively narrow $(1.0 < h/h_{ef} < 2.0)$ and the choice of the appropriate exponent is not of the utmost importance. The choice of the characteristic member thickness appears to be more relevant. While the exponent of 0.5 proposed by Asmus [23] seems to provide a good shape for the modification factor, the characteristic member thickness (see Table 2.1) seems to be too large, especially for the larger edge distances, leading to relative capacities that differ far from the numerical results. In contrast, the proposal of Hüer [25] with the exponent of 1/3 and the exponent of 0.25 introduced by Nilforoush [21] for the in-field installation, although slightly smaller

than the exponents obtained by fitting the numerical results, seem to provide a better estimate due to the smaller characteristic thickness.
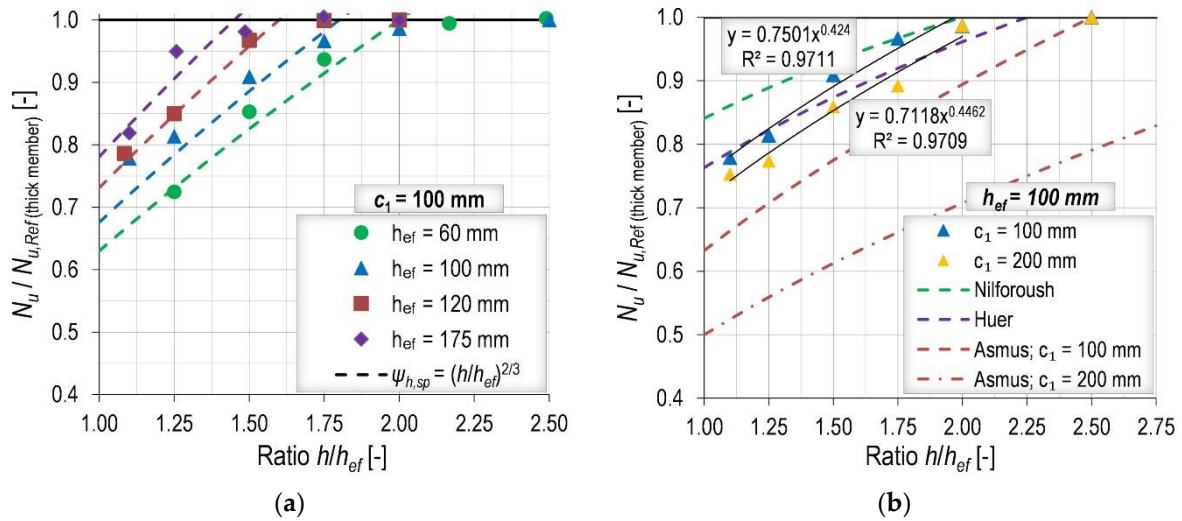
Figure 4.8 Influence of member thickness: (a) relative capacities for different embedment depths; (b) relative capacities compared to the existing design models in the literature

To conclude, the influence of member thickness is considered differently by several authors and the possible reason for this probably lies in the range of the investigated ratios h/h_{ef} ratios and in the choice of boundary conditions. In general, as mentioned above, the current modification factor of EN 1992-4 [26] is sufficiently accurate and its exponent, which is the largest of all the exponents considered, ensures the strongest influence of member thickness.

4.2.2.2 Influence of edge distance

While the influence of edge distance has been extensively studied for the concrete breakout failure mode, experimental and numerical investigations are lacking for concrete splitting. Currently, the characteristic edge distance is set to $3h_{ef}$ in both the USA and Europe. However, the numerical results showed that this distance can be larger than the value of the code provisions for the case of thin members. As an example, it can be observed in Figure 4.9a, that for the embedment depth $h_{ef} = 100$ mm and member thickness $h = 125$ mm, only 80% of the in-field value was obtained for the edge distance of $3h_{ef}$. Figure 6a also shows curves representing the expected reduction

in concrete capacity performing a calculation according to EN 1992-4 [26] and AC232 [40]. Comparing the curves representing the splitting failure with the numerically obtained points, the capacity reduction with decrease of the relative edge distance c_1/h_{ef} in the simulations is less pronounced than that of the current code provisions. In other words, the simulations show larger capacities than those calculated for small edge distances and smaller capacities for larger edge distances.

Considering all the simulation results for small h/h_{ef} ratios, it was found that the influence of the edge distance can be well approximated by a linear function of the relative edge distance c_1/h_{ef} (Figure 4.9b). This linear function becomes equal to one for $c_1 = 6h_{ef}$, which is twice the value of the current characteristic edge distance in the code. The function does not reduce to zero for the theoretical edge distance c_1 equal to zero. This is considered acceptable because very small edge distances ($c_1 < 40$ mm) are excluded due to the qualification procedure and the concrete breakout verification becomes decisive as the edge distance decreases.
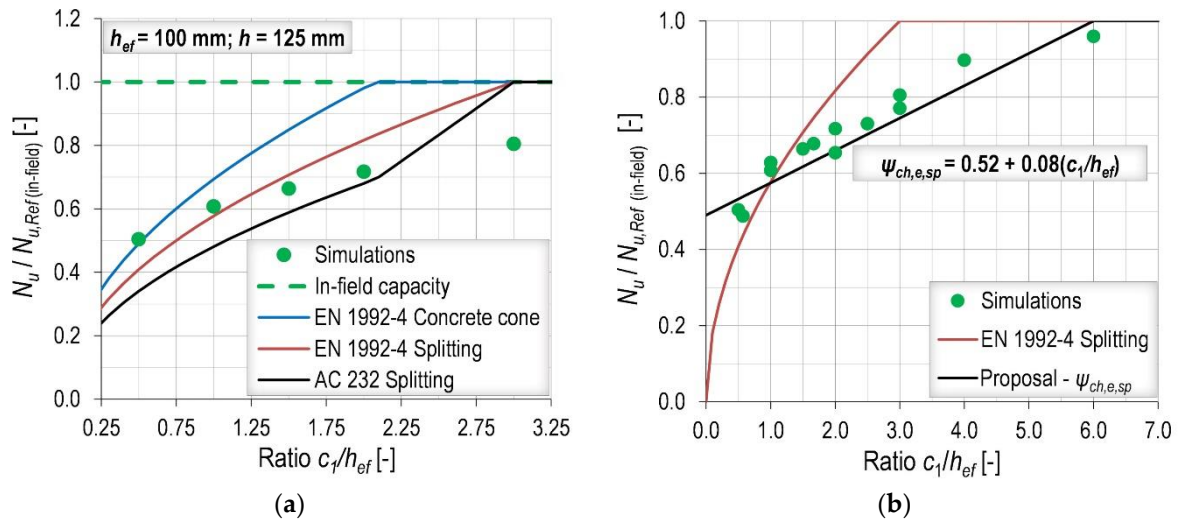
**Figure 4.9** Influence of edge distance: (a) numerical results compared to the current code provisions; (b) numerical results for different embedment depths and small h/h_{ef} ratios described by a linear function

4.2.2.3   Influence of anchor spacing

Similar to the influence of edge distance, the numerical results for thin members showed that the characteristic anchor spacing $s_{cr,sp}$ should be larger than the current

value of EN 1992-4 [26] which is currently defined as the double of the characteristic edge distance ($s_{cr,sp} = 2c_{cr,sp}$). As can be seen in Figure 4.10a for the member thickness $h = 75$ mm, the influence of anchor spacing was not relevant for s/c_1 ratios greater than 12. Moreover, the results obtained for member thickness $h = 125$ mm in Figure 4.10b (green and orange data points) showed that the curve representing the influence of anchor spacing for splitting according to EN 1992-4 [26] should have a smaller inclination. Knowing that the minimum value of the factor $\Psi_{ch,s,N}$ is 0.5 for the theoretical anchor spacing equal to zero, such an inclination can be achieved only by increasing the characteristic anchor spacing. Therefore, it is proposed to increase the characteristic anchor spacing $s_{cr,sp} = 2c_{cr,sp} = 12h_{ef}$, which is consistent with the definition of EN 1992-4 [26] and with the proposal for the characteristic edge distance. The expected $N_u/N_{u,ref}$ ratios are reported with the dashed curves in Figure 4.10a,b. A further increase of the slab thickness to $h = 200$ mm (black points in Figure 4.10b) leads to conditions in which the splitting failure is no longer decisive anymore and the concrete breakout equation (EN 1992-4 [26]) is able to correctly estimate the obtained failure loads.
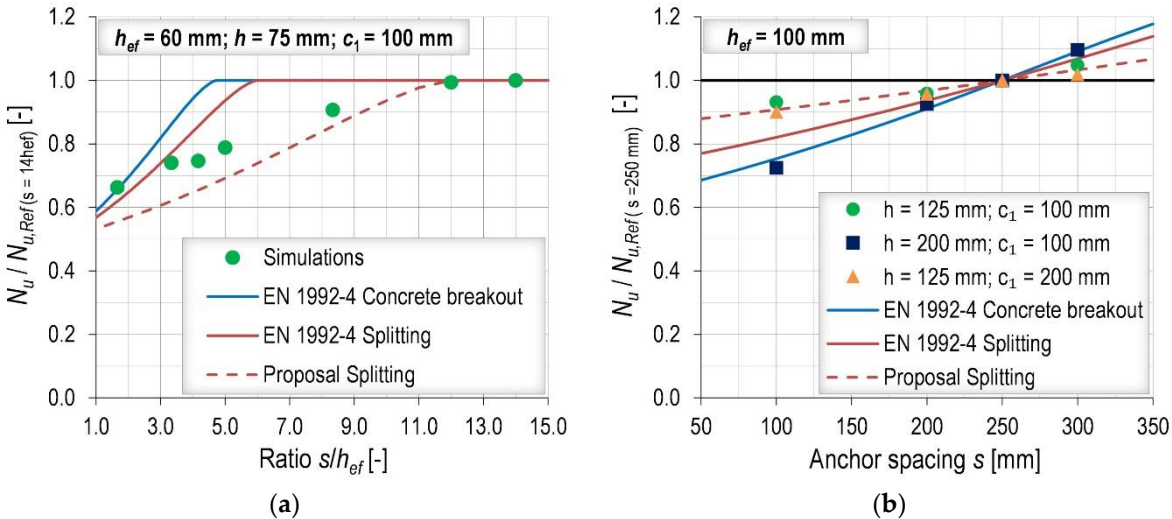
Figure 4.10 Influence of anchor spacing - numerical results compared to the current code provisions for: (a) shallow embedment depth – $s_{cr,N}$ is calculated for actual h_{ef}; (b) typical embedment depth

4.2.3 Proposed modifications of the current design model for concrete splitting (EN 1992-4)

To summarize the above results of the parametric study, it is recommended to improve the splitting verification of the current model of EN 1992-4 [26] with the following modifications.

In the modification factor to account for the influence of the member thickness, the h_{min} should be replaced by h_{ef}:

$$\Psi_{h,sp} = \left(\frac{h}{h_{ef}}\right)^{2/3} \leq max\left\{1; \left(\frac{h_{ef} + c_{cr,N}}{h_{min}}\right)^{2/3}\right\} \leq 2.0 \, . \tag{4.4}$$

The embedment depth, being a physical quantity, is a more convenient choice, and is not dependent on the manufacturer's choices.

For the influence of edge distance, the existing exponential function in Equation (2.35) should be replaced by a linear function:

$$\Psi_{ch,e,N} = 0.52 + 0.08\frac{c_1}{h_{ef}} \leq 1.0 \, . \tag{4.5}$$

As mentioned above, according to this equation the characteristic edge distance is set to $c_{cr,sp} = 6h_{ef}$, although this is not explicitly stated. Moreover, according to the obtained results, the characteristic anchor spacing should also be increased, and in order to be consistent with the characteristic edge distance, the following value is proposed:

$$s_{cr,sp} = 2c_{cr,sp} = 12h_{ef} \, . \tag{4.6}$$

To illustrate how the proposed modifications perform for different configurations, an example is given in Figure 4.11a for the embedment depth $h_{ef} = 100$ mm. The numerically obtained points for different edge distances and two thicknesses ($h = 125$ mm and $h = 200$ mm) are compared with the current model for concrete breakout and with the new design proposal for splitting. As can be seen, the linear function that takes into account the influence of the edge distance accurately predicts the numerical

results, while the modification factor for the influence of member thickness allows the linear function to move upward. It is worth noting that the greater the member thickness, the narrower the range in which concrete splitting is the decisive failure mode.

These modifications also require an adjustment of the constant pre-factor of the basic capacity N^0_{Rk} to ensure optimal agreement between the results (numerical and experimental) and the proposed model for concrete splitting. Therefore, a factor of 1.15 is introduced in Equation (2.34) to increase the basic capacity and allow the model to be more predictable:

$$N^0_{Rk} = 1.15 \cdot min\left(N^0_{Rk,c}, N_{Rk,p}\right).$$ (4.7)

Without this factor, the model predictions, i.e., the calculated concrete splitting resistances, would be on the safe side. A comparison of all numerical results (100 simulations) with the modified design proposal shows excellent predictability with a mean of 1.09 and a standard deviation of 6%. It should be noted that the mean value is slightly higher than 1.0 to ensure that for any case the simulation results do not fall short of the predicted values.

Figure 4.11b shows all the simulation results in dependence to the three investigated parameters. The fact that the results do not show any particular trend with respect to the investigated parameters proves the reliability of the proposed modifications.

The basic concrete breakout capacity $N^0_{Rk,c}$ was considered as the basic characteristic resistance for splitting N^0_{Rk}, as the governing failure mode in all simulations was concrete breakout. The summary of all numerical results can be found in Appendix C. For the short anchors (h_{ef} = 60 mm), the basic characteristic concrete breakout resistance was calculated following the proposal of Grosser et al. [22].
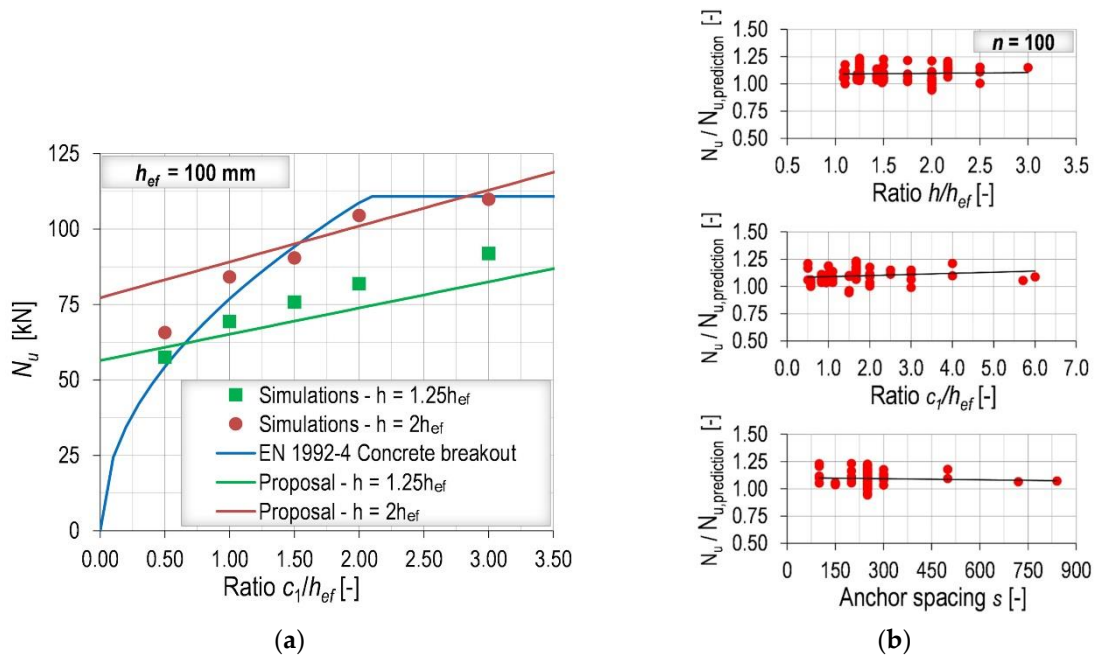
Figure 4.11 (a) Illustration of the principle of the modified design proposal; (b) Numerical results compared to the modified design proposal as a function of investigated parameters.

4.2.4 Experimental results

Due to the actual trend towards thinner concrete members and to check the validity of the simulations, especially for thicknesses that were not already investigated in the literature, the HAC-60 anchor channels equipped with short anchors (h_{ef} = 65 mm) were experimentally tested. This embedment depth is currently not covered by the code as $h_{ch}/h_{ef} > 0.4$ and/or $b_{ch}/h_{ef} > 0.7$. The experimental program was aimed at investigating the influence of member thickness, both for anchor channels with and without edge influence, and the influence of edge distance. The tests were carried out under the same conditions explained in chapter 3.2.2, and the ultimate loads were normalized to the concrete cylinder compressive strength of f_c = 20 N/mm².

The results for anchor channels tested without edge influence are shown in Table 4.7. The tests showed an increase in concrete breakout capacity with the increase in slab thickness. Even though the current design model of EN 1992-4 [26] does not consider the influence of member thickness, calculating the concrete capacity for shallow embedment still leads to a very conservative estimation of the capacity. Indeed, the calculated capacity $N_{u,code}$ is 24.47 kN, which was calculated with the

reduced h_{ef} of 30 mm, is far below the average failure loads $N_{u,m}$ between 40.5 kN and 57.4 kN for the slab thicknesses between 70 mm and 130 mm. In order to calculate the capacity more accurately, the proposal of Grosser et al. [22] for the $\alpha_{ch,N}$ can be considered. With this modification, a capacity $N_{u,Grosser}$ of 50.37 kN is obtained, which more accurately predicts the failure loads of the experiments. In general, since the experimental results show that the influence of the member thickness cannot be neglected, this should be taken into account in the design.

Additionally, the expected reductions according to the proposal of Nilforoush [21] $((h/2h_{ef})^{0.25})$ are reported in the last column of Table 4.7. These reductions vary between 0.86 and 1.00 for the slab thicknesses between 70 mm and 130 mm and therefore are not sufficient to properly represent the experimentally obtained reductions $N_{u,m}/N_{u,m,Ref}$. The reason why the proposal of Nilforoush [21] is not capable of predicting the reductions may be attributed to a larger minimum investigated h/h_{ef} ratio of 1.5, beside the fact that different fastening system was investigated (headed studs).

Table 4.7 Experimental results – in-field installation; 3 tests were performed for each configuration

| h	$N_{u,m}$	$N_{u,m}/N_{u,m,Ref\,(h\,=\,130\;mm)}$	σ	CoV	$N_{u,code}$	$N_{u,Grosser}$	$(h/2h_{ef})^{0.25}$
[mm]	[kN]	[-]	[kN]	[%]	[kN]	[kN]	[-]
70	40.51	0.71	1.26	2.81	24.27	50.37	0.86
100	49.71	0.87	1.63	2.96	24.27	50.37	0.94
130	57.44	1.00	4.69	7.38	24.27	50.37	1.00

The test results for anchor channels installed close to the edge are summarized in Table 4.8. The influence of member thickness was investigated for the same three thicknesses (h = 70, 100, 130 mm). Due to a problem with the acquisition system, only 1 and 2 results are respectively available slab thickness of h = 100 mm and h = 130 mm. Considering the proposed design modifications and calculating the concrete capacity $N_{u,proposal}$ for the tested configurations, the experimental results accurately estimated by the modified design model for concrete splitting (Figure 4.12a) with ratios $N_{u,m}/N_{u,proposal}$ between 0.98 and 1.09. In this case, too, the basic capacity was calculated with the factor

$\alpha_{ch,N}$ according to the proposal introduced by Grosser at al. [22], and the proposed modification factors are applied.

Table 4.8 Experimental results – installation near the edge

c_1	h_{ef}	h	$N_{u,m}$	n_{test}	σ	CoV	$N_{u,proposal}$	$N_{u,m}/N_{u,proposal}$
[mm]	[mm]	[mm]	[kN]	[-]	[kN]	[%]	[kN]	[-]
100	65	70	26.08	4	4.10	14.20	25.09	1.04
100	65	100	31.20	1	-	-	31.82	0.98
100	65	130	41.27	2	1.97	4.31	37.90	1.09
150	65	100	36.06	4	2.04	5.10	34.86	1.03
200	65	100	36.19	4	3.56	8.89	37.91	0.95

Two configurations with larger edge distances ($c_1 = 150$ and $c_1 = 200$ mm) were also tested to check how the edge distance affects the results and further validate the design proposal for splitting failure mode. Also in these cases, the proposed design model was able to estimate accurately the obtained experimental results, as shown in Figure 4.12b (with $N_{u,m}/N_{u,proposal}$ ratios between 0.95 and 1.04.). Among other, it is worth noting that for the ratio $c_1/h_{ef} = 3$ ($c_1 = 200$ mm), the ultimate load was only 73% of the in-field capacity, which shows the correct formulation of the proposed characteristic edge distance.

(a)   (b)
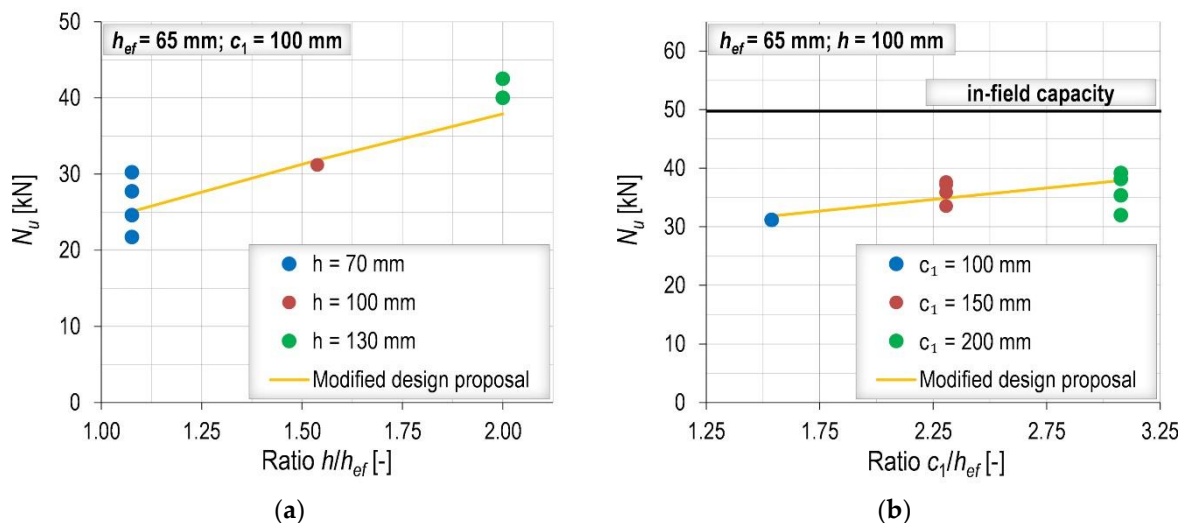
Figure 4.12 Experimental results: (a) influence of member thickness; (b) influence of edge distance

The breakout patterns for the in-field and near the edge installations are shown in Figure 4.13. When installed in-field, a typical cone-shaped pattern was formed.

Simulations also showed that before formation of the cone, bending cracks appear in the slab, especially for small h/h_{ef} ratios. On the other hand, installation near the edge leads to the typical splitting failure, i.e., cracking and separation of the concrete in front of the channel for the full slab thickness, which is again preceded by the bending cracks.

| (a) | (b) |

Figure 4.13 Breakout patterns: (a) in-field installation – $h = 100$ mm; (b) installation near the edge – $c_1 = 150$ mm

4.2.5 Concluding remarks

In this chapter, anchor channels subjected to tension loads were investigated. The focus was set on thin concrete members and shallow embedment depths. Due to the different design rules in the USA and Europe and the limited number of investigations, the focus was placed on the splitting failure mode, which can occur especially for anchor channels placed close to edges in thin members. Based on the numerical and experimental results, the following can be concluded:

- The influence of member thickness should be considered in the design model for concrete splitting. It was found that the existing factor of EN 1992-4 [26] predicts the influence of member thickness with a good accuracy. An improvement for the modification factor to take the slab thickness into account is proposed. The value h_{min} (chosen by the manufacturer for qualification testing) should be replaced by the embedment depth h_{ef} (physical dimension) together with a different calibrating factor of 1.15. The experimental results showed also that the influence of member

thickness is present for anchor channels without edge influence, which is consistent with the findings of Nilforoush [21] for headed studs, although with slightly different results.

- Currently, the characteristic edge distance for splitting is set to $c_{cr,sp} = 3h_{ef}$. According to the numerical and experimental results, a larger value is required to attain the capacity without edge influence, especially when the concrete member is relatively thin. In addition, it was found that the influence of edge distance can be well approximated by a linear function that yields to the limit value for $c_1 = 6h_{ef}$.

- The numerical results indicated that the proportion between the characteristic edge distance and characteristic anchor spacing should be $s_{cr,sp} = 2c_{cr,sp} = 12h_{ef}$.

- The doubling of the critical edge and spacing distances may seem excessive but, together with the other proposed modifications, results in the splitting failure only being decisive for small slab thicknesses compared to the concrete breakout failure.

- The experimental results showed that the modified design model for splitting is able to accurately predict the tensile capacity of anchor channels in thin slabs. This is very important as the basis for the design of anchor channels in composite slabs, where an additional reduction factor should be applied to account for the complex geometry of the concrete above the metal deck.

- In the prospective of the harmonization of the US and European verifications, it is recommended keeping the two verifications for splitting and concrete breakout separately as per EN 1992-4 [26], accordingly modifying the splitting verification, as this approach was proven to provide an overall excellent accuracy.

5

# ANCHOR CHANNELS IN COMPOSITE SLABS

5.1   Introduction

In general, the ribs of the steel decking can be oriented perpendicular or parallel to the edge. The steel decking often protrudes over the flange of the steel beam and thus forms a cantilever. Common details with decking cantilevers are illustrated in Figure 5.1 for perpendicular and parallel orientation.

(**a**)   (**b**)
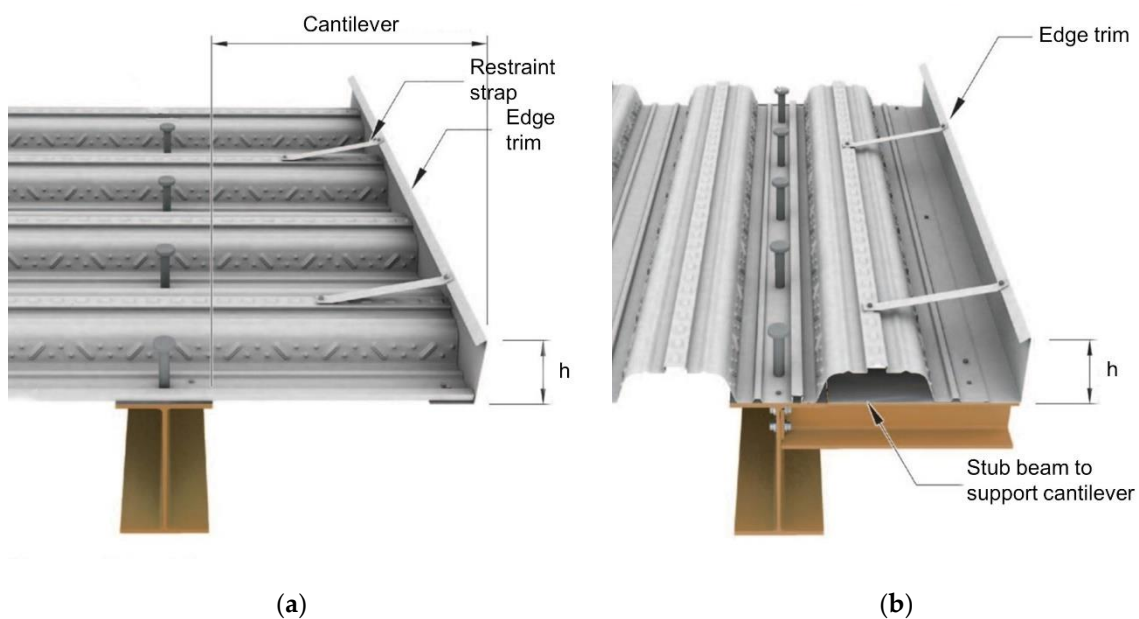
Figure 5.1 Typical edge configurations with cantilever: (a) perpendicular orientation of the steel decking (b) parallel orientation of the steel decking [63]

When the steel decking is oriented parallel to the edge beam, an anchor channel may be installed in various positions with respect to the flange of the steel decking, depending on the edge distance, width of the flange, etc. In the case of perpendicular orientation, anchor channels will be placed over the steel decking. Intuitively, the resistance of anchor channels installed under such conditions should be lower compared to the capacity in the plain concrete slab of the same overall thickness.

In cases where the decking is not cantilevered passed the flange of the steel beam, a perimeter beam is generally provided. This beam is made of plain concrete in the same overall thickness of the concrete slab as shown in Figure 5.2. In this case, the shear capacity should be influenced less by the steel decking since the anchor channel is generally placed in the perimeter beam, which is wider due to the presence of shear connectors. Therefore, the edges with decking cantilevers are of particular interest for this study.
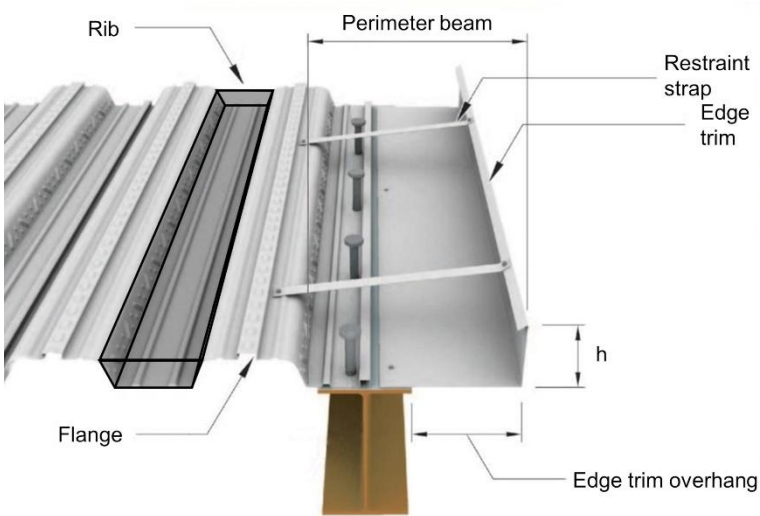
Figure 5.2 Typical edge configurations with wide perimeter beam - parallel orientation of the steel decking [63]

On the market, two types of trapezoidal steel decking are generally distinguished: trapezoidal and re-entrant. Therefore, the influence of steel decking was investigated for two commonly used steel decking profiles: Ribdeck S60, as a representative of trapezoidal profiles, and Superib, as a representative of re-entrant profiles. The dimensions and shape of the profiles are shown in Figure 5.3. It should be noted that

the height of Superib was increased from 51 mm to 60 mm to correspond to Ribdeck S60 to allow a better comparison between the two geometries in the simulations.

(a)   (b)
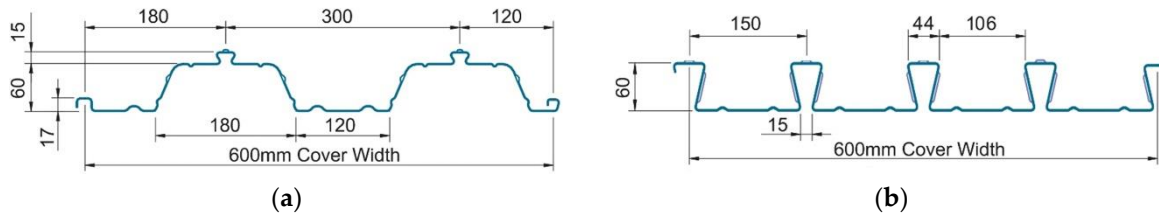
Figure 5.3 Geometry of the steel decking profiles used for the simulations: (a) trapezoidal profile Ribdeck S60; (b) re-entrant profile Superib

5.2   Shear load

5.2.1   Numerical parametric study

Scope of the numerical parametric study was to investigate the vast majority of possible configurations. Each composite slab configuration was also investigated in the equivalent plain concrete slab of the same overall thickness to allow a direct comparison. The study was divided into three series. In Series 1 and 2 the perpendicular orientation of the steel decking with respect to the anchor channel was investigated for deep and shallow anchors, whereas the parallel orientation was investigated in Series 3. In Series 1, where asymmetric configurations were simulated, models were discretized according to Figure 3.4a. Symmetry was exploited in Series 2 and Series 3, as well as in reference models, to optimize computational efforts. In such cases, all nodes on the symmetry plane were restrained in the direction perpendicular to the symmetry plane (x-axis). In all series the HAC-50 anchor channel with two anchors was adopted [57]. The embedment depth and anchor spacing were varied to cover as many configurations as possible.

In Series 1 (perpendicular orientation with standard anchors), commonly used anchors with the embedment depth h_{ef}= 106 mm were considered. It should be noted that the length of the selected anchors exceeded the thickness of the concrete layer above the steel decking. Therefore, the anchor spacing was varied to cover various

configurations. One of the main objectives was to investigate how different positions of anchors inside the rib affect the shear capacity. The chosen anchor spacing should be compatible with the dimensions of the steel decking. For Ribdeck S60 (see Table 5.1), anchor channels with the anchor spacing $s = 250$ and $s = 300$ mm were placed symmetrically over the flange (symmetric configuration) and moved to one side (asymmetric configuration).

Table 5.1 Investigated configurations in Series 1 for Ribdeck S60

Configuration	Anchor spacing $s = 250$ mm	Anchor spacing $s = 300$ mm
Symmetric		
Asymmetric		

Shorter anchor channels with the spacing $s = 150$ and $s = 200$ mm were modeled in the case of the re-entrant profile to fit into the ribs (see Table 5.2). However, for the anchor spacing $s = 200$ mm only a symmetric configuration was investigated due to the limited space around the anchors to move the channel. For both profile types, the investigation was performed for the edge distances $c_1 = 50$ and $c_1 = 100$ mm. To better understand the influence of the edge distance, one configuration (Ribdeck S60, $s = 250$ mm, symmetric) was additionally investigated for larger edge distances of $c_1 = 150$, 200 and 300 mm.

Table 5.2 Investigated configurations in Series 1 for Superib

| Configuration	Anchor spacing $s = 150$ mm	Anchor spacing $s = 200$ mm
Symmetric		
Asymmetric		/

The main objective of Series 2 (perpendicular orientation with shallow anchors) was to examine the validity of the commonly used design approach for anchor channels with reduced embedment depth of $h_{ef} = 60$ mm. The advantage of such configuration would be the flexibility with respect to the position of the anchor channel, independently of the position of the ribs. For edge distances $c_1 = 50$ and $c_1 = 100$ mm and member thickness $h = 130$ mm, two opposite configurations were investigated. In one case both anchors were placed over the flanges and in the other anchors were placed over the center of the ribs (see Table 5.3). In order to provide a general design approach, a thicker composite slab ($h = 160$ mm) and larger edge distances $c_1 = 100$ and $c_1 = 200$ mm were investigated for the installation over the flange. As an additional reference, a thin plain concrete slab ($h = 70$ and $h = 100$mm) was also simulated to represent the concrete layer above the steel decking.

Table 5.3 Investigated configurations in Series 2

c_1 [mm]	h [mm]	Installation over the flange	Installation over the rib
50, 100	130		
100, 200	160		/

In Series 3 (parallel orientation), anchor channels with shallow anchors ($h_{ef} = 60$ mm) were investigated for orientation parallel to the steel decking. Member thicknesses $h = 130$ and $h = 160$ mm were considered for the edge distances $c_1 = 100$ and 200 mm. For the smaller edge distance the re-entrant profile was studied, whereas the trapezoidal profile was used with the edge distance $c_1 = 200$ mm. Larger edge distance was paired with the trapezoidal profile to allow installation on the back of the decking due to the flange width. As shown in Figure 5.4, the edge distances were kept constant and the position of steel decking was varied in regular steps of 50 mm.
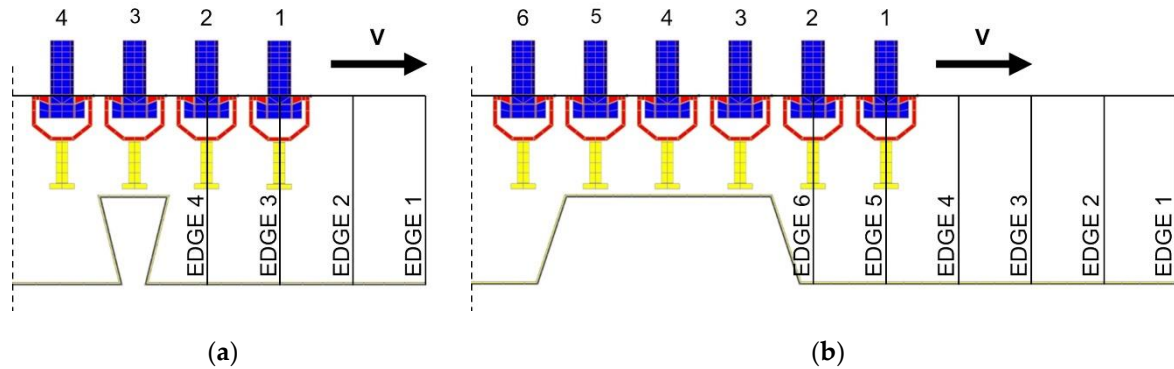
Figure 5.4 Various positions of anchor channel with respect to the steel decking for: (a) Superib, edge distance $c_1 = 100$ mm and member thickness $h = 130$ mm; (b) Ribdeck S60, edge distances $c_1 = 200$ mm and member thickness $h = 130$ mm

5.2.2 Evaluation of numerical results

5.2.2.1 Series 1

The aim of the Series 1 was to investigate the anchor channel with standard anchors installed perpendicular to the steel decking. Figure 5.5 provides a summary of the ultimate loads, normalized with respect to the capacity of the equivalent plain concrete slab ($h = 130$ mm). In general, it turned out that the capacity reductions for composite slabs were all very similar for a given profile, regardless of the anchor position inside a rib. The reductions were more pronounced in the case of trapezoidal profile Ribdeck S60, with values between 0.72 and 0.79 in comparison with the range of 0.78 to 0.87 for Superib. This can be attributed to the larger volume of concrete missing due to the geometry of the decking.

Regarding the simulations with different edge distances for Ribdeck S60 (Figure 5.6a), the load capacities were within the range of 0.68 to 0.79 of the capacity in the plain concrete slab, not showing any particular trend. Note that the investigated configurations showed the largest discrepancy in Figure 5.5a. The observed small deviations can be explained as follows. With increase of anchor spacing or edge distance, the location of the cracks changes, so that the weakened cross-sections (concrete layer over the flange) are intersected differently. This may affect the results

to some extent, but generally less than 10%. Therefore, it can be concluded that the edge distance also has a relatively small influence on the reduction.
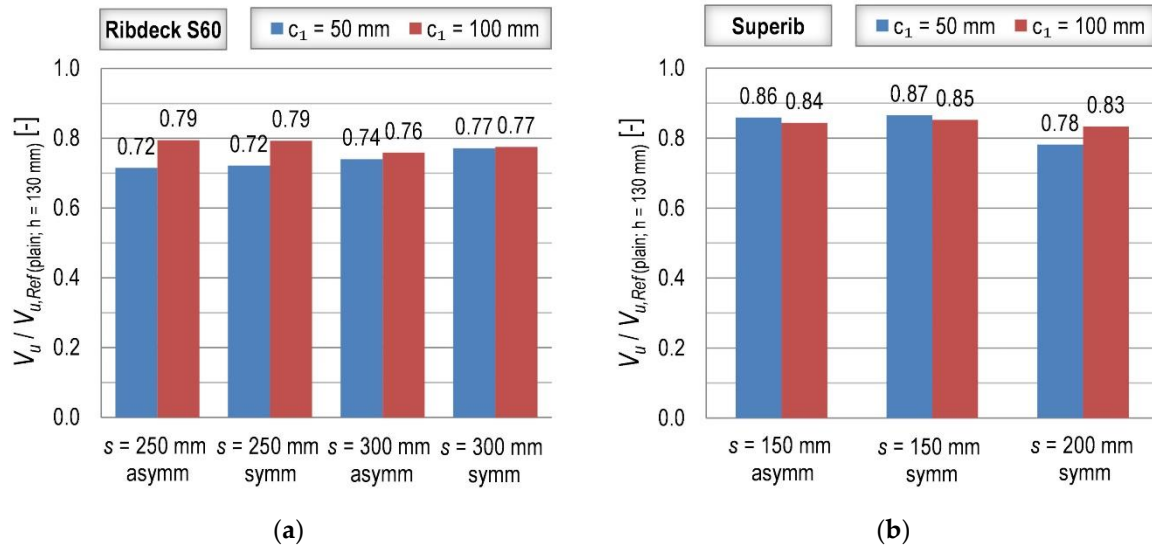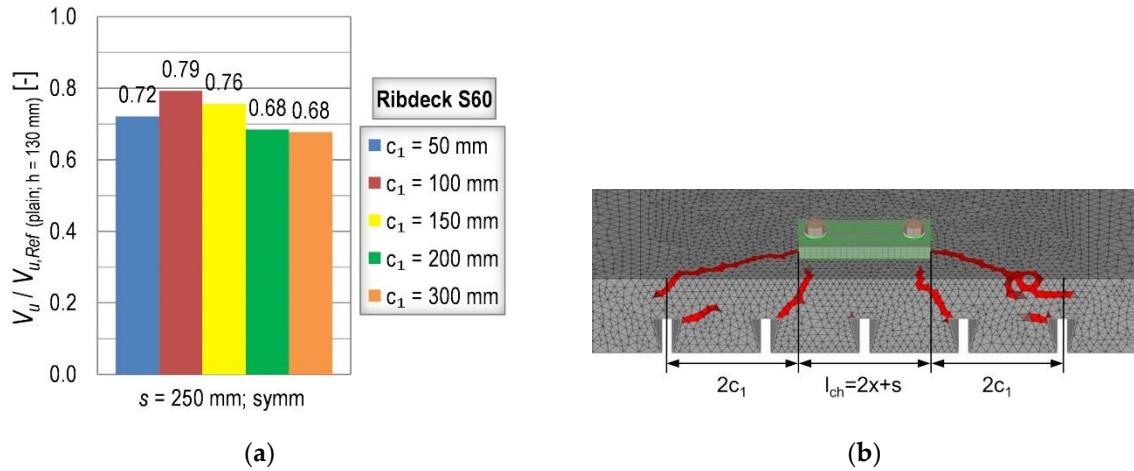

Figure 5.5 Relative capacities for: (a) Ribdeck S60 for edge distances $c_1 = 50$ and 100 mm; (b) Superib for edge distances $c_1 = 50$ and 100 mm; (c) Ribdeck S60 for edge distances $c_1 = 50$ to 300 mm

In addition, the typical breakout pattern is shown in Figure 5.6b for the re-entrant profile. It can be observed that the edges of the upper flange that are closer to the channel represent weak sections in the breakout body. The dimensions of the breakout body are in line with the current code provisions. It should be noted that according to the current code provisions, the critical corner distance is:

$$c_{cr,V} = 2c_1 + b_{ch} \tag{5.1}$$

where the b_{ch} stands for the channel profile width. However, in the performed simulation the cracks started to propagate from the channel corners, thus the end distance x is introduced in the denotation of dimensions instead of the channel width as a more reasonable option.
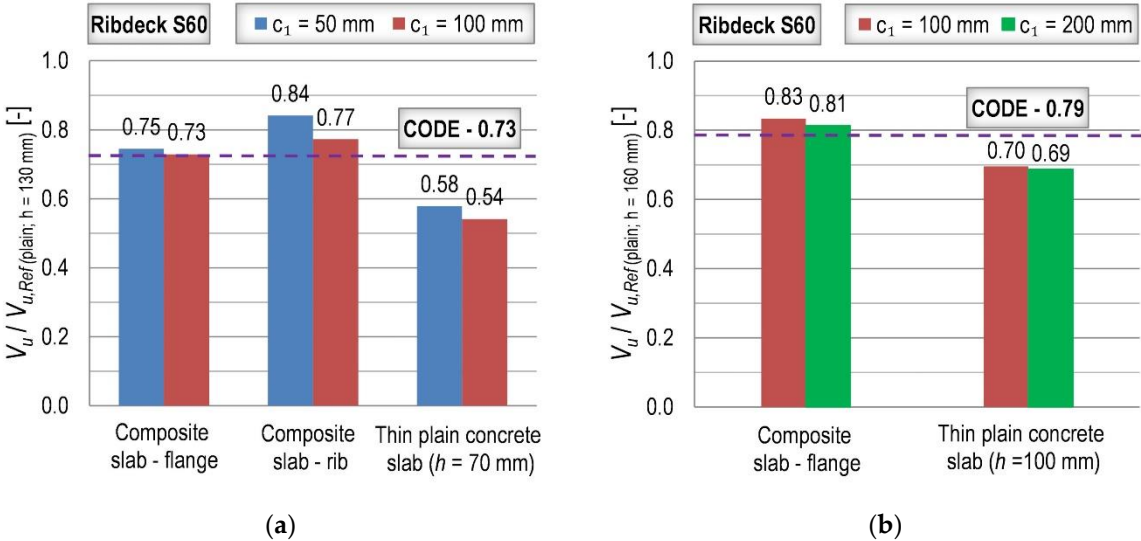
Figure 5.6 (a) Relative capacities for Ribdeck S60 for edge distances c_1 = 50 to 300 mm; (b) Typical breakout pattern for Superib (l_{ch} – channel length)

5.2.2.2 Series 2

The objective of Series 2 was to evaluate the capacity of anchor channels with reduced embedment depth installed perpendicular to the ribs and to compare it with the capacity of the concrete above the steel decking. In Figure 5.7, the capacity reductions with respect to the plain concrete slabs are compared between the composite slabs, the concrete slabs with the thickness of the concrete layer above the steel decking and current code provisions. For both investigated member thicknesses, the relative capacities calculated based on the factor $\Psi_{ch,h,V}$ with the reduced member thickness, i.e. the thickness of the concrete above the profile, were comparable with the numerical results. However, the reductions for the concrete layer above the decking alone (concrete slab) were significantly larger than expected from current code provisions, i.e. up to 19% for the overall member thickness h = 130 mm (Figure 5.7a) and up to 10% for h = 160 mm (Figure 5.7b). This inconsistency agrees with the findings in chapter 4.1, i.e., the influence of the concrete slab thicknesses is not realistically accounted for in the current code provisions.

In Series 1 the results showed that the anchor position and the edge distance have a minor influence on the reduction, which was also confirmed in Series 2. A small difference that can be observed in Figure 5.7a between the investigated configurations, which reduces as the edge distance increases, can be attributed to the position of the

78

ribs in the breakout body. Namely, the reduction was more pronounced in the case where more concrete was missing in the widest part of the breakout body (Figure 5.8c). It should also be noted that the crack patterns on the concrete surface are very similar for different configurations (Figure 5.8). Moreover, the relative capacities are similar for Series1 and Series 2 (see Figure 5.6a – s = 300 mm and Figure 5.7a – composite slab), thus showing that the embedment depth does not have an influence on the reduction.
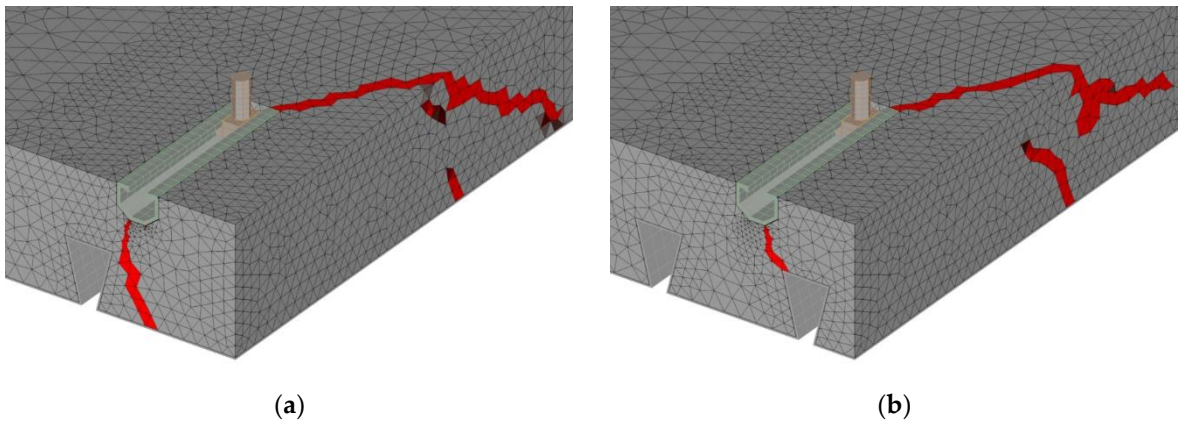

Figure 5.7 Relative capacities in composite slabs, plain concrete slabs and code provisions for overall member thickness: (a) h = 130 mm and Ribdeck S60; (b) h = 160 mm and Ribdeck S60
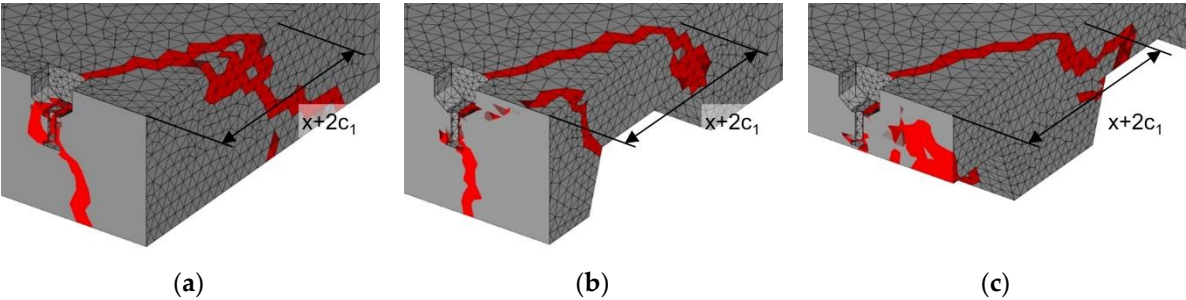
Figure 5.8 Isometric view with the section through the anchor of the post-peak crack patterns obtained for anchor channels with an edge distance c_1 = 100 mm in: (a) plain concrete slab with the thickness h = 130 mm; (b) composite slab in which anchors were installed over the rib; (c) composite slab in which anchors were installed over the flange
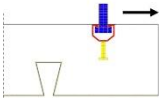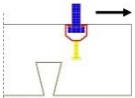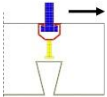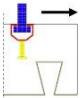
5.2.2.3 Series 3

For parallel orientation of the steel decking, the relative position of an anchor channel with respect to the profile significantly affects the shear capacity. In Table 5.4, the numerical results are shown for various positions of anchor channel in composite slabs with the re-entrant profile for both investigated member thicknesses. As expected, for the channel placed in front of the decking profile (position 1) the capacities were not affected by the profile. However, the capacity reduction was obtained in both cases for the position 2 (Figure 5.9a) where the anchor channel was also installed in front of the steel decking, although closer to the profile. The observed reduction might be unexpected, as the breakout body was not visibly affected by the profile. The reason for the lower capacity can be attributed to the tendency of anchor channels to rotate more easily around their longitudinal axis. Due to the presence of the void in the vicinity of the anchor channel, the slab stiffness is reduced, which facilitates crack formation. The reductions were more pronounced for the overall member thickness $h = 130$ mm, but the trend was very similar. The installation at the back side of the profile (position 4) resulted in the lowest capacity in both cases. As can be seen in Figure 5.9b, the crack ran directly into the closest upper edge of the profile, with a significant reduction to the load capacity. It can be concluded that the reduction in capacity depends on the extent to which the void interferes with the breakout body.


| (a) | (b) |

Figure 5.9 Post-peak crack patterns and corresponding relative capacities for composite slabs with the re-entrant profile Superib: (a) position 2 (in front of the profile); (b) position 4 (at the back of the profile)

Table 5.4 Numerical results for the edge distance $c_1 = 100$ mm and re-entrant profile Superib

Position	$V_{u\ (h=130\ mm)}$ [kN]	$V_u/V_{u,Ref\ (plain;\ h=130\ mm)}$ [-]	$V_{u\ (h=160\ mm)}$ [kN]	$V_u/V_{u,Ref\ (plain;\ h=160\ mm)}$ [-]
1	25.91	0.99	29.41	0.99
2	23.04	0.88	28.13	0.95
3	20.04	0.77	23.94	0.81
4	17.56	0.67	22.46	0.76

For the edge distance $c_1 = 200$ mm and trapezoidal profile (Ribdeck S60) very similar behavior was observed. The numerical results are summarized in Table 5.5. As shown in the table, the largest reduction was also obtained from the channel that was installed at the backside of the profile, where the upper flute was located entirely in the breakout body.

In Figure 5.10, the results for the member thicknesses $h = 130$ mm and $h = 160$ mm are compared in more detail. The reduction, which depends on the position of the anchor channel with respect to the upper flange, could be well approximated by the linear function. The slope of the trend lines for the edge distance $c_1 = 100$ mm was approximately two times the slope of the edge distance $c_1 = 200$ mm in both cases. Moreover, for a given edge distances the slopes were very similar for both investigated thicknesses. However, the intercepts were slightly larger for the composite slabs with the thickness $h = 160$ mm, which indicates that the thickness of the concrete above the steel decking has an influence on the reduction. According to the results and fitted linear trend lines, the distance at which no capacity reduction can be observed gets larger as the edge distance increases, which can be attributed to the higher loads that are transferred into the concrete.

(a)   **(b)**
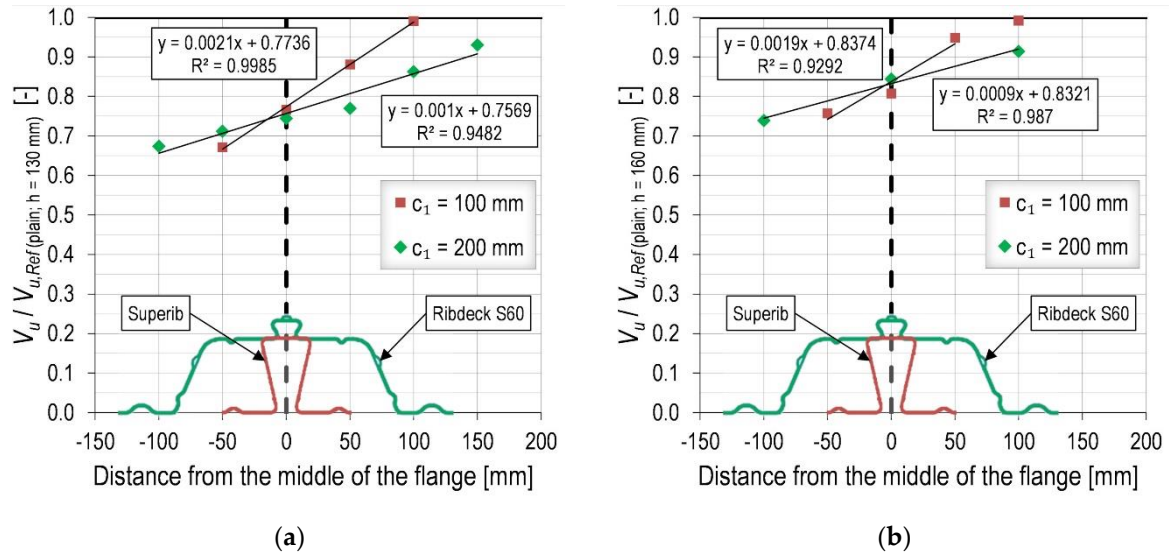
Figure 5.10 Relative capacities as a function of distance between the anchor channel and the middle of the flange for the member thickness: (a) $h = 130$ mm; (b) $h = 160$ mm

Table 5.5 Numerical results for the edge distance $c_1 = 200$ mm and trapezoidal profile Ribdeck S60

	Position	V_u ($h=130$ mm) [kN]	$V_u/V_{u,Ref (plain; h=130 mm)}$ [-]	V_u ($h=160$ mm) [kN]	$V_u/V_{u,Ref (plain; h=160 mm)}$ [-]
1		39.92	0.93	-	-
2		37.02	0.86	45.18	0.91
3		33.04	0.77	-	-
4		31.96	0.74	41.71	0.84
5		30.55	0.71	-	-
6		28.93	0.67	36.25	0.74

5.2.3   Design recommendations and experimental results

With the growing demand for slimmer and lighter concrete elements, the use of anchorage systems in thin concrete slabs will certainly become more frequent. In
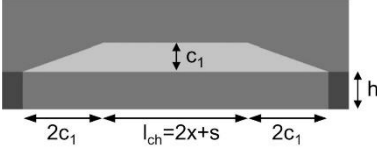
general, the current regulations provide a good basis for calculating the concrete edge capacity, although some improvements are recommended to increase accuracy. In order to take into account the negative influence of complex concrete geometry in composite slabs, an additional factor is proposed:

$$\Psi_{com,V} = \Psi_{com,90°,V} \text{ for perpendicular orientation of the steel decking.}$$

$$= \Psi_{com,0°,V} \text{ for parallel orientation of the steel decking.}$$

(5.2)

The first opportunity to predict the capacity reduction for the perpendicular orientation of the steel decking could be the comparison of the projected areas in front of the slab of the breakout bodies. This approach is based on the well-known CC method [18]. The numerical and experimental results showed that for both plain concrete and composite slabs, the crack propagates almost perpendicular to the lower surface of the slab if the thickness is limited. It was also observed that the crack intersects the slab edge at approximately $x + 2c_1$ from the anchor, as shown in Figure 5.6b and Figure 5.8. Therefore, the typical breakout body for thin plain concrete slabs could be idealized by the trapezoidal prism, as shown in Table 5.6. In order to be consistent with the code provisions, the end spacing x can be replaced by the channel width b_{ch} in the idealized breakout body. The difference between these values is generally very similar, and the choice of the parameter does not significantly affect the dimensions of the idealized breakout body. However, the approach based on the projected area does not distinguish between the void position, whether it is located directly below the anchor channel or intersects the breakout surface in the narrower part at the sides of the breakout body. Due to these observations, it was proposed to correlate the reduction due to complex geometry with the volume of concrete in the breakout body. This approach was found to be more effective. The summary and comparison of all the considered values are shown in Table 5.6.

Table 5.6 Comparison of two ratios with the numerical results obtained in Series 2 (Ribdeck S60) for the edge distance $c_1 = 100$ mm and overall member thickness $h = 130$ mm

Configuration	Idealized breakout body	$V_{u,sim}/V_{u,sim,Ref\,(plain)}$ [-]	Projected area ratio [-]	Exact volume ratio [-]
Plain slab (reference)		1.00	1.00	1.00
Composite slab - rib		0.77	0.71	0.76*
Composite slab - flange		0.73	0.80	0.74*

*$k_{com,90°,V} = 0.75$ *according to Equation* (5.4)

However, both approaches would require a separate design for each anchor channel, which would be time-consuming. Therefore, to bridge the gap between accuracy and simplicity, i.e., applicability in practice, a simpler engineering approach is also proposed. This approach uses the Concrete Volume V_c [m³/m²], which is specified for each profiled steel decking, as a reduction for the concrete edge capacity. The parameter provides the information about the concrete volume per square meter depending on the composite slab thickness. In other words, it is very similar to the above mentioned volume of the breakout body, however, the influence of edge distance and the position of the anchor channel are neglected. As the results of Series 1 and 2 showed, the proposed simplification is acceptable since the differences were relatively small. Therefore, for the perpendicular orientation, the factor $k_{com,90°,V}$ is proposed as follows:

$$\Psi_{com,90°,V} = \frac{V_c}{h}\left[\frac{m^3/m^2}{m}\right] \tag{5.3}$$

where h represents the overall member thickness. With this approach the modification factor for the re-entrant profile is 0.91, however, numerically obtained relative capacities were on average only 0.84. The observed deviation can be attributed to the shape of the profile, where the spacing between the flanges is smaller than for trapezoidal profiles and has a "notching" effect for the slab, facilitating the formation of multiple cracks in front of the anchor channel. An additional modification factor for considering the shape of the profile is therefore introduced. This factor is equal to $k_p = 0.95$ for the re-entrant profiles and $k_p = 1.0$ for the trapezoidal profile. For profiles, which geometry differs significantly from those investigated, a specific k_p should be determined via experiments and numerical simulations. The final form of the modification factor from Equation (5.3) is given as:

$$\Psi_{com,90°,V} = \frac{V_c}{h} \cdot k_p \ [-]. \tag{5.4}$$

In general, the exact volume ratio and the proposed modification factor provide very similar reductions, whereas small differences (up to 5%) were observed for the edge distance $c_1 = 50$ mm, as can be seen from Table 5.7.

Table 5.7 Additional comparison of exact volume ratio and the proposed modification factor $\Psi_{com,90°,V}$ (for symmetric configurations)

c_1 [mm]	h [mm]	s [mm]	h_{ef} [mm]	Steel decking	$V_{u,sim}/V_{u,sim,Ref\,(plain)}$ [-]	Exact volume ratio [-]	$k_{com,90°,V}$ [-]
50	130	300	106	Ribdeck S60	0.77	0.80	0.75
50	130	150	106	Superib	0.87	0.86	0.86
150	130	250	106	Ribdeck S60	0.76	0.75	0.75
200	160	250	60	Ribdeck S60	0.81	0.79	0.79

Furthermore, the comparison between the proposed modification factor and numerical results is given in Figure 5.11. The average simulation-to-prediction with the engineering approach ratio is 1.0 with the standard deviation of 0.053. In addition to the test results introduced in chapter 3.2.1, further tests were carried out to verify the effectiveness and accuracy of the proposed approach for thicker composite slabs

and larger edge distances. The results are summarized in Table 5.8 and the obtained test-to-prediction ratios are highlighted in Figure 5.11. The ratios range between 0.94 and 1.06, which is consistent with the proposal.
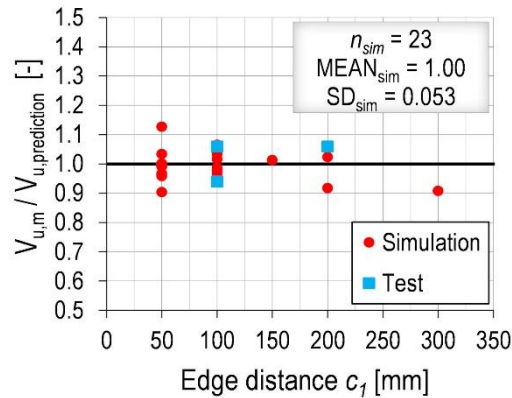
Figure 5.11 Comparison of numerical and experimental results with the proposed design approach for perpendicular orientation of the steel decking

In general, the size effect in fastening technology is rather strong, close to that predicted by LEFM, and it is accounted for accordingly [1]. Since the range of edge distances and member thicknesses in the application of anchor channels in composite slabs is rather limited, no systematic size effect study has been carried out. Such a study would be very demanding as a systematic variation in the size of concrete composite slabs and anchor channels should be performed.

Table 5.8 Test results obtained for the anchor channel HAC-60 (s = 200 mm) and profiled steel decking Cofraplus 60

Slab type*	c_1 [mm]	h [mm]	h_{ef} [mm]	n_{test} [-]	$V_{u,m}$[+] [kN]	CoV [%]	$k_{com,90°,V}$ (test)	$k_{com,90°,V}$ (prediction)	Test-to-prediction
P	100	130	106	4	25.17	7.80	0.77	0.73	1.06
C	100	130	106	4	19.49	8.31			
P	100	160	66	2	33.10	4.72	0.73	0.78	0.94
C	100	160	66	6	24.13	6.63			
P	200	130	66	3	39.93	1.59	0.78	0.73	1.06
C	200	130	66	3	31.01	7.18			

* P – plain concrete slab, C – composite slab

*[+] shear capacities normalized to the $f_{c,mean}$ = 20 N/mm²*

For parallel orientation of profiled steel decking, the situation is more complex because the reduction significantly depends on the position of anchor channels and the edge distance. The proposed approach uses a fundamental parameter, the distance d_f between the anchor channel and front edge of the upper flange, as shown in Figure 5.12a. This parameter provides an indication of the extent in which the void interferes with the breakout body. The influence of the edge distance should be accounted for due to the difference in dimensions of the breakout bodies, i.e., the observed trend in capacity reduction with the edge distance is steeper for smaller edge distances (Figure 5.10). Therefore, the relative distance γ is proposed as:

$$\gamma = \frac{d_f}{c_1} \left[\frac{m}{m} \right]. \tag{5.5}$$

The relative distance is the main parameter in an empirical linear function that should account for the negative influence of both the complex concrete geometry and the member thickness, i.e., the thickness of the layer above the steel decking. The modification factor for the parallel installation of profiled steel decking is then proposed as:

$$\Psi_{com,0°,V} = 0.2\gamma + 1.12 \left(1 - \frac{h_p}{h} \right)^{0.5} \leq 1.0 \, [-] \, , \tag{5.6}$$

where h_p represents the height of the profile. In Figure 5.12b, the comparison of numerical results with the proposed modification factor clearly shows that the factor is able to realistically predict the capacity reduction in composite slabs with the average simulation-to-prediction ratio of 1.0 and the standard deviation of 0.024.
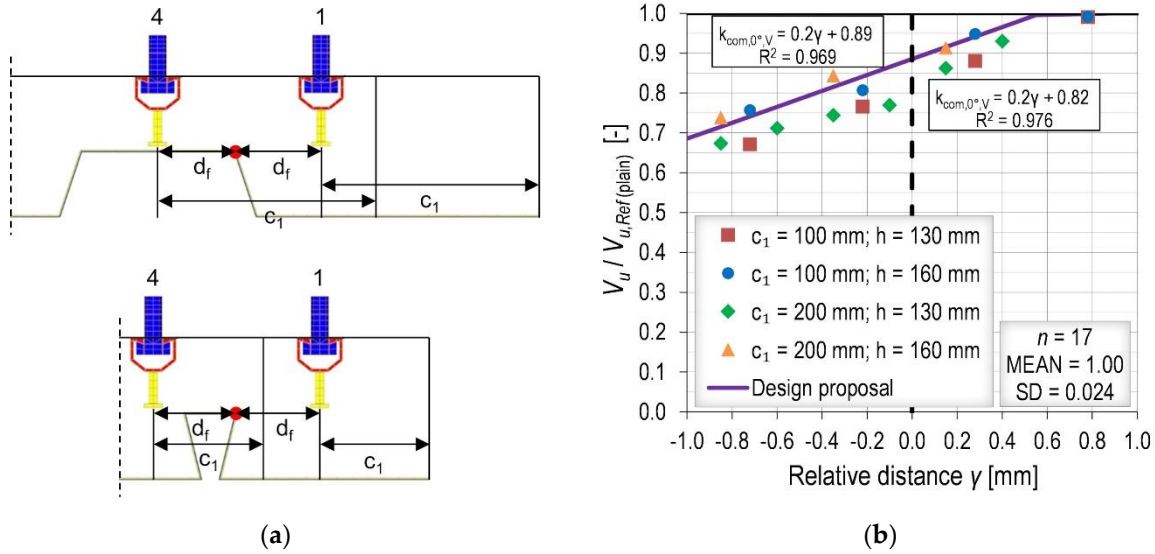
Figure 5.12 Design proposal: (a) geometry and (b) comparison with the numerical results

The proposed factor is intended to cover typical applications in engineering practice. For perpendicular orientation, $\Psi_{com,V}$ is generally greater than 0.70 for trapezoidal profiles and 0.85 for re-entrant profiles. The value increases with increasing member thickness, however, in general this increase is not greater than 0.10 for trapezoidal profiles and 0.05 for re-entrant profiles, e.g. for Ribdeck S60 the reduction factor is $\Psi_{com,V} = 0.746$ for $h = 130$ mm, while increases to $\Psi_{com,V} = 0.835$ for $h = 200$ mm. For the parallel orientation, the minimum value of the factor $\Psi_{com,V}$ would occur when d_f approaches zero, which is unlikely in practice. If minimum slab thicknesses are assumed as $h = 100$ mm (Superib) and $h = 130$ mm (Ribdeck S60), the reduction factor is in the range between 0.6 and 1.0. However, additional experiments are required to validate the proposed modification factor for composite slabs, especially for the parallel orientation. The results of numerical simulation are summarized in Appendix D.

5.2.4 Conclusions

In this chapter, anchor channels in composite slabs with profiled steel decking subjected to shear load were investigated. An extensive numerical parametric study and experimental tests were performed to understand how the complex slab geometry

affects the concrete edge breakout capacity. A common approach in engineering practice, which is based on the design utilizing the reduced slab thickness, was also validated. Based on the numerical and experimental results, the following can be concluded:

- For the perpendicular orientation of steel decking, it was found that the influence of anchor position can be neglected, especially for larger edge distances. Moreover, the capacity reductions with respect to the plain concrete are almost constant as the edge distance is varied. The difference in resistance between the trapezoidal and re-entrant profile can be observed. Namely, re-entrant profiles generally have smaller voids and thus smaller negative influence on the concrete edge breakout capacity. Based on these findings and the behavior of anchor channels in thin plain concrete slabs, it was shown that the capacity reduction can be accurately predicted by the volume of concrete that is missing in the breakout body. The simplified engineering design approach is proposed, based on the Concrete Volume parameter. In general, the modification factor takes the minimum value of 0.70 for trapezoidal profiles and 0.85 for re-entrant profiles. The comparison with the numerical and experimental results proved its effectiveness and accuracy.

- For the parallel orientation of steel decking, the reduction significantly depends on the anchor channel position with respect to the steel decking and the edge distance. The negative influence on the concrete capacity of the complex concrete geometry can be well approximated by a linear function of the position of the channel. Based on these observations, an empiric design approach is proposed. For the most critical case, i.e., when the profile is installed very close to the edge of the thin slab, the reduction factor is approximately 0.60 and its value increases with wider perimeter beams or with thicker concrete layers above the steel decking. The factor takes the value of 1.0 if the profiled steel decking is placed at a sufficient distance behind the anchor channel.

- According to the performed investigation, the engineering judgment based on the reduced member thickness corresponded quite well with the obtained reductions. However, this can be considered as a coincidence as the current codes for very thin concrete members are not accurate. Therefore, a more accurate approach based on numerical and experimental results is proposed.

5.3 Tension load

5.3.1 Numerical parametric study

In chapter 4.2, it was shown that the spacing between the anchor and the vertical support does not have pronounced influence on the results for plain concrete slabs. However, for composite slabs, the influence of the support span is much more pronounced, due to the lower local flexural stiffness. For example, Figure 5.13 shows the breakout patterns at the ultimate load for the support spans 2.5h_{ef} and 4.5h_{ef} for the steel decking oriented parallel to the edge. The finite elements colored in red correspond to a crack width of approximately 0.1 mm or larger. In this case, the thinnest section overlying the flange is the weakest part of the model and causes the failure crack to form behind the channel (at the distance l_1), regardless of how far away the vertical support is. The reduction increases with the support span, as the lever arm between the point of load application and the support (distance l_2) becomes larger without significantly increasing the flexural stiffness, thus without a notable increase in resistance (Table 5.9). The same analogy can be applied for the steel decking oriented perpendicular to the edge. Also, for large support spans, the slab failure occurs before anchorage failure. Therefore, the question arises whether this bending failure should be treated as a global problem or as a local failure, since in practice the location of the vertical supports is not known in advance. In this study, the support span was set at 2.5h_{ef}, in a consistent way with the specification according to qualification tests in the current guidelines [40], [38]. Nevertheless, the interaction between the global stresses

(due to shear or bending) and the local stresses introduced by the fastening element for thin members is one of the problems that need to be considered in further research.
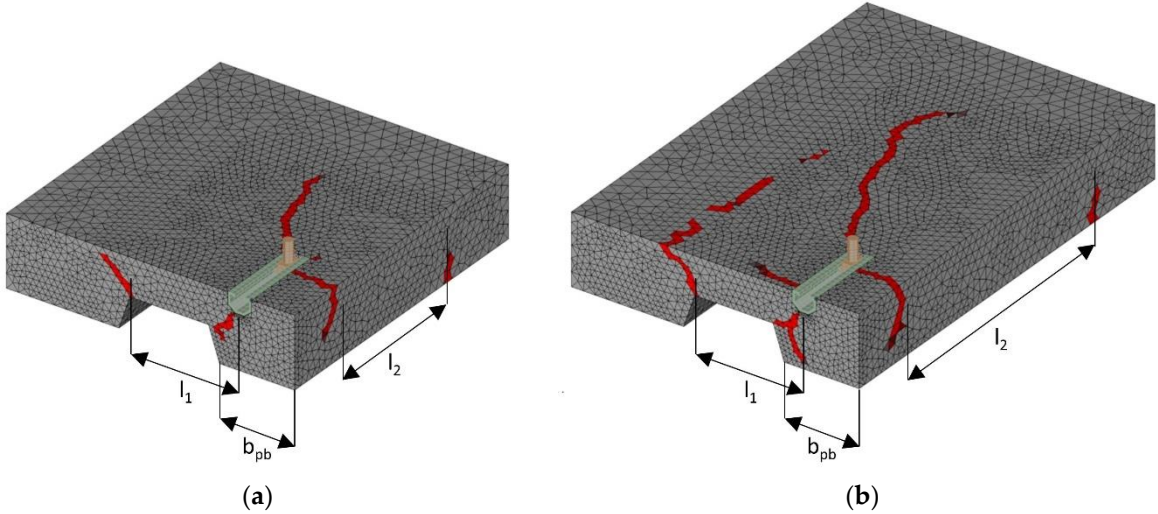

Figure 5.13 Breakout patterns at the ultimate load for: (a) support span 2.5h_{ef}; (b) support span 4.5h_{ef} (symmetry was utilized)

Table 5.9 The influence of support span

Support span	N_u [kN]	$N_u/N_{u,ref}$ [-]
2.5h_{ef}	66.95	1.00
3.5h_{ef}	58.82	0.88
4.5h_{ef}	47.33	0.71
10h_{ef}	26.57	0.40

In the scope of this parametric study, three cases were distinguished based on the orientation of the steel decking and the position of anchor channels. Unless otherwise stated, the overall member thickness of 130 mm, which is fairly common in practice, was selected.

The most important parameters are illustrated in Figure 5.14. The parameter d_w represents the distance between the anchor and the web of the profile, which depends on the width of the perimeter beam b_{pb}. In addition, the angle α is acute for trapezoidal profiles, obtuse for re-entrant profiles, and right angle for the perpendicular orientation of the steel decking.
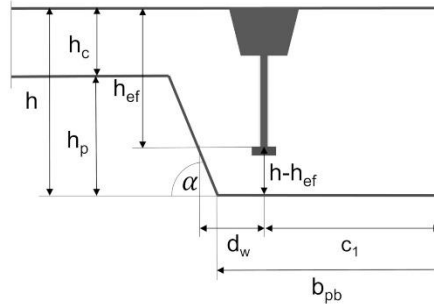
Figure 5.14 Parameters of the numerical model

In Series 1, the profiled steel decking was oriented parallel to the edge and the width of the perimeter beam b_{pb} was varied for a constant edge distance $c_1 = 100$ mm. Embedment depths $h_{ef} = 91$, 106 and 120 mm, which are common for these applications and the two profile types were investigated, as shown in Table 5.10. Shorter anchors were excluded from this study as in this case the influence of bending would be less pronounced, since the concrete cone failure becomes decisive rather than concrete splitting.
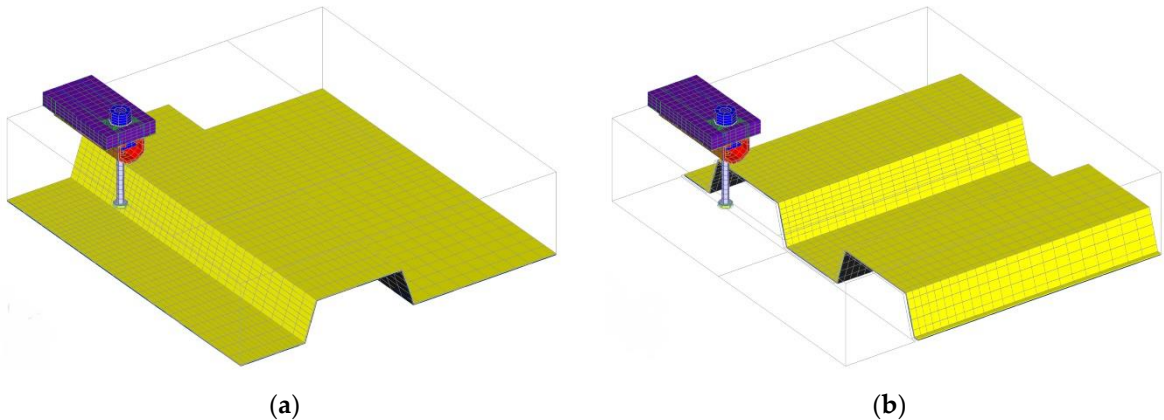
Table 5.10 Series 1 – anchor channel in the perimeter beam, parallel to the steel decking profile

Orientation	Installation	Profile type	c_1 [mm]	h [mm]	h_{ef} [mm]	d_w [mm]	s [mm]
Parallel	Perimeter beam	Ribdeck S60	100	130	91, 106, 120	15, 30, 45, 60, 100	250
			100	180	91, 106, 120	15, 30, 45, 60, 100	250
			200	130	106	15, 30, 45, 60, 100	250
		Superib	100	130	91, 106, 120	15, 30, 45, 60, 100	250

In order to investigate the influence of member thickness, the width of the perimeter beam was varied, simulating additional member thickness $h = 180$ mm with the trapezoidal profile Ribdeck S60. In addition, a single configuration ($h_{ef} = 106$ mm, $h = 130$ mm, Ribdeck S60) was investigated for the edge distance $c_1 = 200$ mm to understand whether this parameter also affects the capacity reduction.

In Series 2, anchor channels with embedment depths of $h_{ef} = 91$, 106 and 120 mm were also placed in the perimeter beams with various widths, but the orientation of the steel decking was perpendicular to the beam. Since this configuration is very

similar to Series 1 (see Figure 5.15), only trapezoidal profile Ribdeck S60 was simulated, as shown in Table 5.11.

(a)   (b)

Figure 5.15 The geometry (model) representing: (a) Series 1; (b) Series 2

Table 5.11 Series 2 – anchor channel in the perimeter beam, perpendicular to the steel decking

Orientation	Installation	Profile type	c_1 [mm]	h [mm]	h_{ef} [mm]	d_w [mm]	s [mm]
Perpendicular	Perimeter beam	Ribdeck S60	100	130	91, 106, 120	15, 30, 45, 60, 100	250

The main objective of Series 3 was to investigate the installation of anchor channels over the decking profile, when it is oriented perpendicular to the edge (see Table 5.12). Since the considered embedment depths exceeded the thickness of the concrete layer above the steel decking, the anchor spacing was varied to be compatible with the dimensions of the steel decking. The anchor spacing $s = 250$ mm and $s = 300$ mm were simulated for the trapezoidal profile, whereas anchor spacings $s = 150$ mm and $s = 200$ mm were chosen for the re-entrant profile. Moreover, in order to cover a number of configurations, the anchor channels were placed symmetrically over the flange (symmetric configuration), but also shifted to one side (asymmetric configuration), as shown in Table 5.1 and Table 5.2.

**Table 5.12** Series 3 – anchor channel over the decking profile, perpendicular to the decking profile

Orientation	Installation	Profile type	c_1 [mm]	h [mm]	h_{ef} [mm]	d_w [mm]	s [mm]
Perpendicular	Over the profile	Ribdeck S60	100	130	91, 106, 120	Depends on configuration	250, 300
			100	180	120		250, 300
		Superib	100	130	91, 106, 120	Depends on configuration	150, 200

5.3.2 Numerical results

5.3.2.1 Series 1

The numerical results of Series 1 are reported in Figure 5.16 in terms of relative capacity $N_u/N_{u,Ref}$ as a function of the anchor lateral distance d_w from the decking profile, whereby N_u is the ultimate tensile concrete capacity in composite slabs and $N_{u,Ref}$ is the reference ultimate capacity in the plain concrete slab. According to the obtained numerical results, the capacity reduction does not depend significantly on the width of the perimeter beam, as long as the parameter d_w is not small enough to provoke a sort of blowout failure. As shown in Figure 5.16a, reducing d_w below approximately 30 mm, the relative capacity for all investigated cases decreases rapidly. For larger d_w distances, reductions of less than 20% were observed compared to the reference plain concrete slab, with no particular trend. As the width of perimeter beam b_{pb} increases, one would expect smaller reductions. At the same time, however, an opposite effect occurs, as the lever arm between the applied forces and the weakest cross section behind the channel l_1 also increases (see Figure 5.13). For comparison, Figure 5.17 shows the post-peak breakout patterns for the distances $d_w = 15$ and $d_w = 45$ mm and the corresponding reference plain concrete slab. For the reference slab, a typical cone-shaped pattern developed. In contrast, a sort of blowout failure can be observed for the smallest distance d_w, accompanied by a flexural crack behind the channel starting from the corner of the flange. For the distance $d_w = 45$ mm, a cone-shaped breakout pattern developed together with clearly visible flexural cracks. However, the

dimension of the cone behind the channel was smaller than that of the reference plain slab due to the disturbance caused by the steel decking.

(a)   (b)
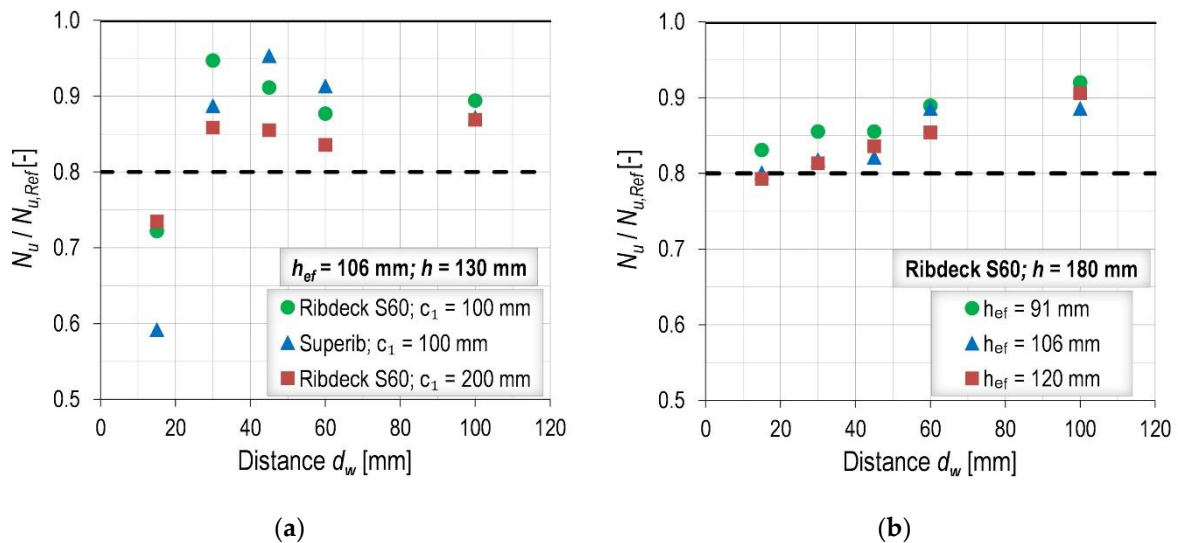
Figure 5.16 Numerical results of Series 1 for: (a) the embedment depth h_{ef} = 106 mm; (b) the overall member thickness h = 180 mm

Moreover, it can be also observed from Figure 5.16a that the results for both investigated edge distances are comparable, thus also the edge distance does not have a pronounced influence on the reductions. The results for the 180 mm thick composite slabs are shown in Figure 5.16b. In a similar way as for the 130 mm thick slab, the relative capacity in case of composite slabs was in all the cases over the 80%. However, a larger reduction was not obtained for the smallest value of d_w since the anchor length did not exceed the thickness of the layer above the steel decking, and the blowout failure could not develop.

(a)   (b)   (c)
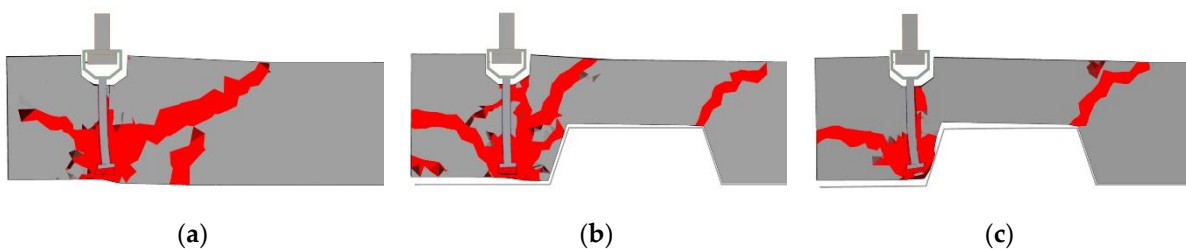
Figure 5.17 Post-peak breakout patterns (section through the anchor for h_{ef} = 120 mm) for: (a) plain concrete slab; (b) composite slab – d_w = 45 mm; (c) composite slab – d_w = 15 mm

5.3.2.2 Series 2

In Series 2, the steel decking profile was oriented in direction perpendicular to the perimeter beam. In general, there was no significant difference between the investigated embedment depths and the results were comparable with the Series 1 results, as shown in Figure 5.18. Also in this case, the largest reduction was again observed for the smallest value of the parameter d_w, while for the other studied values the reductions in capacity in composite slabs did not exceed 20%. It should be mentioned that the anchors were placed in the direction of flanges (refer to Figure 5.15b). Consequently, as the parameter d_w decreases, the anchors approach the voids and the failure mode turns into a sort of blowout failure.
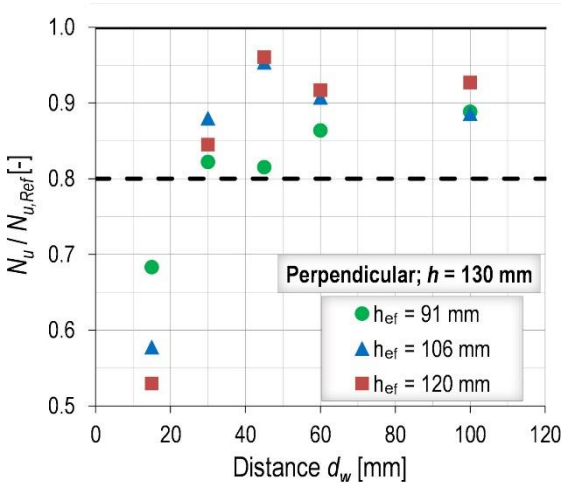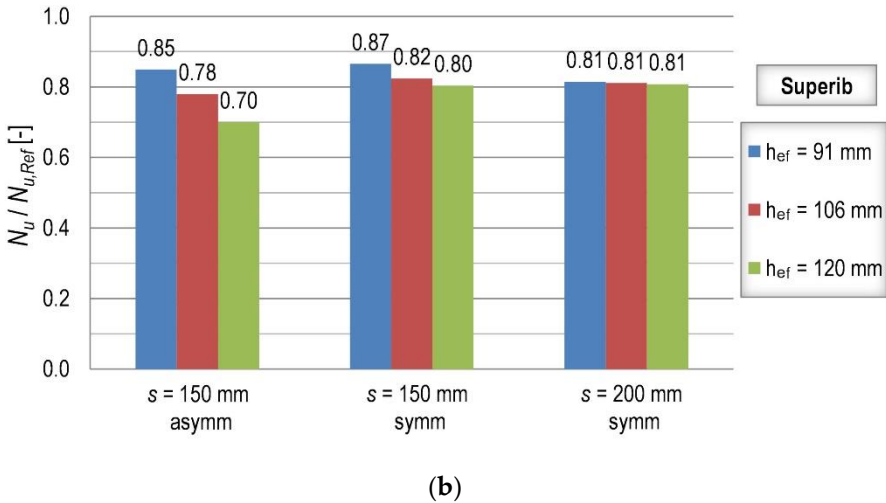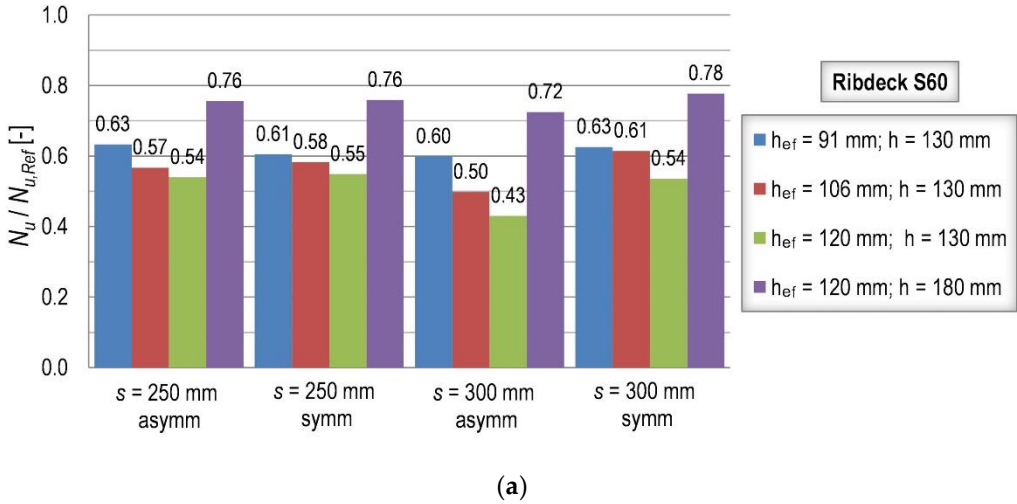

Figure 5.18 Numerical results of Series 2

5.3.2.3 Series 3

Various positions of the anchors in the ribs of the decking profile were investigated in Series 3. The relative capacity $N_u/N_{u,Ref}$ for the trapezoidal and the re-entrant profiles are shown in Figure 5.19a and Figure 5.19b, respectively. It can be observed that the relative capacities between the investigated configurations were comparable between the different embedment depths, although slightly larger reductions were observed with increasing embedment depth. The most critical case was the configuration with both anchors in the vicinity of the steel decking, which would correspond to the anchor spacing $s = 300$ mm and asymmetric configuration (see Table 5). Unlike in Series 1, the

influence of member thickness cannot be neglected. As can be seen from Figure 5.19a, there was a difference in the relative capacities for the embedment depth h_{ef} = 120 mm installed in the 130 mm and 180 mm thick slabs between 0.21 and 0.29.

(a)

(b)

Figure 5.19 Numerical results of Series 3 for: (a) the trapezoidal profile; (b) the re-entrant profile

The shape of the steel decking had a significant effect on the capacity reduction. The reductions for composite slabs with the trapezoidal profile Ribdeck S60 were more than 20 % larger than for the re-entrant profile Superib. To explain this fact, Figure 5.20 shows the cross-sections through the longitudinal axis of the channel and the corresponding principal stresses σ_{33} at the ultimate load for both decking profiles. As can be seen, a sort of strut-and-tie mechanism develops in case of re-entrant profiles, where the compressive forces are transferred from the anchor head to the corners of

the flanges (green area in Figure 5.20b). Therefore, the re-entrant profile provides a confinement and higher stresses can be generated around the anchor head. For fasteners loaded in tension, this directly increases the concrete capacity.


(a)   (b)
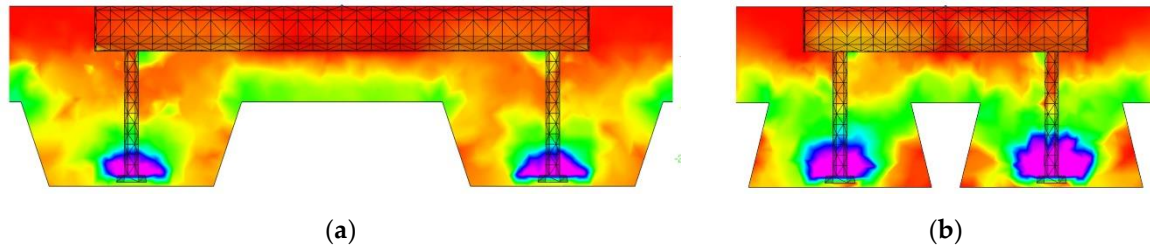
Figure 5.20 Principal stress σ_{33} at the ultimate load: (a) the trapezoidal profile; (b) the re-entrant profile

5.3.3 Experimental investigation

In experimental test program, aimed to verify the numerical results, a total of four configurations in composite slabs in addition to the reference in plain concrete were tested. An example of a composite slab used for testing is shown Figure 5.21. The composite slabs had a length of 1800 mm, a width of 1700 mm and a thickness of 150 mm, whereas a Cofraplus 60 profiled steel decking was used. Using all the four edges of the composite slabs resulted in two anchor channels parallel an in two perpendicular to the decking profile in each slab. The large amount of reinforcement visible in Figure 5.21 was placed outside of the possible breakout bodies and was aimed to avoid any kind of splitting or corner influence, but also to avoid the influence of possible cracks on the subsequent tests. The reference plain concrete slab was squared with a length of 1800 mm and the same overall thickness as composite slabs. The two configurations with a channel parallel to the profiled steel decking were aimed to investigate the behavior in narrower (d_w = 25 mm – configuration 1) and wider (d_w = 125 mm – configuration 2) perimeter beams. These tests correspond to the simulations performed within Series 1. For the perpendicular orientation of the steel decking, the installation in a narrow perimeter beam (d_w = 25 mm – configuration 3) was designed according to Series 2, whereas the installation over the profile (configuration 4) was designed to validate the numerical results obtained in Series 3.
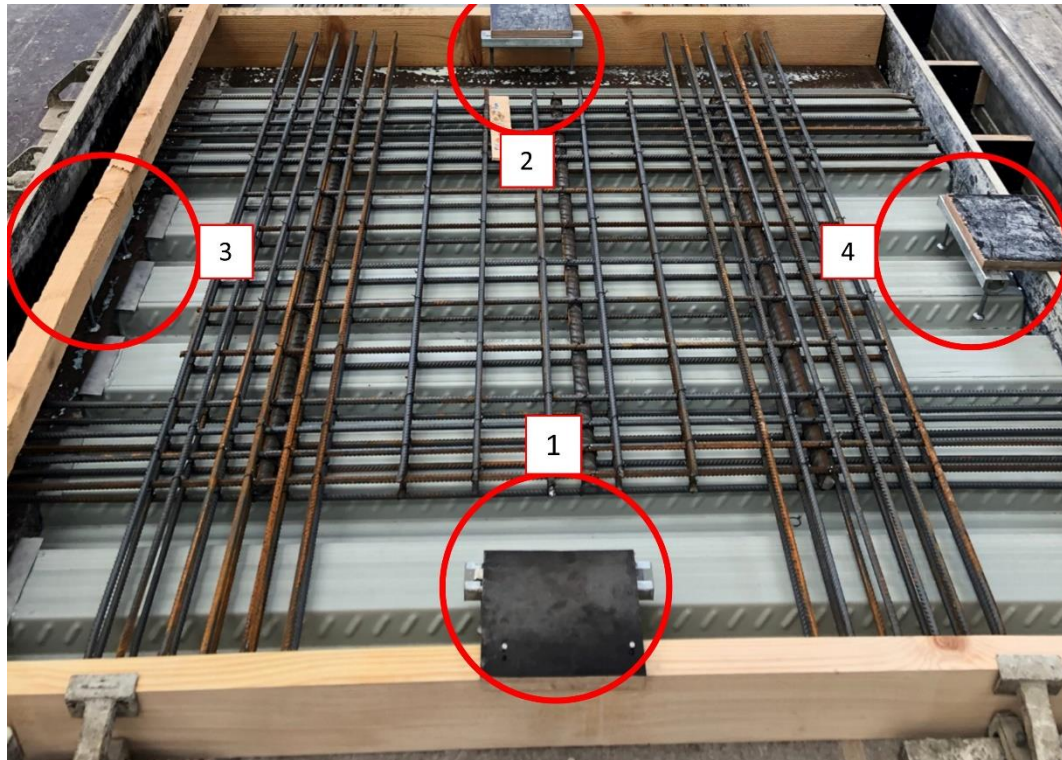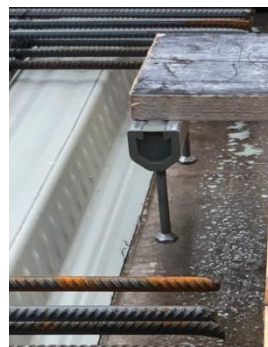
| Configuration 1 | Configuration 2 | Configuration 3 | Configuration 4 |

Figure 5.21 Composite slab layout

Anchor channels (HAC-60 profile provided by the company Hilti [57]) equipped with two anchors at a distance of $s = 200$ mm were utilized. The edge distance $c_1 = 100$ mm and the embedment depth $h_{ef} = 106$ mm were chosen because these values are common in real curtain wall applications. The tests were performed in accordance with EAD [38] in the laboratory of the Faculty of Civil Engineering in Rijeka, Croatia. Zwick Roell servo-hydraulic actuator was utilized and the load was evenly distributed on two channel bolts (HBC-C M20x80 8.8F) inserted directly over the anchors. A constant displacement rate of 0.05 mm/s was applied and controlled by machine stroke. All slabs were made of the same batch of a low strength concrete. Crushed (edged)

aggregate with a maximum size of 16 mm was used. The tests were performed about a month after casting, and in the meantime the slabs were stored in the laboratory. The concrete compressive strength of $f_{cc} = 20.80 \, \text{N/mm}^2$ (the corresponding $f_c = 16.64 \, \text{N/mm}^2$) was measured on 3 cubes (150 mm × 150 mm × 150 mm) with a coefficient of variation of $CoV = 5.98\%$ at the time of testing.

The test results are summarized in Table 5.13. Configuration 1 was one of the most critical configurations with a relative capacity of 0.71. This result is consistent with the numerical results obtained in Series 1, where the largest reductions were observed for $d_w < 30$ mm. As shown in Figure 5.22a, the crack run directly into the steel decking as anchor heads were placed near the steel decking, resulting in a smaller breakout body. The installation parallel to the steel decking in a 225 mm wide perimeter beam (configuration 2) was the most favorable configuration. The reduction of 10% can be attributed to the reduced flexural stiffness of the slab due to the presence of the steel decking at the distance of $d_w = 125$ mm with only minor influence on the breakout size, as shown in Figure 5.22b. It should be noted that this result agree well with the numerical results in Series 1 for larger distances d_w. Very similar relative capacity of 0.87 was also observed for anchor channels placed in a narrow perimeter beam and perpendicular orientation of the steel decking (configuration 3). A greater reduction might have been expected, however, the anchors were placed in the direction of the ribs, right in the area of major stiffness of the composite slab. Thus, the anchor heads were not located near voids and consequently the development of blowout failure was prevented, as shown in Figure 5.22c. As expected, the most unfavorable configuration was the installation over the profile (configuration 4) with a relative capacity of 0.66 with respect to the mean reference capacity in the plain concrete slab. The breakout pattern, shown in Figure 5.22d, reveals that the cracks developed at the flange corners followed by the formation of a typical cone-shaped pattern. This results also agrees well with the numerical results that showed a reduction of approximately 40% for the

given embedment depth and symmetric configurations in slightly thinner composite slab.

(a)

(b)

(c)

(d)
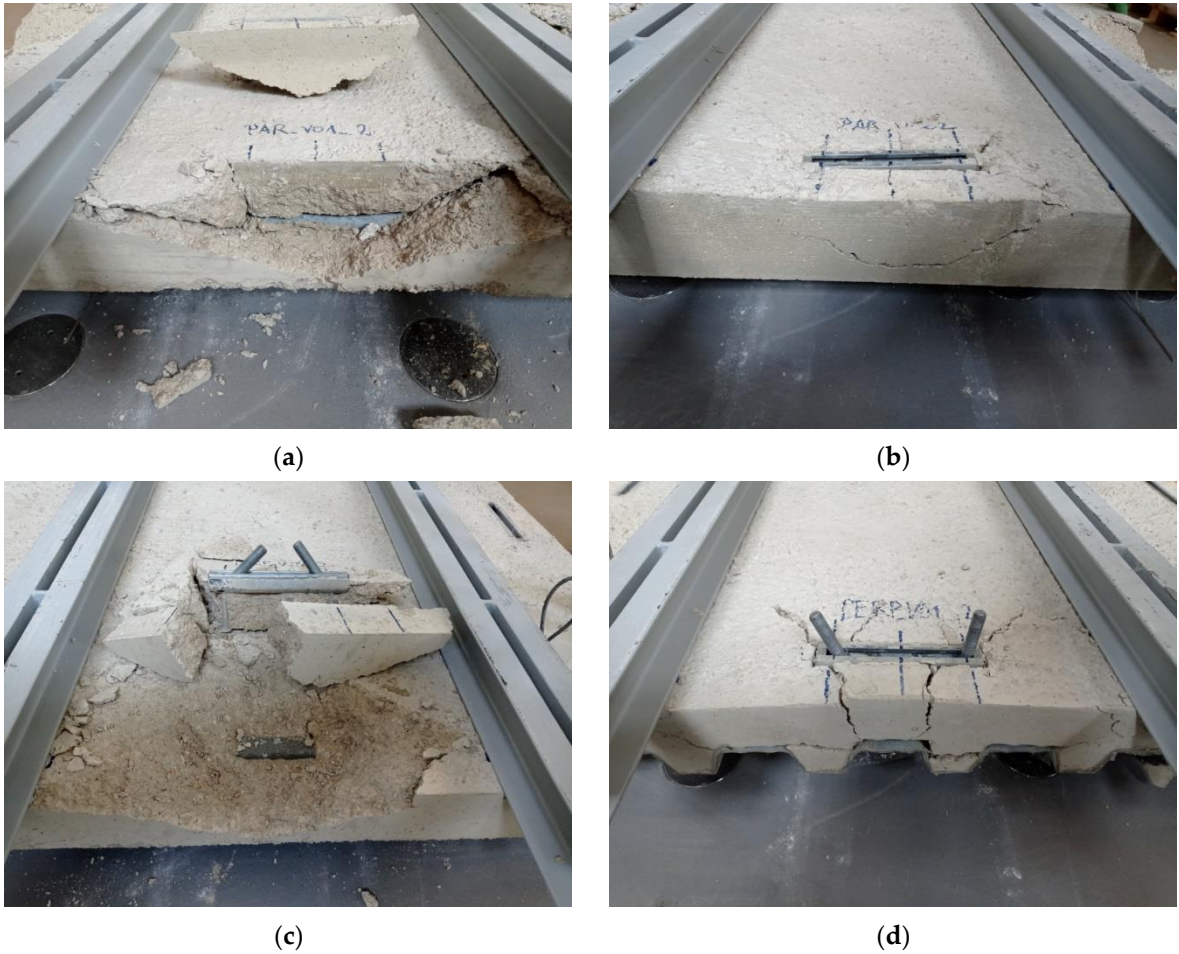
Figure 5.22 Breakout patterns for: (a) configuration 1; (b) configuration 2; (c) configuration 3; (d) configuration 4

Table 5.13 Test results

Configuration	$N_{u,m}$ [kN]	n_{test} [-]	σ [kN]	CoV [%]	$N_{u,m}/N_{u,m,ref}$ [-]
Reference	65.18	4	1.87	2.86	1.00
1	46.30	3	2.28	4.93	0.71
2	58.40	3	2.39	4.09	0.90
3	43.21	3	1.54	3.56	0.66
4	56.59	3	3.60	6.35	0.87

5.3.4   Design recommendations

According to the obtained numerical and experimental results, anchor channels in perimeter beams exhibit very similar capacity reduction if they are placed sufficiently

far from the steel decking. Therefore, a constant reduction factor, which should be included in Equation (2.33), is proposed for the installation of anchor channels in perimeter beams:

$$\Psi_{com,N} = 0.8 \, . \tag{5.7}$$

In case the embedment depth exceeds the thickness of the concrete layer above the steel decking, the required distance to preclude the blowout failure is relatively small, i.e., a distance of approximately 30 mm is sufficient according to the results.

For the installation over the decking profile, the capacity reduction is more pronounced in case of trapezoidal profiles and depends on the member thickness. Therefore, the following expression should be considered for this configuration:

$$\Psi_{com,N} = \frac{h_c}{h} \, , \tag{5.8}$$

where h_c represents the thickness of the concrete layer above the steel decking and h is the overall member thickness. The shape of the re-entrant profiles is more favorable in this case and thus a constant factor of 0.8 should be applied. It should be mentioned that for thicker composite slabs the value of 0.8 might be slightly conservative, but for the sack of simplicity the proposed approach could be considered in design. The overview of the numerical results is given in Appendix E.

5.3.5 Conclusions

This chapter deals with anchor channels loaded in tension in composite slabs with profiled steel decking. An extensive numerical parametric study and a corresponding experimental program were carried out to investigate how the complex geometry of composite slabs affects the capacity of concrete failure modes. In order to cover as many possibilities as possible in practice, the orientation of the steel decking and the position of anchor channels were varied. Based on the numerical and experimental results, the following conclusion can be drawn:

- The influence of bending affects the concrete capacity of tension loaded fasteners in thin concrete members. It was shown that the influence of support span is not so pronounced when installed in plain concrete slabs. However, for composite slabs the influence is significant, and the interaction between the global stresses and the local stresses caused by the fastening system should be considered for further discussion.

- When anchor channels are installed in perimeter beams, the orientation of the profiled steel decking does not have a pronounced influence. If anchors are placed sufficiently far from the steel decking, a reduction of up to 20% can be expected for the studied geometry, regardless of the width of perimeter beam, embedment depth, edge distance or member thickness. Therefore, a constant reduction factor of 0.8 is proposed if the distance between the anchor and the steel decking is sufficient to avoid blowout failure. According to the obtained results, this distance should be $d_w > 30$ mm.

- Installation over the steel decking is the most critical position, especially in case of composite slabs with trapezoidal profiles. For a common thickness of 130 mm, capacity reductions up to approximately 50% compared to a plain concrete slab are possible for trapezoidal profiles. The influence of anchor position is minor, as well as the influence of embedment depth. However, the influence of member thickness cannot be neglected in this case. Therefore, a modification factor based on the thickness of the concrete layer above the steel decking and the overall member thickness is proposed. For re-entrant profiles, a constant factor of 0.8 can be adopted as their shape enhances concrete capacity.

- Given the complexity of the topic, the obtained test results can be considered as the first evidence. In order to optimize the design method, further experimental investigations are recommended in the future.

6

TOPICS RELEVANT FOR CURTAIN WALL APPLICATIONS

6.1   Pockets

For the investigation on the effect of pocket geometry on the capacity, the relevant geometry is shown in Figure 6.1, whereby h stands for the slab thickness in the pocket, h_p for the pocket height, d_s for the distance between the anchor and the pocket wall along the longitudinal axis of the channel, d_b for the distance at the back of the channel. The results of the numerical parametric studies for shear and tension loads are given in Appendix F.
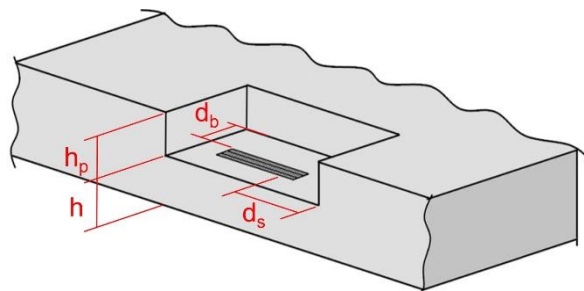
Figure 6.1 Abbreviations – description of pockets

6.1.1 Shear load

6.1.1.1 Numerical parametric study

The numerical parametric study, summarized in Table 6.1, was conducted to propose a design model that takes into account the influence of pockets. In all simulations, a medium size channel profile with anchor spacing $s = 250$ mm was used and the distance $d_b = 75$ mm was kept constant as it has no effect on the shear capacity of anchor channels. The simulations were performed for the pocket dimensions $d_s = 25$, 75 and 125 mm (small, medium, and large, respectively) and for the pocket heights h_p of 25, 50 and 100 mm. In order to obtain the overall picture of the influence of pockets on the shear capacity, three edge distances $c_1 = 100$, 150 and 200 mm were investigated. For each configuration, a reference model without a pocket was also calculated using the member thickness h to determine to what extent the portion of concrete beside the pocket increases the concrete edge capacity.

Table 6.1 Simulation program – installation in pockets for shear load

c_1 [mm]	h [mm]	h_{ef} [mm]	d_s [mm]	h_p [mm]
100	80	60	25, 75, 125	50
100	130	106	25, 75, 125	25, 50, 100
100	300	106	25, 75, 125	25, 50, 100
150	80	60	25, 75, 125	50
150	130	106	25	25, 75, 100
150	130	106	25, 75, 125	50
150	400	106	25, 75, 125	50
200	80	60	25, 75, 125	50
200	130	106	25, 75, 125	25, 50, 100
200	500	106	25, 75, 125	25, 50, 100

#### 6.1.1.2 Evaluation of numerical results for the influence of pockets

As expected, the conducted numerical parametric study revealed that the shear capacity significantly depends on the pocket size (distance d_s) and pocket height. As shown in Figure 6.2a for the edge distance $c_1 = 200$ mm and the member thickness in the pocket of $h = 130$ mm, the increase in capacity for the smallest distance $d_s = 25$ mm

varied between 1.21 and 1.57, whereas for the largest pocket size (d_s = 125 mm) the increase was only between 1.04 and 1.10. Moreover, the edge distance also has a pronounced effect as the breakout body becomes wider and cracks intersect more concrete outside of the pocket for the same pocket size. This can be clearly seen in Figure 6.3a, where for each pocket size the largest increase was obtained for the largest edge distance. In addition, the member thickness in the pocket also plays an important role. Namely, the thicker the member, the less pronounced is the influence of pockets, as shown in Figure 6.2b for edge distance c_1 = 200 mm and pocket height h_p = 50 mm.

(a)   (b)
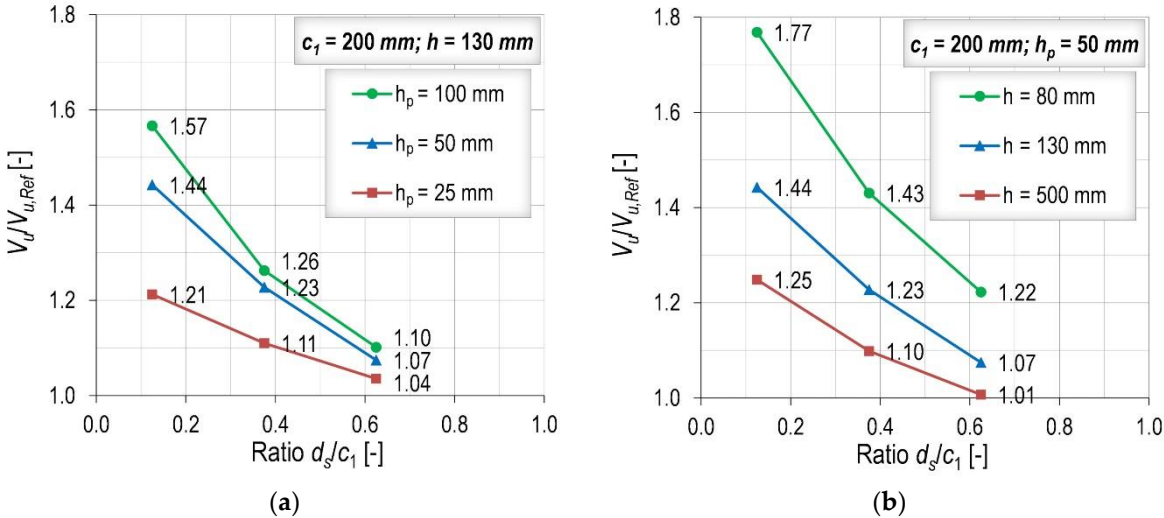
Figure 6.2 Increase in capacity as a function of pocket size for different: (a) pocket heights; (b) member thicknesses in pockets

(a)   (b)
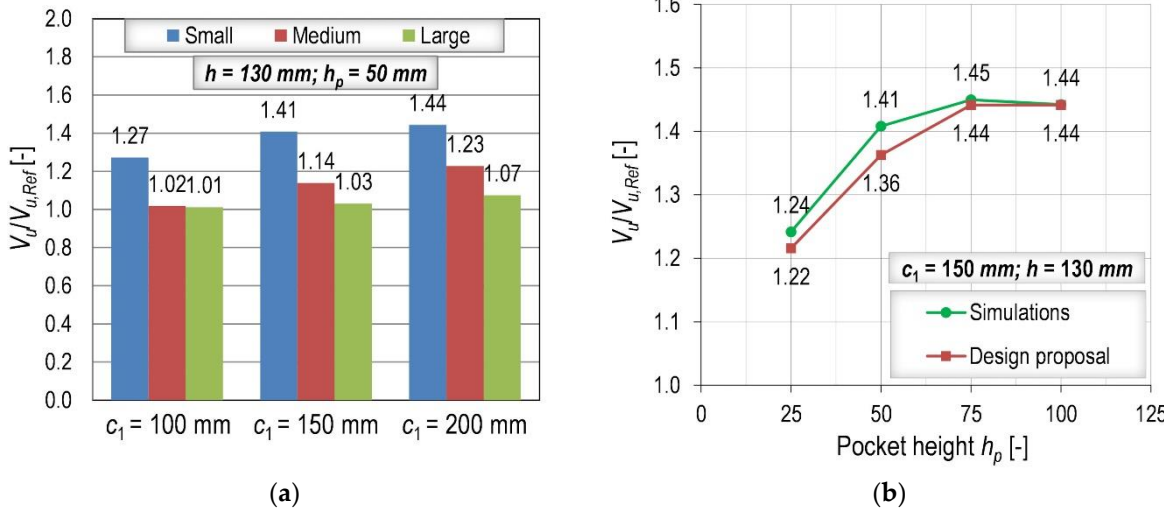
Figure 6.3 (a) Increase in capacity as a function of pocket size for different edge distances; (b) Design proposal compared to the numerical results as a function of pocket height

6.1.1.3 Modification factor for the influence of pockets

Based on the evaluation of numerical results an additional modification factor to consider the influence of the pocket is proposed in the following Equation (6.1). This increasing factor should be multiplied by the basic concrete edge breakout capacity:

$$\Psi_{p,V} = 1 - 0.2 \cdot \left(\frac{h}{h_{cr,V}}\right)^{-\frac{3}{4}} \cdot \left(\frac{h_p}{50}\right)^{\frac{3}{4}} \cdot ln\left(\frac{d_s}{c_1} + 0.15\right) \geq 1$$

(6.1)

with $h_p \leq 65$ mm and $h \leq h_{cr,V}$.

The core of the above equation is the logarithmic function containing the ratio between the anchor distance from the pocket wall and the edge distance. As the ratio d_s/c_1 increases, the positive influence of pocket geometry vanishes (Figure 6.2). It was found that the best agreement between the numerical results and the proposed formula can be achieved when the modification factor reaches the value of one (no positive effect) for the ratio $d_s/c_1 = 0.85$. In other words, for d_s larger than 0.85 c_1 the positive influence of pockets is no longer considered. Consequently, the limit values for d_s/c_1 are set to $0.85 \geq d_s/c_1 > 0$.

The influences of member thickness and pocket height are taken into account by an exponent of 3/4 and these factors multiply and modify the main function. The concrete thickness in the pocket h is limited to the value of the characteristic member thickness since the breakout body does not change when the critical value is exceeded. It should be noted that the characteristic member thickness proposed in previous section was used in the evaluation. In addition, an upper limit for the pocket height h_p is also provided, as it was observed that the increase in capacity decreases as the pocket height increases. Figure 6.3b shows no further increase in the relative capacity $V_u/V_{u,Ref}$ for h_p larger than approximately 75 mm, whereby $V_{u,Ref}$ is the reference capacity for the plain concrete member without the pocket. This trend can be also seen in Figure 6.2a for larger edge distance, i.e., the difference between the pocket heights $h_p = 25$ mm and $h_p = 50$ mm was more pronounced than the difference between $h_p = 50$ mm and

$h_p = 100$ mm. The critical value is set to 65 mm, although in practice pockets higher than the chosen value are rarely encountered. The limit pocket height may increase with the edge distance, but the proposed value is a good fit for the most common edge distances in practical applications. In the case of an anchor channel with more than two anchors, which is unlikely for curtain wall applications, the proposed equation would be valid only for the two outer anchors.

Based on the 54 simulated configurations, the average simulation-to-prediction ratio is 1.0 with a standard deviation of 0.046. Moreover, as shown in Figure 6.4, the trend lines do not show any particular trend with respect to the investigated parameters.
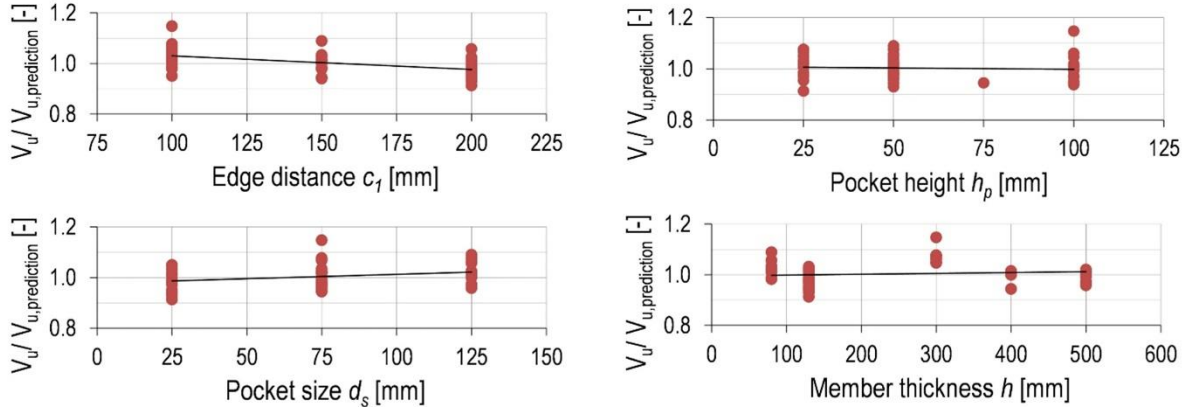
Figure 6.4 Numerical results compared to the design proposal as a function of investigated parameters

6.1.1.4 Experimental investigation

In order to investigate the behavior of anchor channels in pockets and to confirm the numerical results and proposed formula, two configurations were selected for the experimental tests. The pocket dimensions for both configurations were: $d_s = 55$ mm, $d_b = 40$ mm and $h_p = 40$ mm. The selected overall member thickness was 130 mm as a common thickness in curtain wall applications, and consequently the member thickness in the pocket was 90 mm. For the given parameters, two edge distances were investigated, $c_1 = 100$ mm and $c_1 = 200$ mm. The shallow anchor channels (HAC-60, $s = 200$ mm, $h_{ef} = 65$ mm) were used. The reference tests in plain concrete slabs with

same thickness of the slab inside the pocket were also carried out. The slabs were made from the concrete mix presented in Table 3.2 and stored in the laboratory of the University of Rijeka for one month before being tested. In this program, the slabs were not cast from the same batch, meaning they were made over a period of three days. Three tests were performed for each configuration and the ultimate capacities (normalized to $f_c = 20$ N/mm^2) are summarized in Table 6.2. Moreover, concrete compressive strengths are given for each configuration based on cored cylinders taken out at the time of testing. For some configurations, a very low compressive strength was obtained, which can be attributed to a problem with the concrete mixing facility.

Table 6.2 Test results – installation in pockets ($f_c = 20$ N/mm^2)

Installation	c_1 [mm]	$V_{u,m}$ [kN]	n [-]	σ [kN]	CoV [%]	$V_{u,m}/V_{u,m,Ref}$ [-]	$\Psi_{p,V}$ [-]	$V_{u,m}/\Psi_{p,V}$ [-]	$f_{c,core}$ (CoV) [N/mm^2]
Plain	100	21.74	3	0.19	0.88	-	-	-	12.99 (11.24%)
Pocket	100	29.66	3	4.74	15.97	1.36	1.13	1.21	12.99 (11.24%)
Plain	200	28.02	3	2.11	7.54	-	-	-	24.69 (6.18%)
Pocket	200	47.30	3	0.88	1.85	1.69	1.40	1.20	16.36 (0.96%)

Nevertheless, a significant increase in capacity of 1.36 and 1.69 was obtained for investigated configurations without pockets. As expected, this effect was more pronounced for the edge distance $c_1 = 200$ mm due to the larger intersection of concrete breakout body outside the pocket, as shown in Figure 6.5.

The predictions of the proposed modification factor $\Psi_{ch,p,V}$ are approximately 20% smaller than the experimentally obtained values. According to this observation, the proposed factor could be further optimized, however, additional experimental investigations are needed with different pocket sizes.

Figure 6.5 Breakout pattern for anchor channels installed in pockets - $c_1 = 100$ mm (upper) and $c_1 = 200$ mm (lower)

6.1.2   Tension load

6.1.2.1   Numerical parametric study

Table 6.3 summarizes the performed simulations for the tension loaded anchor channels in pockets. In the numerical parametric study, a medium size channel profile was used with anchor spacing $s = 250$ mm and various embedment depths $h_{ef} = 60$, 83 and 106 mm. Unlike for the shear load, the distance d_b at the back of the channel was varied and the vast majority of simulations were performed for the small (25x0), medium (75x50) and large pockets (125x100), as shown in Table 6.3 (d_s x d_b).

Table 6.3 Simulation program – installation in pockets for tension load

h_{ef}	h	c_1	d_s x d_b	h_p
[mm]	[mm]	[mm]	[mm x mm]	[mm]
60	80	100	25x0, 75x50, 125x100	25, 50
60	130	100	25x0, 75x50, 125x100	25, 50
60	130	60	25x0, 75x50, 125x100	50
60	250	100	25x0, 75x50, 125x100	50
83	130	100	25x0, 75x50, 125x100	25, 50
83	130	42, 166	25x0, 75x50, 125x100	50
83	250	100	25x0, 75x50, 125x100	50
106	130	100	25x0, 75x50, 125x100	25, 50
106	130	50, 200	25x0, 75x50, 125x100	50
106	130	100	125x0, 125x50, 75x100, 25x100	50
106	250	100	25x0, 75x50, 125x100	25, 50

In order to investigate how each of pocket dimensions influences the increase in capacity, additional pocket sizes were investigated for the embedment depth

h_{ef} = 106 mm. In addition, potentially important parameters were varied, such as member thickness in pockets h, edge distance c_1 and pocket height h_p.

6.1.2.2 Evaluation of numerical results for the influence of pockets

The behavior of anchor channels subjected to tension is highly dependent on the member thickness (chapter 4.2), and the presence of pockets adds to the complexity. As shown in Table 6.4, several configurations in plain concrete slabs were first simulated and the results can be well predicted by the proposed design model.

Table 6.4 Results of the numerical simulations for plain concrete slabs

c_1	h_{ef}	h	N_u	$N_{u,proposal}$*	$N_u/N_{u,proposal}$
[mm]	[mm]	[mm]	[kN]	[kN]	[-]
100	106	130	73.45	69.45	1.06
100	106	180	88.12	81.49	1.08
100	156	180	115.89	108.77	1.07

According to chapter 4.2.3

These results were compared in Table 6.5 with the capacities influenced by pockets. Namely, three pocket sizes were considered with a constant pocket height of 50 mm and a member thickness in the pocket of 130 mm. Comparison with the thinnest reference model, which represents the thickness in the pocket, showed an increase in capacity of 1.21, 1.38 and 1.52 for the large, medium and small pocket, respectively.

Table 6.5 Results of the numerical simulations for anchor channels in pockets

d_s	d_b	h_p	h	N_u	$N_u/N_{u,Ref\ (h\ =\ 130\ mm)}$	$N_u/N_{u,Ref\ (h\ =\ 180\ mm)}$
[mm]	[mm]	[mm]	[mm]	[kN]	[-]	[-]
25	0	50	130	111.52	1.52	1.27
75	50	50	130	101.67	1.38	1.15
125	100	50	130	88.81	1.21	1.01

Therefore, the smaller the pocket dimensions, the greater the increase in capacity. The relative capacities with respect to the thicker reference model (h = 180 mm) were smaller, but still greater than one. As can be seen, the result for the largest pockets was almost identical to the capacity of the reference model. These two models have the same overall member thickness in the vicinity of vertical supports, and therefore the

similar influence of bending on the results. Furthermore, the influence of the reduced member thickness in the pocket was compensated by the intersected concrete outside the pocket. The comparison of the post-peak breakout patterns is given in Figure 6.6a,b. Based on this observations, in this parametric study the reference models were chosen to have the same overall thickness as the models with pockets to eliminate the influence of bending in the design model for the influence of pockets.

For the smallest possible pocket dimensions, it could be assumed that the embedment depth increases by the pocket height. This assumption seems to be valid, as the result for the smallest pocket was comparable to the reference model with the larger embedment depth (h_{ef} = 156 mm), although with slightly different post-peak breakout patterns. Namely, a cone-shaped breakout pattern influenced by bending cracks developed in plain concrete slab (Figure 6.6c), whereas typical splitting cracks can be seen for the small pocket in Figure 6.6d.

The distance between the anchor and the vertical support in the model depends on the embedment depth. Therefore, the same configurations with pockets were investigated with larger support span, which was determined based on the embedment depth h_{ef} = 156 mm. As the results in Table 6.6 indicate, the obtained capacities were similar to those in Table 6.5, with the largest difference of approximately 4 kN. Therefore, the influence of the support span is almost negligible, which is consistent with the findings in chapter 4.2.1.

(a)

(b)

(c)

(d)
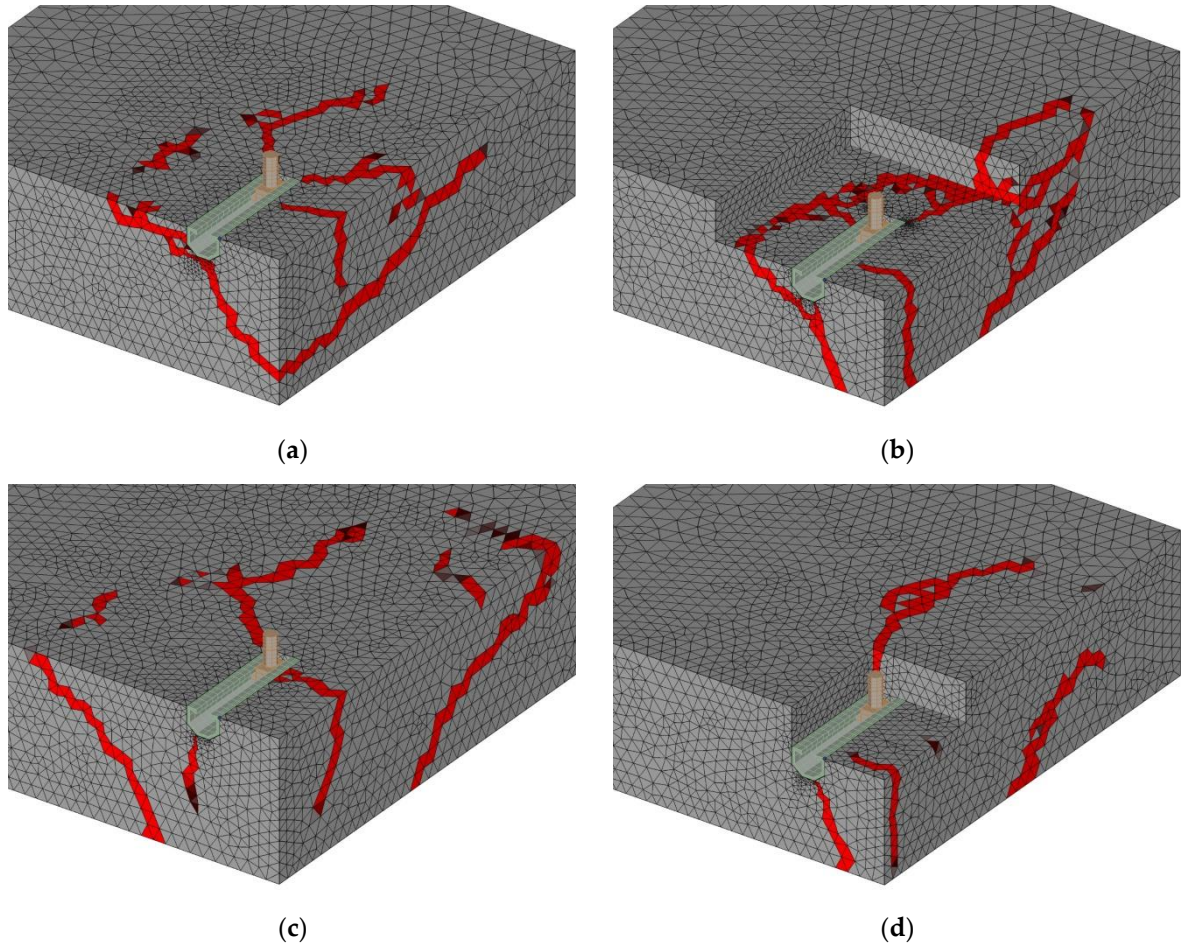
Figure 6.6 Post-peak breakout patterns for: (a) plain slab – h_{ef} = 106 mm; (b) plain slab – h_{ef} = 156 mm; (c) large pocket; (d) small pocket

Table 6.6 Results of the numerical simulations with larger support span for anchor channels in pockets

| d_s	d_b	h_p	h	N_u	$N_u/N_{u,Ref\,(h\,=\,130\,mm)}$	$N_u/N_{u,Ref\,(h\,=\,180\,mm)}$
[mm]	[mm]	[mm]	[mm]	[kN]	[-]	[-]
25	0	50	130	107.30	1.46	1.22
75	50	50	130	100.69	1.37	1.14
125	100	50	130	84.66	1.15	0.96

The pocket dimensions clearly have a significant influence on the results. In order to investigate how each of the two dimensions affects the behavior, further simulations were performed in which one dimension was kept constant and the other dimension was varied. The results in Table 6.7 for a constant distance d_b of 100 mm are very similar to those in Table 6.5, indicating that the dimension of the pocket at the back of the channel has no significant influence on the results. This can be attributed to the fact

113

that the fracture process in case of pockets mostly develops towards the edge. Therefore, the results are presented below are shown as a function of the side distance d_s.

Table 6.7 Results of the numerical simulations for anchor channels in pockets with a constant distance d_b

d_s	d_b	h_p	h	N_u	$N_u/N_{u,Ref\,(h=130\,mm)}$	$N_u/N_{u,Ref\,(h=180\,mm)}$
[mm]	[mm]	[mm]	[mm]	[kN]	[-]	[-]
25	100	50	130	109.71	1.49	1.24
75	100	50	130	98.77	1.34	1.12
125	100	50	130	88.81	1.21	1.01

Figure 6.7 shows the relative capacities $N_u/N_{u,Ref}$ for different embedment depths in relatively thin members as a function of the ratio d_s/h_{ef}. The same configurations were investigated for two pocket heights, i.e., h_p = 25 and 50 mm. A comparable behavior was obtained for different embedment depths. Namely, the influence of pockets can be explained sufficiently well by a linear function, although the results for thinner pocket show a somewhat larger scatter. As can be observed, the slope of the trend line obtained for the thicker pocket is nearly twice as steep as the slope in Figure 6.7b.
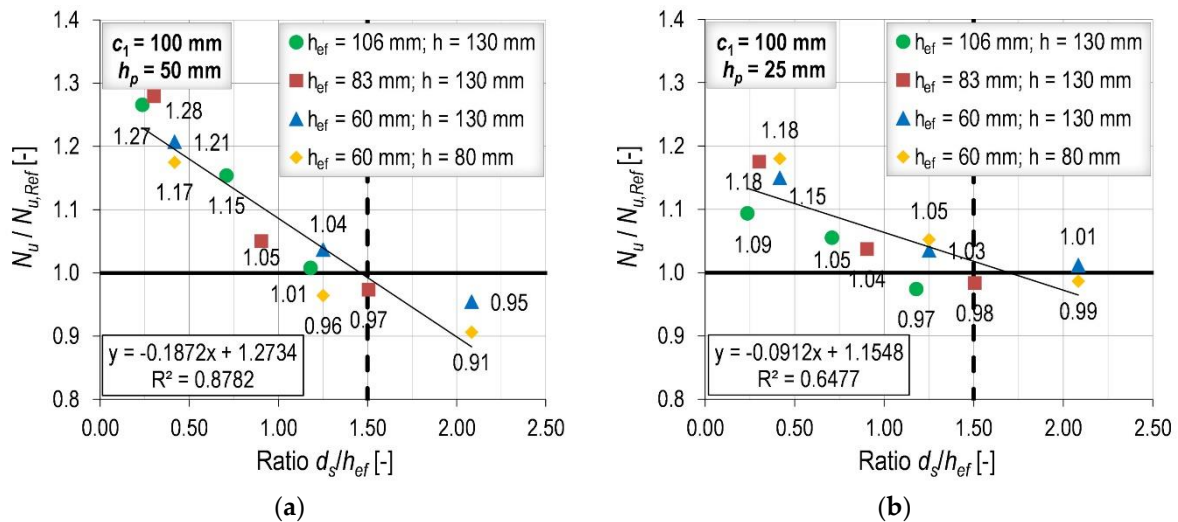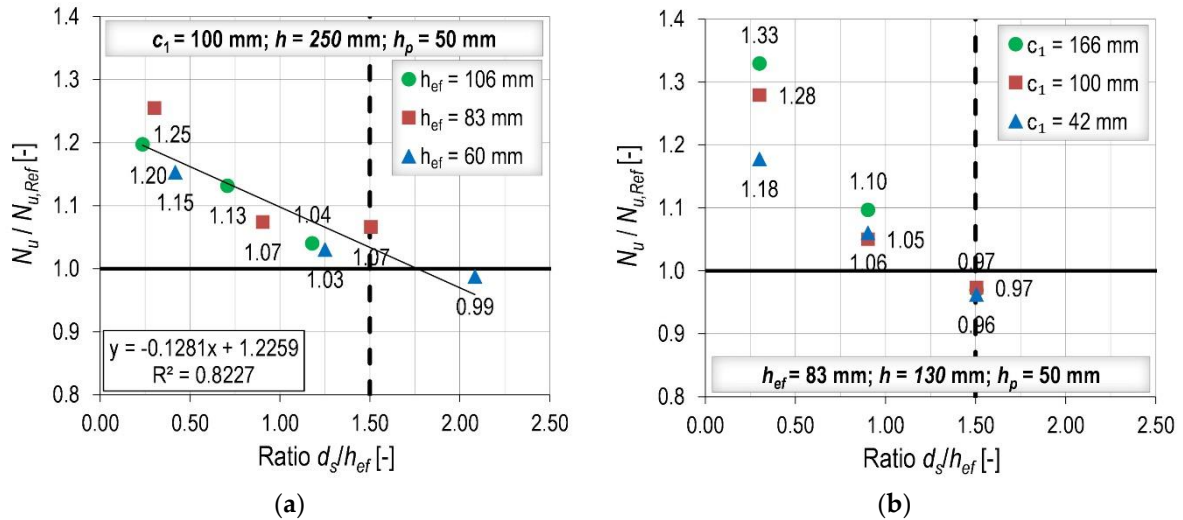

Figure 6.7 Relative capacity as a function of pocket size obtained for different embedment depths and: (a) pocket height of 50 mm; (b) pocket height of 25 mm

The member thickness was found to have a relatively small influence on the capacity in pockets. First, the results for the member thickness h_{ef} = 60 mm are obtained for the member thicknesses in the pocket h = 80 and 130 mm. As can be seen in Figure

6.7, the results are comparable for both investigated pocket heights. Furthermore, Figure 6.8a shows the results for different embedment depths investigated for thicker members, i.e. h = 250 mm. A comparison with the results in thinner members shows a slightly smaller steepness of the fitted trend line.

In addition, the influence of edge distance was investigated as well. The results obtained for the embedment depth h_{ef} = 83 mm are summarized in Figure 6.8b. While the results for the edge distances c_1 = 100 and 166 mm are similar, the relative capacity obtained for the smallest edge distance and the smallest pocket is slightly below these values. However, considering all the obtained results for the influence of edge distance, no significant effect on the capacity in pockets can be observed.

Figure 6.8 Relative capacity as a function of pocket size obtained for: (a) different embedment depths in thick members; (b) different edge distances

### 6.1.2.3 Modification factor for the influence of pockets

As mentioned above, the reference value should be calculated according to chapter 4.2 considering the overall member thickness (h + h_p) and not only the member thickness in the pocket, in order to take into account the influence of bending. The influence of pocket should be accounted for by the following modification factor:

$$\Psi_{p,N} = 1 + 0.004 h_p \cdot \left(-\frac{d_s}{h_{ef}} + 1.5 \right)$$ (6.2)

According to the proposed factor, the behavior of anchor channels in pockets subjected to tension load is described by a linear function based on the ratio between the anchor distance from the pocket wall d_s and the embedment depth h_{ef}. According to the numerical results, this function should intersect the value of one for the ratio d_s/c_1 of about 1.5, as illustrated in Figure 6.7 and Figure 6.8. Therefore, for d_s greater than $1.5h_{ef}$ the modification factor is less than one. In this case, the capacity is smaller than the reference capacity due to the fact that the fracture process takes place within the pocket, i.e. inside the region of reduced member thickness.

Based on the results, the influence of member thickness and the influence of edge distance can be neglected in the design due to their minor effect on the capacity. Therefore, Equation (6.2) account for the influence of pocket height, which multiplies the linear function and changes its slope. The range of pocket heights is relatively narrow in practice, so the proposed modification factor could be simplified by replacing the pocket height with a constant factor. As for the shear load, for an anchor channel with more than two anchors, the proposed equation would apply only for the two outer anchors.

In this form, the proposed modification factor showed an excellent predictability. Based on the 55 simulated configurations with pockets, the average simulation-to-prediction ratio is 1.0 with a standard deviation of 0.048. Moreover, the results do not show any particular trend with respect to the main investigated parameters, as shown in Figure 6.9.
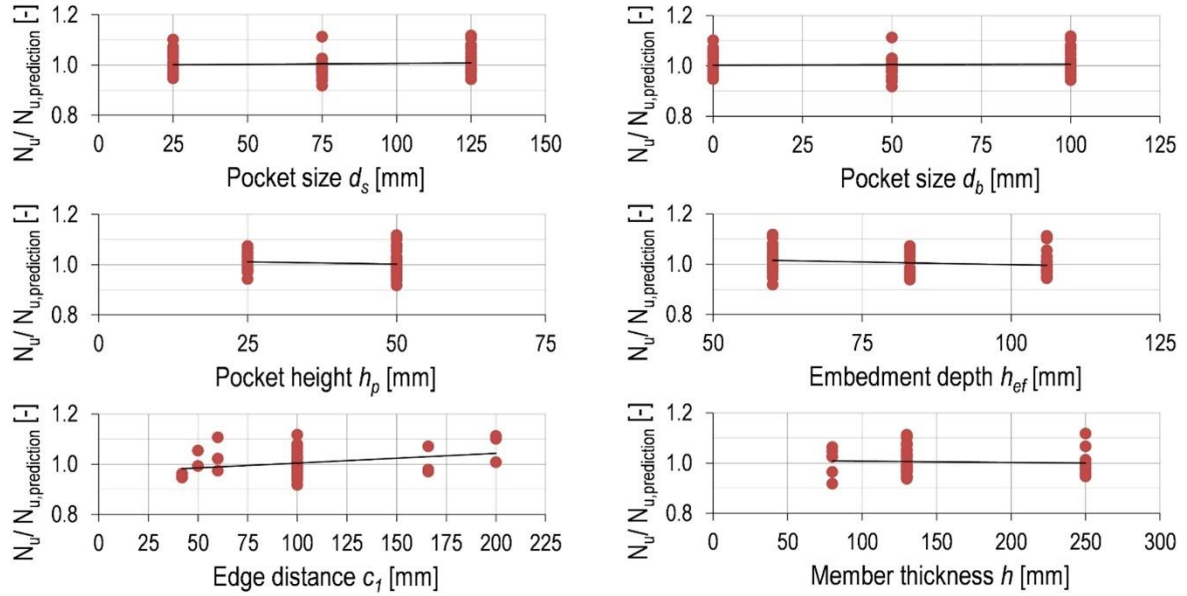
Figure 6.9 Numerical results compared to the design proposal as a function of investigated parameters

6.1.2.4 Experimental investigation

Only one configuration was investigated to serve as a preliminary result for anchor channels in pockets subjected to tension. It was performed as a part of the experimental program in which shear load was investigated (chapter 6.1.1.4). Therefore, everything that was written about the concrete mix applies here as well. The dimensions of the pocket were as follows: d_s = 60 mm, d_b = 40 mm and h_p = 40 mm. As for the shear load, the overall member thickness of 130 mm was chosen and the anchor channels were installed at the edge distance c_1 = 100 mm. The reference tests in plain concrete slabs with the same thickness of the slab inside the pocket (h = 90 mm) were also performed. To enable installation in thin concrete slabs, the shallow anchor channels (HAC-60, s = 200 mm, h_{ef} = 65 mm) were installed. A total of six tests were carried out and the ultimate capacities (normalized to f_c = 20 N/mm^2) are summarized in Table 6.8.

Table 6.8 Test results – installation in pockets (f_c = 20 N/mm²)

Installation	c_1 [mm]	$V_{u,m}$ [kN]	n [-]	σ [kN]	CoV [%]	$V_{u,m}/V_{u,m,Ref}$ [-]	$\Psi_{p,N}$ [-]	$V_{u,m}/\Psi_{p,N}$ [-]	$f_{c,core}$ (CoV) [N/mm²]
Plain	100	33.11	3	1.74	5.27	-	-	-	24.69 (6.18%)
Pocket	100	54.21	3	1.89	3.49	1.64	1.40	1.17	12.99 (11.24%)

As can be seen, the capacity in the pocket was 64% larger than the capacity in the plain concrete slab. This can be attributed to the increased overall member thickness and the intersection with the concrete layer outside the pocket. The breakout pattern typical for splitting failure developed, as shown in Figure 6.10.

Figure 6.10 Breakout pattern for anchor channels in tension installed in pocket

An increase of 40% can be calculated according to the proposal for anchor channels subjected to tension load. This is a significant increase in capacity compared to simply calculating the capacity with the member thickness in the pockets, which could be an approach in engineering judgments. However, the difference between the experimentally obtained value and the calculated value opens up room for further optimization of the modification factor or may be attributed to the very low concrete strength in the case of pockets. Therefore, further experimental investigations are necessary for the installation of anchor channels in pockets.

6.1.3 Conclusions

The effects of pockets, which are common in curtain wall applications to prevent brackets from occupying the usable floor area, were studied. Based on the numerical and limited experimental results, the following conclusions are drawn:

- Several parameters were found to have a significant influence on the shear capacity of anchor channels in pockets, and those are the edge distance, pocket size and height and member thickness.

- An additional modification factor is proposed to be included in the verification of the concrete edge breakout. It is based on a logarithmic function that includes the two most influential factors, i.e., pocket size and edge distance. The comparison with the numerical results were in excellent agreement, while the results of the limited experimental program were slightly on the safe side.

- For the tension load, the ratio between the distance d_s and the embedment depth and the pocket height h_p are the most influential parameters.

- The capacity in pockets should be calculated according to the modified design proposal for tension loaded anchor channels with the overall member thickness and an additional modification factor should be applied. Based on the numerical results, it is based on a linear function that takes the value of one for the ratio $d_s/h_{ef} = 1.5$. Regardless of its simplicity, the modification factor showed good predictability of numerical results.

- Further experimental investigations are needed to confirm and possibly improve the proposed modification factors for shear and tension load.

6.2 Surface reinforcement

According to the current design models, the influence of surface reinforcement cannot be accounted for. However, there is some evidence that it has a positive effect

on the concrete capacity [36], [21]. Indeed, this could be very helpful in the application of anchor channels in curtain walls, especially for the frequently decisive concrete edge capacity. Therefore, the influence of surface reinforcement was briefly investigated numerically and experimentally to obtain preliminary results and lay the foundations for further research.

6.2.1 Shear load

An experimental program was conducted to investigate the influence of reinforcement mesh on concrete edge capacity. The reference configuration was a composite slab with Cofraplus steel decking and an overall member thickness of 160 mm. Anchor channels (HAC-60, $s = 200$ mm) equipped with two shallow anchors ($h_{ef} = 65$ mm) were installed at the edge distance $c_1 = 100$ mm. In addition, three configurations with the presence of reinforcement mesh Q-188 ($\Phi 6 / 150$ mm) were investigated. The concrete cover was varied, i.e., the distance from the concrete surface was 40, 50 and 60 mm. The layout of the mesh is illustrated in Figure 6.11 for two extreme cases. A total of three tests were performed for the reference configuration and one for each of the configurations with reinforcement mesh. The slabs were made from the concrete mix in Table 3.2 and stored under laboratory conditions for one month before being tested. At the time of testing, a concrete cylinder compressive strength $f_c = 20.79$ N/mm^2 was obtained based on the cored cylinders taken out from slabs ($f_{c,core} = 24.69$ N/mm^2, $n = 3$, $CoV = 6.18\%$).

| (a) | (b) |
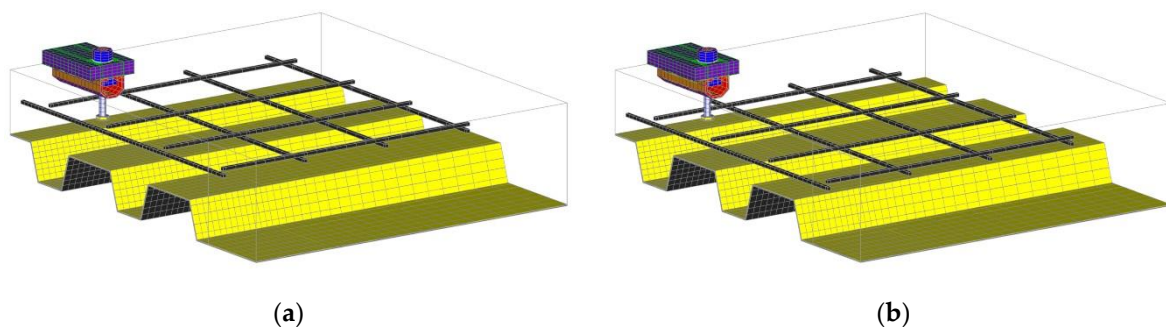
Figure 6.11 The geometry (model) representing: (a) concrete cover of 40 mm; (b) concrete cover of 60 mm

The same configurations, except the configuration with medium concrete cover, were also numerically investigated. The reinforcement was modeled with hexahedral solid elements, assuming a perfect connection with concrete. The orthogonal layers of the reinforcement mesh were not connected to each other, as this would lead to an excessive stiffness of the mesh. The 3D Von Mises yield criterion was used for the simulation of reinforcement with a bilinear stress-strain relationship. The properties of the steel are given in Table 6.9, where $f_{y,s}$ is the steel yield strength, $f_{u,s}$ is the steel ultimate strength and H is the hardening modulus. The macroscopic properties of concrete were determined based on the obtained compressive strength [59]. Symmetry was utilized in the numerical simulations to reduce computational costs, as shown in Figure 6.11.

Table 6.9 Material properties of reinforcement in numerical simulations

| $f_{y,s}$ [N/mm²]	$f_{u,s}$ [N/mm²]	H [N/mm²]	ν [-]	E_s [MPa]
480	580	2000	0.18	210000

The results are summarized in Table 6.10. The experimental results showed that the influence of surface reinforcement strongly depends on the concrete cover. For the smallest concrete cover, an increase of 43% was observed compared to the reference configuration, while it was only 14% for the largest concrete cover. The lower the reinforcement, the smaller the influence of reinforcement. Furthermore, the numerical result for the reference configuration agree excellent with the experimental results, but the configurations with reinforcement show somewhat higher capacities ($V_{u,m}/V_{u,sim} = 0.90$). This can be attributed to the perfect bond between the reinforcement and concrete. The model should be refined in the future with appropriate contact elements that realistically account for stress-slip relationship. Nevertheless, the simulation results showed exactly the same trend as the experimental results.

Table 6.10 Summary of the experimental and numerical results (f_c = 20.79 N/mm²)

Slab type	c_c* [mm]	$V_{u,m}$ [kN]	$V_{u,m} / V_{u,m,Ref}$ [-]	$V_{u,sim}$ [kN]	$V_{u,sim} / V_{u,sim,Ref}$ [-]	$V_{u,m} / V_{u,sim}$ [-]
Plain	-	23.30	1.00	23.15	1.00	1.01
Reinforced	40	33.26	1.43	37.15	1.60	0.90
Reinforced	50	28.06	1.20	-	-	-
Reinforced	60	26.47	1.14	29.33	1.27	0.90

c_c – concrete cover

In general, the configurations with the reinforcement mesh exhibit more ductile behavior. As can be seen in Figure 6.12a, cracking occurs approximately at the failure load of the reference configuration, and thereafter the influence of reinforcement takes place. The previously explained difference between the numerically and experimentally obtained failure loads can be observed, as well as the slightly smaller displacement at the failure load in the simulations due to the slippage in the tests. The breakout patterns for the configurations with the reinforcement mesh had comparable dimensions to the reference model, as shown in Figure 6.12b. However, an additional fracture surface developed in the breakout body at the reinforcement level.
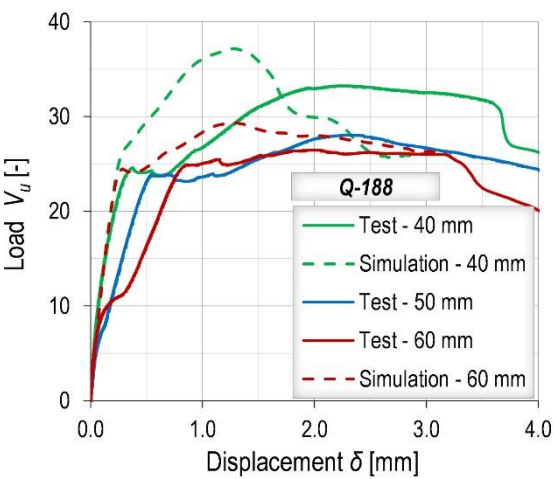

(a)   (b)

Figure 6.12 (a) Comparison between experimental and numerical LD curves obtained for configurations with reinforcement mesh Q-188; (b) Breakout patterns for the reference configuration (upper) and the reinforced configuration with the smallest concrete cover (lower)

6.2.2 Tension load

Two configurations with reinforcement were tested experimentally, as well as the reference tests in plain concrete slabs ($h = 130$ mm). All slabs were reinforced with the reinforcement used for handling purposes to prevent the whole slab from splitting, as shown in Figure 3.2b. The configurations with reinforcement were additionally reinforced in the fracture zone. As illustrated in Figure 6.13, this zone was additionally reinforced with edge reinforcement (2Φ10), hairpin reinforcement (3Φ10 / 300 mm) and reinforcement mesh Q-188. Such an arrangement can be seen on the construction site, especially when diaphragm action of the slab is required (e.g. [64]). The influence of reinforcement was investigated for anchor channels (HAC-60, $s = 250$ mm, $h_{ef} = 106$ mm) installed at two edge distances. A typical edge distance of 100 mm was chosen, as well as the edge distance $c_1 = 216$ mm that represents the characteristic edge distance for concrete (cone) breakout failure for the given parameters.
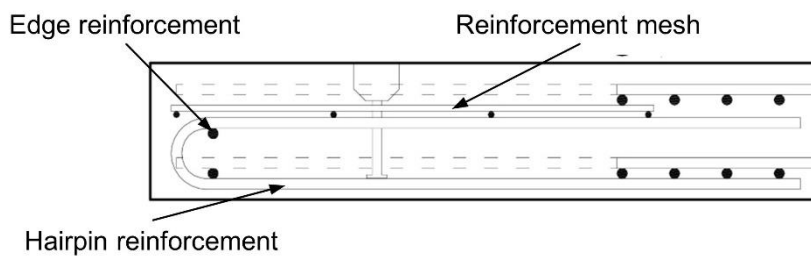
Figure 6.13 Arrangement of reinforcement in the vicinity of anchor channel (cross-section)

The results are summarized in Table 6.11 and normalized to $f_c = 20$ N/mm². Since these tests were part of the experimental program in which pockets were also investigated, the information on the concrete mix, curing and concrete strengths can be found in chapter 6.1.1.4. According to these results, the effectiveness of reinforcement depends on the edge distance. Namely, an increase of 33% was observed for the larger edge distance compared to the reference result (plain concrete), whereas it was 12% for the smaller edge distance. As shown in Figure 6.14 for the larger edge distance, the configuration with reinforcement exhibited a slightly larger displacement at the ultimate load, preceded by the stiffer response.

123
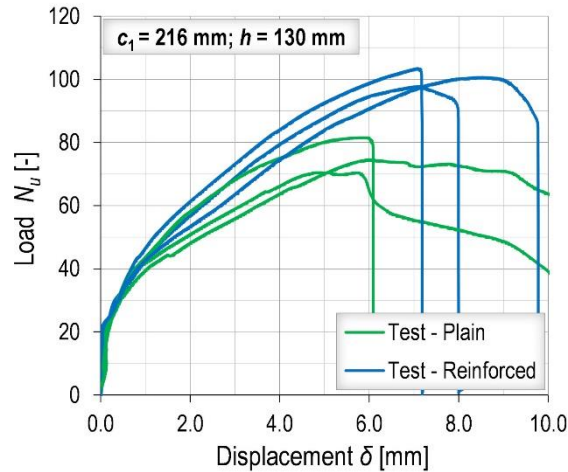
Figure 6.14 Comparison of experimentally obtained LD curves for anchor channels in plain concrete slabs and reinforced slabs

In terms of breakout patterns, the configurations in plain concrete slabs showed a splitting failure influenced by bending, as can be seen in Figure 6.15a. On the other hand, reinforcement increases the stiffness of the edge, i.e. it prevents the separation of concrete in front of the channel. Therefore, the breakout pattern was similar to a typical concrete cone (Figure 6.15b). Moreover, the results for the configurations in plain concrete slabs agree well with the proposed modification of the current code provisions in chapter 4.2.3.

Table 6.11 Summary of the experimental results (f_c = 20 N/mm²)

Slab type	c_1 [mm]	$V_{u,m}$ [kN]	n [-]	σ [kN]	CoV [%]	$N_{u,m}/N_{u,m,Ref}$ [-]	$N_{u,m}/N_{u,proposal}$ [-]	$f_{c,core}$ (CoV) [N/mm²]
Plain	100	69.39	3	0.26	0.38	-	1.00	12.99 (11.24%)
Reinforced	100	77.66	3	3.59	4.62	1.12	-	12.99 (11.24%)
Plain	216	75.53	3	5.61	7.43	-	0.95	16.36 (0.96%)
Reinforced	216	100.60	3	2.84	2.83	1.33	-	16.36 (0.96%)
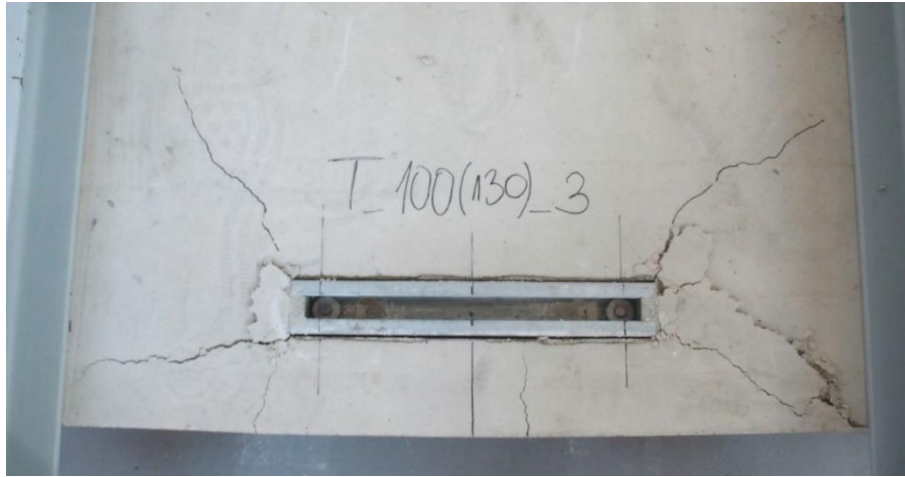
(a)

(b)

Figure 6.15 Breakout pattern for $c_1 = 100$ mm: (a) Plain concrete slab; (b) Reinforced slab

Numerical simulations were performed modeling the reinforcement mesh Q-188 with a concrete cover of 40 mm to determine exclusively the influence of surface reinforcement. The reinforcement was modeled as for shear load. The boundary conditions were applied according to chapter 4.2.1 and the concrete parameters presented in chapter 3.3 were used ($f_c = 20$ N/mm²). As can be seen in Table 6.12, the numerically obtained capacities slightly overestimate the experimental results obtained in plain concrete slabs. This may be due to the limited dimensions of the slabs in the tests, whereas the edges were fixed in the model, or the concrete parameters did not fully correspond to the actual concrete mix. Nevertheless, the relative capacity $N_{u,sim}/N_{u,sim,Ref}$ for the smaller edge distance is equal to the experimentally obtained relative capacity. Therefore, surface reinforcement seems to be much more effective

than edge reinforcement and hairpin reinforcement, although hairpin reinforcement could have been distributed more densely. For the larger edge distance, a relative capacity of 1.19 was observed in the simulations, whereas it was 1.33 in the experiments. According to these results, surface reinforcement contributes the most in the increase of capacity as it reduces the influence of bending in thin members. This is in agreement with the findings of Nilforoush [21] for the headed studs without the edge influence, where an increase of up to 30% was observed in thin members. However, further investigations are necessary to investigate all potentially influencing parameters (edge distance, reinforcement arrangement, etc.).

Table 6.12 Summary of the numerical results (f_c = 20 N/mm²)

Slab type	c_1 [mm]	$V_{u,sim}$ [kN]	$N_{u,sim}/N_{u,sim,Ref}$ [-]	$N_{u,m}/N_{u,sim}$
Plain	100	73.39	-	0.95
Reinforced	100	82.46	1.12	-
Plain	216	83.06	-	0.91
Reinforced	216	98.83	1.19	-

6.2.3 Conclusions

Based on the numerical and experimental results, the positive influence of surface reinforcement is definitely benefit that should be accounted for. According to the performed preliminary investigation, the following conclusions are drawn:

- Concrete edge breakout is usually the decisive failure mode in the curtain wall applications. The limited capacity can be significantly increased by surface reinforcement, up to almost 50% with relatively small amount of reinforcement, although its effectiveness depends on the concrete cover.

- The performance of anchor channels loaded in tension can also be improved by adding surface reinforcement, especially in thin members where the reinforcement reduces the influence of bending. Based on this investigation, reinforcement mesh (Q-188) can bring up to 20% for the investigated configurations.

- Further numerical and experimental studies are necessary to investigate this topic in detail, considering various positions and amount of reinforcement.

7
CONCLUSIONS

7.1   Summary

In this thesis, anchor channels installed at the top of the un-cracked slabs were investigated under static tension and shear load. The main focus was placed on the influence of the complex geometry of composite slabs with profiled steel decking and pockets on the concrete capacity, as there are no existing guidelines on this subject. Moreover, due to an increasing need for anchor channels with shallow embedment depths and to provide a sound reference for additional modification factor, the current design models were examined. The results and contributions of the thesis are summarized as follows:

- Concrete edge breakout is frequently decisive failure mode in curtain wall applications and its capacity significantly depends on the member thickness. It was observed that the modification factor $\Psi_{ch,h,V}$ in the current form overestimates the capacity for thin members, whereas the characteristic member thickness tends to be conservative for larger edge distances. Therefore, a linear function is proposed for the small $h/h_{cr,V}$ ratios:

$$\Psi_{ch,h,V} = \left(\frac{h}{h_{cr,V}}\right)^{0.5} \leq 1.0 \quad \text{if } \frac{h}{h_{cr,V}} > 0.5 \tag{7.1}$$

$$\Psi_{ch,h,V} = \sqrt{2}\,\frac{h}{h_{cr,V}} \qquad\qquad \text{if } \frac{h}{h_{cr,V}} \le 0.5\,,$$

and the characteristic member thickness is modified by decreasing the exponent of the edge distance:

$$h_{cr,V} = 8.25 c_1^{2/3} + 2 h_{ch}\,. \tag{7.2}$$

- In order to investigate the influence of complex geometry of composite slabs on the shear capacity, various parameters were varied (e.g., orientation and type of the steel decking, member thickness, edge distance, etc.). Based on the results, an additional modification factor $\Psi_{com,V}$ is proposed:

$$\Psi_{com,V} = \Psi_{com,90°,V} \quad \text{for perpendicular orientation of the steel decking.}$$
$$= \Psi_{com,0°,V} \quad \text{for parallel orientation of the steel decking.} \tag{7.3}$$

For the perpendicular orientation, it was found that the influence of anchor position and edge distance can be neglected. The capacity reduction can be accurately predicted by the volume of concrete that is missing in the breakout body. Therefore, the simplified engineering design approach is proposed, based on the Concrete Volume parameter V_c:

$$\Psi_{com,90°,V} = \frac{V_c}{h} \cdot k_p \le 1.0\,[-]\,, \tag{7.4}$$

with $k_p = 0.95$ for re-entrant profiles, and $k_p = 1.0$ for trapezoidal profiles.

In case of parallel orientation, on the other hand, the capacity reduction significantly depends on the position of anchor channel with respect to the steel decking and on the edge distance and member thickness. Therefore, a linear function is proposed:

$$\Psi_{com,0°,V} = 0.2\gamma + 1.12\left(1 - \frac{h_p}{h}\right)^{0.5} \le 1.0\,[-]\,, \tag{7.5}$$

where parameter γ represents the ratio between the position of anchor channel and edge distance:

$$\gamma = \frac{d_f}{c_1} \left[\frac{m}{m}\right].\tag{7.6}$$

- The behavior of anchor channels subjected to shear in pockets significantly depends on the pocket size and edge distance, i.e. on the volume of the intersected concrete outside the pocket. In addition, member thickness and pocket height are also parameters that should be accounted for. Therefore, the reference value should be calculated with the member thickness in the pocket and the influence of pocket geometry is taken in account as follows:

$$\Psi_{p,V} = 1 - 0.2 \cdot \left(\frac{h}{h_{cr,V}}\right)^{-\frac{3}{4}} \cdot \left(\frac{h_p}{50}\right)^{\frac{3}{4}} \cdot ln\left(\frac{d_s}{c_1} + 0.15\right) \geq 1.0\ [-]\tag{7.7}$$

with $h_p \leq 65$ mm and $h \leq h_{cr,V}$.

- Additional modification factors $\Psi_{com,V}$ and $\Psi_{p,V}$ for shear load should be included in the basic equation for concrete edge breakout:

$$V_{Rk,c} = V_{Rk,c}^0 \cdot \Psi_{ch,s,V} \cdot \Psi_{ch,c,V} \cdot \Psi_{ch,h,V} \cdot \Psi_{ch,90°,V} \cdot \Psi_{re,V} \cdot \Psi_{com,V} \cdot \Psi_{p,V}\ [N],\tag{7.8}$$

- The model for concrete splitting failure is modified to improve its predictability. Due to different design rules in Europe and the US, the current model in EN 1992-4 [26] is chosen as the basis and the necessary modification are proposed:

$$N_{Rk,sp} = N_{Rk}^0 \cdot \Psi_{ch,s,N} \cdot \Psi_{ch,c,N} \cdot \Psi_{ch,e,N} \cdot \Psi_{re,N} \cdot \Psi_{h,sp}\ [N].\tag{7.9}$$

First, an additional calibrating factor of 1.15 is included in the equation for the basic resistance:

$$N_{Rk}^0 = 1.15 \cdot min\left(N_{Rk,c}^0, N_{Rk,p}\right).\tag{7.10}$$

Next, only minor change is proposed for the modification factor that takes into account the influence of member thickness. Namely, the value h_{min} is replaced by the embedment depth h_{ef} as it is a physical dimension:

$$\Psi_{h,sp} = \left(\frac{h}{h_{ef}}\right)^{2/3} \leq max\left\{1; \left(\frac{h_{ef} + c_{cr,N}}{h_{min}}\right)^{2/3}\right\} \leq 2.0 .\tag{7.11}$$

A linear function is proposed for the influence of edge instead of exponential function with an exponent of 0.5:

$$\Psi_{ch,e,N} = 0.52 + 0.08\frac{c_1}{h_{ef}} \leq 1.0 . \tag{7.12}$$

According to the equation, the edge influence vanishes for the edge distance $c_1 = 6h_{ef}$, which is substantially greater value than the current characteristic edge distance $c_{cr,sp} = 3h_{ef}$. Due to this, the characteristic anchor spacing is also doubled:

$$s_{cr,sp} = 2c_{cr,sp} = 12h_{ef} . \tag{7.13}$$

- The influence of support span is pronounced for anchor channels subjected to tension in composite slabs. The investigation was performed with a support span of $2.5h_{ef}$ and the following modification factor is proposed based on the position of the anchor channels:

$$\Psi_{com,N} = 0.8 \text{ for the installation in perimeter beam.}$$
$$= h_c/h \text{ for the installation over the steel decking,} \tag{7.14}$$

where h_c represents the concrete layer above the trapezoidal steel decking.

- The behavior of anchor channels subjected to tension in pockets can be well explained by a linear function that depends on the pocket size d_s and embedment depth h_{ef}. In addition to these two most influential factors, the pocket height h_p is another parameter that should be considered. The reference capacity should be calculated with the overall member thickness and the following factor accounts for the influence of pockets:

$$\Psi_{p,N} = 1 + 0.004h_p \cdot \left(-\frac{d_s}{h_{ef}} + 1.5\right) \tag{7.15}$$

- The reference capacity should be determined by evaluating all the concrete failure modes and the decisive value should be multiplied by the additional modification factors.

7.2 Future research

Given the current trend in the construction industry towards thinner and lighter concrete members, the fastening technology and the corresponding design models should adapt. The challenges in defining an appropriate design method for anchor channels, and in general for all fastening systems in thin concrete members, are mainly due to the fact that the load introduced by the fastening system often causes substantial stresses in the concrete member. This is particularly important for anchor channels subjected to tension. The author sees a need for further research on the following topics:

- The interaction between the global stresses (due to shear or bending) and the local stresses introduced by the fastening element should be considered, especially in composite slabs.

- The influence of corners on the capacity of anchor channels in thin members should be clarified.

- Further numerical and experimental investigations for anchor channels without edge influence are required to determine how to consider the influence of member thickness in the verification for concrete (cone) breakout.

- The influence of surface reinforcement should be studied in detail, as the performance of anchor channels in thin members could be significantly improved without the need for specific solutions.

Other than that, further experimental investigations on configurations with complex geometries, such as composite slabs and pockets, would be useful. These additional results could serve to verify the proposed models or to improve and simplify them.

REFERENCES

[1] Eligehausen, R., Mallee, R., Silva, JF. (2006) *Anchorage in concrete construction*. Ernst & Sohn, Berlin, Germany.

[2] Mahrenholtz, C., Ayoubi, M., Müller, S., Bachschmid, S. (2019) Tension and shear performance of anchor channels with channel bolts cast in Fibre Reinforced Concrete (FRC). *IOP Conference Series: Materials Science and Engineering* **615**, 012089.

[3] Hilti (2019) *Cast-in Anchor Channel Fastening Technical Guide*. Hilti Inc. (U.S.), Dallas, TX.

[4] Rackham, JW., Couchman, GH., Hicks, SJ. (2009) *Composite slabs and beams using steel decking: Best practice for design and construction*. MCRMA/SCI, London, UK.

[5] Ožbolt, J., Li, Y., Kožar, I. (2001) Microplane model for concrete with relaxed kinematic constraints. *International Journal of Solids and Structures* **38(16)**, 2683-2711.

[6] Bažant, ZP., Oh, B. (1983) Crack band theory for fracture of concrete. *Materials and Structures* **16(93)**, 155-177.

[7] Oluokun, FA., Burdette, EG. (1993) Behavior of channel anchors in thin slabs under combined shear and tension (pullout) loads. *ACI Structural Journal* **90(4)**, 407-413.

[8] Kraus, J. (2003) *Tragverhalten und Bemessung von Ankerschienen unter zentrischer Zugbelastung (Load bearing behavior and design of channel bars under centric tension loads)*. University of Stuttgart, Stuttgart, Germany, Doctoral thesis.

[9] Potthoff, M. (2008) *Tragverhalten und Bemessung von Ankerschienen unter Querbelastung (Behavior and design of anchor channels under shear load)*. University of Stuttgart, Stuttgart, Germany, Doctoral thesis.

[10] Wohlfahrt, R. (1996) *Tragverhalten von Ankerschienen ohne Rückhängebewehrung (Behavior of anchor channels without supplementary reinforcement)*. University of Stuttgart, Stuttgart, Germany, Doctoral thesis.

[11] Park, J., Plamper-Hellwig, D. (2012) Untersuchung des Tragwiderstandes von Ankerschienensystemen unter Erdbebenbeanspruchungen (Investigation of the

capacity of anchor channel systems under earthquake loads). *Bauingenieur* **87**, 3-8.

[12] Güres, S. (2005) *Zum Tragverhalten von Ankerschienenbefestigungen unter Nichtruhenden Beanspruchungen (Load bearing behaviour of anchor channels under fatigue loads)*. Ruhr University Bochum, Bochum, Germany, Doctoral thesis.

[13] Hanenkamp, W., Güres, S. (2004) Zum Tragverhalten von Ankerschienen unter ermüdungsrelevanten Ein-wirkungen. *Stahlbau* **73**, 668-675.

[14] Fröhlich, T., Lotze, D. (2021) Testing and evaluation of anchor channels under fatigue loading. *CivilEng* **2(1)**, 1-13.

[15] Mahrenholtz, C., Sharma, A. (2019) Qualification and design of anchor channels with channel bolts according to the new EN 1992-4 and ACI 318. *Structural Concrete* **21(1)**, 94-106.

[16] Furche, J. (1994) *Zum Trag- und Verschiebungsverhalten von Kopfbolzen bei zentrischem Zug (Load-bearing and displacement behaviour of headed anchors under axial tension loading)*. University of Stuttgart, Stuttgart, Germany, Doctoral thesis.

[17] Hofmann, J., Eligehausen, R. (2002) Lokaler Betonausbruch bei randnahen Befestigungen mit Kopfbolzen (Local blow-out failure with headed anchors close to an edge). In : *fib Special Acitivty Group*, Beijing, China.

[18] Fuchs, W., Eligehausen, R., Breen, JE. (1995) Concrete capacity design (CCD) approach for fastenings to concrete. *ACI Structural Journal* **2(1)**, 73-94.

[19] Eligehausen, R., Ožbolt, J. (1990) Size effect in anchorage behavior. In : *ECF8, Fracture Behavior and Design of Materials and Structures*, Turin, Italy.

[20] EN 1994-1-1 (2004) *Eurocode 4 – Design of composite steel and concrete structures – Part 1-1: General rules and rules for buildings.*, European Committee for Standardization (CEN), Brussels, Belgium.

[21] Nilforoush, R. (2017) *Numerical and experimental evaluations of load-carrying capacity of cast-in-place headed anchors and post-installed adhesive anchors*. University of Lulea, Lulea, Sweden, Doctoral thesis.

[22] Grosser, P., Dimitrova, T., Winkler, B. (2017) Anchor channels with short embedment depth used in composite slab construction. In : *3rd International Symposium on Connections between Steel and Concrete*, Stuttgart, Germany.

[23] Asmus, J. (1999) *Bemessung von zugbeanspruchten Befestigungen bei der Versagensart Spalten des Betons (Design of tension loaded anchorages for the splitting failure mode)*. University of Stuttgart, Stuttgart, Germany, Doctoral thesis.

[24] Asmus, J., Eligehausen, R. (2007) Design method for splitting failure mode of fastenings. In : *2nd International Symposium on Connections between Steel and Concrete*, Stuttgart, Germany.

[25] Hüer, T. (2014) *Tragverhalten von randnahen zugbeanspruchten Befestigungen bei der Versagensart Spalten des Betons (Behavior of tension loaded fasteners near the edge for the concrete splitting failure mode)*. University of Stuttgart, Stuttgart, Germany, Doctoral thesis.

[26] EN 1992-4 (2018) *Eurocode 2 – Design of concrete structures – Part 4: Design of fastenings for use in concrete (EN 1992-4:2018).*, European Committee for Standardization (CEN), Brussels, Belgium.

[27] Zhao, G. (1993) *Tragverhalten von randfernen Kopfbolzenverankerungen bei Betonbruch (Behaviour of headed anchors remote to an edge at concrete failure)*. University of Stuttgart, Stuttgart, Germany, Doctoral Thesis.

[28] Eligehausen, R., Lehr, B. (1993) *Querzugtragfähigkeit von Dübeln mit großem Randabstand (Shear capacity of anchors with large edge distances).*, Report No. 10/20-93/11, University of Stuttgart, Stuttgart, Germany.

[29] Jebara, K. (2018) *Pryout capacity and bearing behavior of stocky headed stud anchorages*. University of Stuttgart, Stuttgart, Germany, Doctoral thesis.

[30] Zhao, G., Fuchs, W., Eligehausen, R. (1989) *Einfluß der Bauteildicke auf das Tragverhalten von Dübelbefestigungen im ungerissenen Beton unter Querzugbeanspruchung (Influence of component thickness on the load-bearing behaviour of anchors in non-cracked concrete under shear loading).*, Report No. 10/12A-89/5, University of Stuttgart, Stuttgart, Germany.

[31] Hofmann, J. (2004) *Tragverhalten und Bemessung von Befestigungen am Bauteilrand unter Querlasten mit beliebigem Winkel zur Bauteilkante (Load-bearing behaviour and design of fasteners close to an edge under shear loading in an arbitrary angle to the edge)*. University of Stuttgart, Stuttgart, Germany, Doctoral thesis.

[32] Grosser, P. (2012) *Load-bearing behavior and design of anchorages subjected to shear and torsion loading in uncracked concrete*. University of Stuttgart, Stuttgart, Germany, Doctoral thesis.

[33] Potthoff, M., Grewin, Y., Eligehausen, R. (2004) Design of channel bars under shear load. In : *FRAMCOS 5, Fracture Mechanics of Concrete Structures*, Vail, USA.

[34] Schmid, K. (2010) *Tragverhalten und Bemessung von Befestigungen am Bauteilrand mit Rückhängebewehrung unter Querlasten rechtwinklig zum Rand (Behavior and design of fastenings at the edge with anchor reinforcement under shear loads towards the edge)*. University of Stuttgart, Stuttgart, Germany, Doctoral thesis.

[35] Sharma, A., Eligehausen, R., Asmus, J. (2017) A new model for concrete edge failure of multiple row anchorages with supplementary reinforcement - reinforcement failure. *Structural Concrete* **18(6)**, 893-901.

[36] Konertz, D., Kocur, GK., Häusler, F., Mark, P. (2017) Concrete breakout strength of anchor channels in edge and corner situations under perpendicular shear

loading. In : *3rd International Symposium on Connections between Steel and Concrete*, Stuttgart, Germany.

[37] CEN/TS1992-4 (2009) *Part 1 to 5: Design of fastenings for use in concrete.*, European Committee for Standardization (CEN), Brussels, Belgium.

[38] EAD330008-03-0601 (2018) *Anchor channels, European assessment document, OJEU 2018/C.*, European Organisation for Technical Approvals (EOTA), Brussels, Belgium.

[39] ACI 318 (2014) *Building code requirements for structural concrete (ACI 318-14) and commentary (ACI 318R-14).*, American Concrete Institute, Farmington Hills, MI.

[40] AC232 (2019) *Acceptance criteria for anchor channels in concrete elements.*, International Code Council Evaluation Service (ICC-ES), Whittier, CA.

[41] Mahrenholtz, C., Sharma, A. (2020) Load capacity of shallow embedded anchor channels. *CivilEng* **1(3)**, 243-252.

[42] Casucci, D., Grosser, P., Schwenn, M., Zeman, O. (2019) Influence of edge reinforcement on the concrete breakout strength of anchor channels close to the edge of a concrete member. *CE papers* **3(2)**, 219-225.

[43] EOTA TR 047 (2015) *Calculation Method for the Design of Anchor Channels.*, European Organisation for Technical Approvals (EOTA), Brussels, Belgium.

[44] Ožbolt, J., Tonković, Z., Lacković, L. (2015) Microplane model for steel and application on static and dynamic fracture. *Journal of Engineering Mechanics* **142(2)**, 04015086.

[45] Gambarelli, S., Ožbolt, J. (2021) 3D hygro-mechanical meso-scale model for wood. *Construction and Building Materials* **311**, 125283.

[46] Taylor, GI. (1938) Plastic strains in metals. *Journal of the Institute of Metals* **62**, 307-324.

[47] Bažant, ZP., Gambarova, P. (1984) Crack shear in concrete: Crack band microplane model. *Journal of Engineering Mechanics* **110**, 2015-2035.

[48] Bažant, ZP., Pratt, PC. (1988) Microplane model for brittle-plstic materials - parts I and II. *Journal of Engineering Mechanics* **114(10)**, 1672-1702.

[49] Bažant, ZP., Ožbolt, J. (1990) Nonlocal microplane model for fracture, damage and size effect in structures. *Journal of Engineering Mechanics* **116(11)**, 2485-2504.

[50] FEMAP® (2015) *v11.2.2, [Computer Software]*.

[51] Jirasek, M., Bauer, M. (2012) Numerical aspects of the crack band approach. *Computers and Structures* **110**, 60-78.

[52] Ožbolt, J., Gambarelli, S. (2018) Microplane model with relaxed kinematic constraint in the framework of micro polar Cosserat continuum. *Engineering Fracture Mechanics* **199**, 476-488.

[53] Oliver, J. (1989) A consistent characteristic length for smeared cracking models. *International Journal for Numerical Methods in Engineering* **28(2)**, 461-474.

[54] Ožbolt, J., Sharma, A., Reinhardt, HW. (2011) Dynamic fracture of concrete compact tension specimen. *International Journal of Solids and Structures* **48(10)**, 1534-1543.

[55] Ožbolt, J., Bošnjak, J., Sola, E. (2013) Dynamic fracture of concrete compact tension specimen: experimental and numerical study. *International Journal of Solids and Structures* **50**, 4270-4278.

[56] Ožbolt, J., Oršanić, F., Balabanić, G. (2014) Modeling pull-out resistance of corroded reinforcement in concrete: Coupled three-dimensional finite element model. *Cement and Concrete Composites* **46**, 41-55.

[57] ETA-11/0006 (2016) *Hilti anchor channels (HAC) with channel bolts (HBC).*, DIBt, Berlin, Germany.

[58] RILEM TC50-FMC (1985) Determination of the fracture energy of mortar and concrete by means of three-point bend tests on notched beams. *Materials and Structures* **18(106)**, 285-290.

[59] CEB-FIP (1993) *Model Code 90.*, Comité Euro-International du Béton (CEB) and Fédération Internationale de la Précontrainte (FIP), London, UK.

[60] Fichtner, S. (2005) *Implementierung einer Kontaktschicht mit Reibeigenschaften für kleine Verformungen in das Programm MASA.*, Prüfbericht Nr. HT 141/01-04/8, University of Stuttgart, Stuttgart, Germany.

[61] Jebara, K., Ožbolt, J., Hoffman, J. (2016) Pryout failure of single headed stud anchor : 3D numerical FE analysis. *Materials and Structures* **49**, 4551-4563.

[62] Bede, N., Grosser, P., Ožbolt, J. (2017) Shear breakout capacity of various fastening systems in concrete elements. *Građevinar* **69(12)**, 1093-1100.

[63] SMD (2013) *Metal Decking Specialists: Technical Manual and Guidance Notes*. Structural Metal Decks ltd, Dorset, UK.

[64] Clifton, GC., El Sarraf, R. (2005) *Composite floor construction Handbook.*, Report R4-107. N. Z. HERA, Manukau City, New Zealand.

LIST OF FIGURES

LIST OF TABLES

APPENDICES

Appendix A – Validation of numerical model

Table A.1 Numerical results – the influence of concrete properties, boundary conditions and mesh size

Description	$f_{c,mean}$ [N/mm²]	c_1 [mm]	h [mm]	s [mm]	h_{ef} [mm]	$\delta(V_u)$ [mm]	V_u [kN]
Plain slab – low strength	20	100	130	200	106	0.25	22.92
Composite slab – low strength	20	100	130	200	106	0.22	17.55
Plain slab – medium strength	27.69	100	130	200	106	0.28	28.67
Plain slab – medium strength; boundary conditions	27.69	100	130	200	106	0.28	28.25
Composite slab – medium strength	27.69	100	130	200	106	0.25	22.43
Plain slab – high strength	40	100	130	200	106	0.31	37.24
Composite slab – high strength	40	100	130	200	106	0.25	27.39
Plain slab – medium strength; fine mesh	27.69	100	130	200	106	0.28	28.51
Plain slab – medium strength; coarse mesh	27.69	100	130	200	106	0.25	29.33

Appendix B – Anchor channels in plain concrete slabs (shear)

Table B.1 Numerical simulations – influence of member thickness ($f_{c,mean}$ = 20 N/mm²)

c_1	h	h_{ch}	s	V_u	$V_u/V_{u,Ref}$	$\Psi_{ch,h,V\ code}$	$\Psi_{ch,h,V\ proposal}$
[mm]	[mm]	[mm]	[mm]	[kN]	[-]	[-]	[-]
100	300	31	300	34.98	1.00	1.00	1.00
100	210	31	300	32.59	0.93	0.90	0.94
100	160	31	300	29.67	0.85	0.78	0.82
100	130	31	300	26.16	0.75	0.70	0.74
100	100	31	300	20.64	0.59	0.62	0.59
100	70	31	300	14.17	0.41	0.52	0.41
100	300	17	300	37.93	1.00	1.00	1.00
100	210	17	300	36.81	0.97	0.95	1.00
100	160	17	300	33.48	0.88	0.83	0.87
100	130	17	300	29.94	0.79	0.75	0.78
100	100	17	300	25.48	0.67	0.65	0.67
100	70	17	300	18.05	0.48	0.55	0.47
100	350	48	300	32.98	1.00	1.00	1.00
100	300	48	300	32.34	0.98	1.00	1.00
100	210	48	300	29.38	0.89	0.84	0.88
100	160	48	300	25.82	0.78	0.74	0.76
100	130	48	300	22.00	0.67	0.66	0.67
100	100	48	300	16.71	0.51	0.58	0.52
200	500	31	250	78.67	1.00	1.00	1.00
200	350	31	250	78.22	0.99	0.87	1.00
200	230	31	250	65.20	0.83	0.71	0.82
200	160	31	250	49.44	0.63	0.59	0.66
200	130	31	250	42.93	0.55	0.53	0.53
200	100	31	250	33.98	0.43	0.47	0.41
200	70	31	250	24.27	0.31	0.39	0.29
300	700	31	250	121.19	1.00	1.00	1.00
300	500	31	250	118.16	0.98	0.87	1.00
300	420	31	250	116.47	0.96	0.80	0.99
300	330	31	250	103.66	0.86	0.71	0.87
300	240	31	250	86.17	0.71	0.60	0.75
300	160	31	250	66.43	0.55	0.49	0.52
300	130	31	250	55.95	0.46	0.44	0.43
300	100	31	250	44.51	0.37	0.39	0.33
300	100	31	250	32.53	0.27	0.33	0.23

Appendix C – Anchor channels in plain concrete slabs (tension)

Table C.1 Numerical simulations – influence of member thickness ($f_{c,mean}$ = 20 N/mm^2)

c_1 [mm]	h_{ef} [mm]	h [mm]	s [mm]	N_u [kN]	$N_{u,CB}$ [1] [kN]	$N_{u,proposal}$ [2] [kN]	$N_u/N_{u,decisive}$ [3] [-]
100	60	75	250	33.46	40.20	28.47	1.18
100	60	90	250	39.38	40.20	32.15	1.22
100	60	105	250	43.25	40.20	35.63	1.21
100	60	130	250	45.91	40.20	41.09	1.14
100	60	150	250	46.29	40.20	42.67	1.15
100	60	180	250	46.16	40.20	42.67	1.15
100	100	110	250	66.39	76.87	59.82	1.11
100	100	125	250	69.39	76.87	65.15	1.07
100	100	150	250	77.51	76.87	73.56	1.05
100	100	175	250	82.40	76.87	81.53	1.07
100	100	200	250	84.09	76.87	89.12	1.09
100	100	250	250	85.26	76.87	93.03	1.11
200	100	110	250	79.71	108.72	67.80	1.18
200	100	125	250	81.87	108.72	73.83	1.11
200	100	150	250	90.93	108.72	83.37	1.09
200	100	175	250	94.40	108.72	92.40	1.02
200	100	200	250	104.47	108.72	101.00	1.03
200	100	250	250	105.80	108.72	105.43	1.00
100	120	130	250	80.20	93.66	76.13	1.05
100	120	150	250	86.72	93.66	83.75	1.04
100	120	180	250	98.72	93.66	94.58	1.05
100	120	210	250	101.96	93.66	104.81	1.09
100	120	240	250	102.00	93.66	114.57	1.09
100	175	193	250	129.21	153.06	129.24	1.00
100	175	220	250	149.80	153.06	141.27	1.06
100	175	260	250	154.79	153.06	157.91	1.01
100	175	306	250	158.54	153.06	176.03	1.04
100	175	350	250	157.74	153.06	181.85	1.03

[1] *EN 1992-4 – concrete breakout failure ($\alpha_{ch,N}$ according to [22] for h_{ef} = 60 mm)*

[2] *Modified design proposal for splitting failure mode*

[3] *$N_{u,decisive}$ represents smaller of the two calculated capacities*

Table C.2 Numerical simulations – influence of edge distance ($f_{c,mean}$ = 20 N/mm^2)

c_1	h_{ef}	h	s	N_u	$N_{u,CB}$ [1]	$N_{u,proposal}$ [2]	$N_u/N_{u,decisive}$ [3]
[mm]	[mm]	[mm]	[mm]	[kN]	[kN]	[kN]	[-]
60	60	75	250	31.04	31.14	26.15	1.19
100	60	75	250	33.46	40.20	28.47	1.18
150	60	75	250	36.07	47.90	31.38	1.15
180	60	75	250	38.06	47.90	33.12	1.15
240	60	75	250	44.29	47.90	36.61	1.21
360	60	75	250	47.38	47.90	43.58	1.09
∞	60	75	250	49.37	47.90	/	1.03
60	60	130	250	36.85	31.14	37.73	1.18
100	60	130	250	45.91	40.20	41.09	1.14
150	60	130	250	50.33	47.90	45.28	1.11
180	60	130	250	50.78	47.90	47.79	1.06
240	60	130	250	52.53	47.90	52.82	1.10
∞	60	130	250	53.88	47.90	/	1.12
50	100	125	250	57.55	54.36	60.80	1.06
100	100	125	250	69.39	76.87	65.15	1.07
150	100	125	250	75.83	94.15	69.49	1.09
200	100	125	250	81.87	108.72	73.83	1.11
300	100	125	250	91.89	110.81	82.52	1.11
∞	100	125	250	114.12	110.81	/	1.03
50	100	150	250	63.43	54.36	68.66	1.17
100	100	150	250	77.51	76.87	73.56	1.05
150	100	150	250	86.29	94.15	78.47	1.10
200	100	150	250	90.93	108.72	83.37	1.09
∞	100	150	250	114.12	110.81	/	1.03
50	100	200	250	65.74	54.36	83.18	1.21
100	100	200	250	84.09	76.87	89.12	1.09
150	100	200	250	90.43	94.15	95.06	0.96
200	100	200	250	104.47	108.72	101.00	1.03
300	100	200	250	109.84	110.81	112.88	0.99
∞	100	200	250	123.06	110.81	/	1.11
100	175	193	250	129.21	153.06	129.24	1.00
350	175	193	250	173.13	250.95	155.34	1.11
∞	175	193	250	264.75	250.95	/	1.06
100	175	350	250	157.74	153.06	181.85	1.03
262	175	350	250	193.99	247.74	205.66	0.94
∞	175	350	250	255.28	250.95	/	1.02

[1] *EN 1992-4 – concrete breakout failure ($\alpha_{ch,N}$ according to [22] for h_{ef} = 60 mm)*

[2] *Modified design proposal for splitting failure mode*

[3] *$N_{u,decisive}$ represents smaller of the two calculated capacities*

Table C.3 Numerical simulations – influence of anchor spacing ($f_{c,mean}$ = 20 N/mm²)

c_1 [mm]	h_{ef} [mm]	h [mm]	s [mm]	N_u [kN]	$N_{u,CB}$ [1] [kN]	$N_{u,proposal}$ [2] [kN]	$N_u/N_{u,decisive}$ [3] [-]
100	60	75	100	29.72	27.51	24.17	1.23
100	60	75	200	33.20	36.06	26.95	1.23
100	60	75	250	33.46	40.20	28.47	1.18
100	60	75	300	35.34	41.86	30.09	1.17
100	60	75	500	40.66	41.86	37.21	1.09
100	60	75	720	44.56	41.86	43.49	1.06
100	60	75	840	44.83	41.86	43.49	1.07
100	60	130	100	33.20	27.51	34.88	1.21
100	60	130	200	41.98	36.06	38.89	1.16
100	60	130	250	45.91	40.20	41.09	1.14
100	60	130	300	47.17	41.86	43.41	1.13
100	60	130	500	49.29	41.86	53.69	1.18
100	100	125	100	64.63	57.89	59.13	1.12
100	100	125	200	66.53	70.04	63.06	1.05
100	100	125	250	69.39	76.87	65.15	1.07
100	100	125	300	72.72	83.90	67.31	1.08
100	100	200	100	60.90	57.89	80.89	1.05
100	100	200	200	77.84	70.04	86.27	1.11
100	100	200	250	84.09	76.87	89.12	1.09
100	100	200	300	92.13	83.90	92.08	1.10
200	100	125	100	73.66	81.88	67.02	1.10
200	100	125	200	78.37	99.05	71.47	1.10
200	100	125	250	81.87	108.72	73.83	1.11
200	100	125	300	83.40	118.66	76.29	1.09
100	91	130	150	59.34	57.32	58.43	1.04
100	91	130	200	64.51	63.43	60.55	1.07
100	91	130	250	67.98	69.95	62.76	1.08
100	91	130	300	73.96	76.52	65.06	1.14
100	106	130	150	68.21	68.09	65.51	1.04
100	106	130	200	73.19	74.65	67.53	1.08
100	106	130	250	73.45	81.70	69.63	1.05
100	106	130	300	74.28	89.01	71.81	1.03
100	120	130	150	76.13	79.01	72.15	1.06
100	120	130	200	78.46	86.06	74.11	1.06
100	120	130	250	80.20	93.66	76.13	1.05
100	120	130	300	86.79	101.64	78.22	1.11

[1] *EN 1992-4 – concrete breakout failure ($\alpha_{ch,N}$ according to [22] for h_{ef} = 60 mm)*

[2] *Modified design proposal for splitting failure mode*

[3] *$N_{u,decisive}$ represents smaller of the two calculated capacities*

Appendix D – Anchor channels in composite slabs (shear)

Table D.1 Numerical results – plain concrete slabs ($f_{c,mean}$ = 20 N/mm²)

c_1 [mm]	h [mm]	s [mm]	h_{ef} [mm]	V_u [kN]
50	130	300	106	15.12
50	130	250	106	14.67
50	130	200	106	12.98
50	130	150	106	10.75
100	130	300	106	26.58
100	130	250	106	24.67
100	130	200	106	22.92
100	130	150	106	20.88
150	130	250	106	33.22
200	130	250	106	45.42
300	130	250	106	58.65
50	130	300	60	14.32
50	70	300	60	8.29
100	160	300	60	29.67
100	130	300	60	26.16
100	100	300	60	20.64
100	70	300	60	14.17
200	160	250	60	49.44
200	130	250	60	42.93
200	100	250	60	33.98

Table D.2 Numerical results – Series 1 and Series 2 ($f_{c,mean}$ = 20 N/mm²)

c_1 [mm]	h [mm]	s [mm]	h_{ef} [mm]	Steel decking	Config.	V_u [kN]	$V_u/V_{u,Ref}$ [-]	$\Psi_{com,V}$ [-]	Simulation-to-prediction [-]
50	130	250	106	Ribdeck S60	asymm	10.49	0.72	0.75	0.96
50	130	250	106	Ribdeck S60	symm	10.59	0.72	0.75	0.97
50	130	300	106	Ribdeck S60	asymm	11.19	0.74	0.75	0.99
50	130	300	106	Ribdeck S60	symm	11.66	0.77	0.75	1.03
50	130	150	106	Superib	asymm	9.23	0.86	0.86	0.99
50	130	150	106	Superib	symm	9.31	0.87	0.86	1.00
50	130	200	106	Superib	symm	10.14	0.78	0.86	0.90
100	130	250	106	Ribdeck S60	asymm	19.61	0.79	0.75	1.07
100	130	250	106	Ribdeck S60	symm	19.56	0.79	0.75	1.06
100	130	300	106	Ribdeck S60	asymm	20.17	0.76	0.75	1.02
100	130	300	106	Ribdeck S60	symm	20.60	0.77	0.75	1.04
100	130	150	106	Superib	asymm	17.63	0.84	0.86	0.98
100	130	150	106	Superib	symm	17.80	0.85	0.86	0.99

c_1 [mm]	h [mm]	s [mm]	h_{ef} [mm]	Steel decking	Config.	V_u [kN]	$V_u/V_{u,Ref}$ [-]	$\Psi_{com,V}$ [-]	Simulation -to- prediction [-]
100	130	200	106	Superib	symm	19.09	0.83	0.86	0.96
150	130	250	106	Ribdeck S60	symm	25.13	0.76	0.75	1.01
200	130	250	106	Ribdeck S60	symm	31.10	0.68	0.75	0.92
300	130	250	106	Ribdeck S60	symm	39.75	0.68	0.75	0.91
50	130	300	60	Ribdeck S60	flange	10.67	0.75	0.75	1.00
50	130	300	60	Ribdeck S60	rib	12.04	0.84	0.75	1.13
100	130	300	60	Ribdeck S60	flange	19.07	0.73	0.75	0.98
100	130	300	60	Ribdeck S60	rib	20.20	0.77	0.75	1.04
100	160	300	60	Ribdeck S60	flange	24.74	0.83	0.79	1.05
200	160	250	60	Ribdeck S60	flange	40.20	0.81	0.79	1.02

Table D.3 Numerical results – Series 3 ($f_{c,mean}$ = 20 N/mm^2)

c_1 [mm]	h [mm]	s [mm]	h_{ef} [mm]	Steel decking	Pos.	V_u [kN]	$V_u/V_{u,Ref}$ [-]	$\Psi_{com,V}$ [-]	Simulation -to- prediction [-]
100	130	300	60	Superib	4	17.56	0.67	0.68	0.99
100	130	300	60	Superib	3	20.04	0.77	0.78	0.98
100	130	300	60	Superib	2	23.04	0.88	0.88	1.00
100	130	300	60	Superib	1	25.91	0.99	0.98	1.01
100	160	300	60	Superib	4	22.46	0.76	0.74	1.02
100	160	300	60	Superib	3	23.94	0.81	0.84	0.96
100	160	300	60	Superib	2	28.13	0.95	0.94	1.01
100	160	300	60	Superib	1	29.41	0.99	1.00	0.99
200	130	250	60	Ribdeck S60	6	28.93	0.67	0.65	1.03
200	130	250	60	Ribdeck S60	5	30.55	0.71	0.70	1.01
200	130	250	60	Ribdeck S60	4	31.96	0.74	0.75	0.99
200	130	250	60	Ribdeck S60	3	33.04	0.77	0.80	0.96
200	130	250	60	Ribdeck S60	2	37.02	0.86	0.85	1.01
200	130	250	60	Ribdeck S60	1	39.92	0.93	0.90	1.03
200	160	250	60	Ribdeck S60	6	36.52	0.74	0.72	1.03
200	160	250	60	Ribdeck S60	4	41.71	0.84	0.82	1.03
200	160	250	60	Ribdeck S60	2	45.18	0.91	0.92	1.00

Appendix E – Anchor channels in composite slabs (tension)

Table E.1 Numerical results – Plain concrete slabs ($f_{c,mean}$ = 20 N/mm²)

c_1	h_{ef}	h	s	N_u
[mm]	[mm]	[mm]	[mm]	[kN]
100	91	130	300	73.96
100	91	130	250	67.98
100	91	130	200	64.51
100	91	130	150	59.34
100	91	180	250	75.09
100	106	130	300	79.08
100	106	130	250	73.45
100	106	130	200	73.19
100	106	130	150	68.21
100	106	180	250	87.29
200	106	130	250	87.72
100	120	130	300	86.79
100	120	130	250	80.20
100	120	130	200	78.46
100	120	130	150	76.13
100	120	180	300	107.42
100	120	180	250	98.72

Table E.2 Numerical results – Series 1 ($f_{c,mean}$ = 20 N/mm²)

c_1	h_{ef}	h	s	Steel decking	d_w	N_u	$N_u/N_{u,Ref}$
[mm]	[mm]	[mm]	[mm]		[mm]	[kN]	[kN]
100	91	130	250	Ribdeck S60	15	50.73	0.75
100	91	130	250	Ribdeck S60	30	53.27	0.78
100	91	130	250	Ribdeck S60	45	57.82	0.85
100	91	130	250	Ribdeck S60	60	55.68	0.82
100	91	130	250	Ribdeck S60	100	59.30	0.87
100	91	180	250	Ribdeck S60	15	62.39	0.83
100	91	180	250	Ribdeck S60	30	64.20	0.86
100	91	180	250	Ribdeck S60	45	64.20	0.86
100	91	180	250	Ribdeck S60	60	66.77	0.89
100	91	180	250	Ribdeck S60	100	69.09	0.92
100	91	130	250	Superib	15	44.17	0.65
100	91	130	250	Superib	30	52.29	0.77
100	91	130	250	Superib	45	57.73	0.85
100	91	130	250	Superib	60	56.23	0.83
100	91	130	250	Superib	100	59.62	0.88
100	106	130	250	Ribdeck S60	15	53.05	0.72
100	106	130	250	Ribdeck S60	30	69.56	0.95
100	106	130	250	Ribdeck S60	45	66.95	0.91

c_1	h_{ef}	h	s	Steel decking	d_w	N_u	$N_u/N_{u,Ref}$
[mm]	[mm]	[mm]	[mm]		[mm]	[kN]	[kN]
100	106	130	250	Ribdeck S60	60	64.42	0.88
100	106	130	250	Ribdeck S60	100	65.69	0.89
100	106	180	250	Ribdeck S60	15	69.18	0.79
100	106	180	250	Ribdeck S60	30	70.99	0.81
100	106	180	250	Ribdeck S60	45	72.95	0.84
100	106	180	250	Ribdeck S60	60	74.54	0.85
100	106	180	250	Ribdeck S60	100	79.08	0.91
200	106	130	250	Ribdeck S60	15	64.45	0.73
200	106	130	250	Ribdeck S60	30	75.31	0.86
200	106	130	250	Ribdeck S60	45	75.00	0.86
200	106	130	250	Ribdeck S60	60	73.32	0.84
200	106	130	250	Ribdeck S60	100	76.22	0.87
100	106	130	250	Superib	15	43.49	0.59
100	106	130	250	Superib	30	65.19	0.89
100	106	130	250	Superib	45	70.03	0.95
100	106	130	250	Superib	60	67.09	0.91
100	106	130	250	Superib	100	64.06	0.87
100	120	130	250	Ribdeck S60	15	68.84	0.86
100	120	130	250	Ribdeck S60	30	76.49	0.95
100	120	130	250	Ribdeck S60	45	77.25	0.96
100	120	130	250	Ribdeck S60	60	73.16	0.91
100	120	130	250	Ribdeck S60	100	70.51	0.88
100	120	180	250	Ribdeck S60	15	79.04	0.80
100	120	180	250	Ribdeck S60	30	80.76	0.82
100	120	180	250	Ribdeck S60	45	81.07	0.82
100	120	180	250	Ribdeck S60	60	87.41	0.89
100	120	180	250	Ribdeck S60	100	87.41	0.89
100	120	130	250	Superib	15	44.56	0.56
100	120	130	250	Superib	30	59.64	0.74
100	120	130	250	Superib	45	71.92	0.90
100	120	130	250	Superib	60	81.22	1.01
100	120	130	250	Superib	100	69.58	0.87

Table E.3 Numerical results – Series 2 ($f_{c,mean}$ = 20 N/mm^2)

c_1	h_{ef}	h	s	Steel decking	d_w	N_u	$N_u/N_{u,Ref}$
[mm]	[mm]	[mm]	[mm]		[mm]	[kN]	[kN]
100	91	130	250	Ribdeck S60	15	46.46	0.68
100	91	130	250	Ribdeck S60	30	55.90	0.82
100	91	130	250	Ribdeck S60	45	55.44	0.82
100	91	130	250	Ribdeck S60	60	58.73	0.86
100	91	130	250	Ribdeck S60	100	60.41	0.89
100	106	130	250	Ribdeck S60	15	42.41	0.58

| c_1 | h_{ef} | h | s | Steel | d_w | N_u | $N_u/N_{u,Ref}$ |
[mm]	[mm]	[mm]	[mm]	decking	[mm]	[kN]	[kN]
100	106	130	250	Ribdeck S60	30	64.61	0.88
100	106	130	250	Ribdeck S60	45	70.03	0.95
100	106	130	250	Ribdeck S60	60	66.63	0.91
100	106	130	250	Ribdeck S60	100	65.05	0.89
100	120	130	250	Ribdeck S60	15	42.46	0.53
100	120	130	250	Ribdeck S60	30	67.77	0.85
100	120	130	250	Ribdeck S60	45	77.02	0.96
100	120	130	250	Ribdeck S60	60	73.55	0.92
100	120	130	250	Ribdeck S60	100	74.35	0.93

Table E.4 Numerical results – Series 3 ($f_{c,mean}$ = 20 N/mm²)

| c_1 | h_{ef} | h | s | Steel | Configuration | N_u | $N_u/N_{u,Ref}$ |
[mm]	[mm]	[mm]	[mm]	decking		[kN]	[kN]
100	91	130	250	Ribdeck S60	Asymmetric	43.06	0.63
100	91	130	250	Ribdeck S60	Symmetric	41.14	0.61
100	91	130	300	Ribdeck S60	Asymmetric	44.31	0.60
100	91	130	300	Ribdeck S60	Symmetric	46.30	0.63
100	91	130	150	Superib	Asymmetric	50.38	0.85
100	91	130	150	Superib	Symmetric	51.35	0.87
100	91	130	200	Superib	Symmetric	52.56	0.81
100	106	130	250	Ribdeck S60	Asymmetric	41.66	0.57
100	106	130	250	Ribdeck S60	Symmetric	42.82	0.58
100	106	130	300	Ribdeck S60	Asymmetric	39.38	0.50
100	106	130	300	Ribdeck S60	Symmetric	48.60	0.61
100	106	130	150	Superib	Asymmetric	53.19	0.78
100	106	130	150	Superib	Symmetric	56.18	0.82
100	106	130	200	Superib	Symmetric	59.39	0.81
100	120	130	250	Ribdeck S60	Asymmetric	43.30	0.54
100	120	130	250	Ribdeck S60	Symmetric	44.00	0.55
100	120	130	300	Ribdeck S60	Asymmetric	37.34	0.43
100	120	130	300	Ribdeck S60	Symmetric	46.50	0.54
100	120	130	150	Superib	Asymmetric	53.32	0.70
100	120	130	150	Superib	Symmetric	61.21	0.80
100	120	130	200	Superib	Symmetric	63.39	0.81
100	120	180	250	Ribdeck S60	Asymmetric	74.64	0.76
100	120	180	250	Ribdeck S60	Symmetric	74.92	0.76
100	120	180	300	Ribdeck S60	Asymmetric	77.87	0.72
100	120	180	300	Ribdeck S60	Symmetric	83.49	0.78

Appendix F – Anchor channels in pockets

Table F.1 Numerical simulations – shear load ($f_{c,mean}$ = 20 N/mm²)

c_1 [mm]	h_p [mm]	d_s [mm]	h [mm]	V_u [kN]	$V_u/V_{u,Ref}$ [-]	$\Psi_{p,V\,proposal}$ [-]	Simulation-to-proposal [-]
100	-	-	80	15.71	-	-	-
100	50	25	80	22.11	1.41	1.43	0.98
100	50	75	80	16.73	1.06	1.05	1.01
100	50	125	80	16.05	1.02	1.00	1.02
100	-	-	130	24.66	-	-	-
100	25	25	130	29.99	1.22	1.18	1.03
100	25	75	130	25.69	1.04	1.02	1.02
100	25	125	130	24.82	1.01	1.00	1.01
100	50	25	130	31.39	1.27	1.30	0.98
100	50	75	130	25.15	1.02	1.03	0.99
100	50	125	130	24.98	1.01	1.00	1.01
100	100	25	130	32.00	1.30	1.36	0.95
100	100	75	130	25.53	1.04	1.04	0.99
100	100	125	130	25.14	1.02	1.00	1.02
100	-	-	300	33.45	-	-	-
100	25	25	300	38.95	1.16	1.11	1.05
100	25	75	300	36.15	1.08	1.01	1.07
100	25	125	300	36.02	1.08	1.00	1.08
100	50	25	300	41.48	1.24	1.18	1.05
100	50	75	300	36.77	1.10	1.02	1.08
100	50	125	300	35.96	1.08	1.00	1.08
100	100	25	300	42.82	1.28	1.22	1.05
100	100	75	300	39.37	1.18	1.03	1.15
100	100	125	300	35.48	1.06	1.00	1.06
150	-	-	80	21.71	-	-	-
150	50	25	80	35.79	1.65	1.63	1.01
150	50	75	80	27.76	1.28	1.24	1.03
150	50	125	80	23.88	1.10	1.01	1.09
150	-	-	130	35.05	-	-	-
150	50	25	130	49.35	1.41	1.44	0.98
150	50	75	130	39.95	1.14	1.16	0.98
150	50	125	130	36.15	1.03	1.01	1.02
150	25	25	130	43.52	1.24	1.26	0.99
150	75	25	130	50.82	1.45	1.53	0.95
150	100	25	130	50.55	1.44	1.53	0.94
150	-	-	400	61.09	-	-	-
150	50	25	400	76.30	1.25	1.23	1.02
150	50	75	400	62.66	1.03	1.09	0.94
150	50	125	400	61.28	1.00	1.00	1.00

c_1 [mm]	h_p [mm]	d_s [mm]	h [mm]	V_u [kN]	$V_u/V_{u,Ref}$ [-]	$\Psi_{ch,p,V\ proposal}$ [-]	Simulation-to-proposal [-]
200	-	-	80	28.02	-	-	-
200	50	25	80	49.56	1.77	1.79	0.99
200	50	75	80	40.09	1.43	1.40	1.02
200	50	125	80	34.26	1.22	1.16	1.06
200	-	-	130	45.42	-	-	-
200	25	25	130	55.09	1.21	1.33	0.91
200	25	75	130	50.42	1.11	1.16	0.95
200	25	125	130	47.04	1.04	1.06	0.97
200	50	25	130	65.54	1.44	1.55	0.93
200	50	75	130	55.77	1.23	1.28	0.96
200	50	125	130	48.82	1.07	1.11	0.97
200	100	25	130	71.17	1.57	1.67	0.94
200	100	75	130	57.36	1.26	1.33	0.95
200	100	125	130	50.05	1.10	1.13	0.97
200	-	-	500	85.59	-	-	-
200	25	25	500	96.14	1.12	1.15	0.97
200	25	75	500	91.30	1.07	1.08	1.02
200	25	125	500	88.77	1.04	1.03	1.01
200	50	25	500	106.88	1.25	1.26	0.99
200	50	75	500	94.04	1.10	1.13	0.97
200	50	125	500	86.22	1.01	1.05	0.96
200	100	25	500	113.61	1.33	1.31	1.01
200	100	75	500	95.90	1.12	1.16	0.97
200	100	125	500	91.67	1.07	1.06	1.01

Table F.2 Numerical simulations – tension load ($f_{c,mean}$ = 20 N/mm²)

c_1 [mm]	h_{ef} [mm]	h_p [mm]	d_s [mm]	d_b [mm]	h [mm]	N_u [kN]	$N_u/N_{u,Ref}$ [-]	$\Psi_{p,N\ proposal}$ [-]	Simulation-to-proposal [-]
50	106	-	-	-	180	67.95	-	-	-
50	106	50	25	0	130	89.78	1.32	1.25	1.05
50	106	50	75	50	130	78.23	1.15	1.16	0.99
50	106	50	125	100	130	71.82	1.06	1.06	0.99
100	106	-	-	-	180	88.12	-	-	-
100	106	50	25	0	130	111.52	1.27	1.25	1.01
100	106	50	75	50	130	101.67	1.15	1.16	1.00
100	106	50	125	100	130	88.81	1.01	1.06	0.95
100	106	50	125	0	130	92.97	1.05	1.06	0.99
100	106	50	125	50	130	96.62	1.10	1.06	1.03
100	106	50	25	100	130	109.71	1.24	1.25	0.99
100	106	50	75	100	130	98.77	1.12	1.16	0.97
200	106	-	-	-	180	100.04	-	-	-

c_1 [mm]	h_{ef} [mm]	h_p [mm]	d_s [mm]	d_b [mm]	h [mm]	N_u [kN]	$N_u/N_{u,Ref}$ [-]	$\Psi_{p,N\ proposal}$ [-]	Simulation-to-proposal [-]
200	106	50	25	0	130	138.07	1.38	1.25	1.10
200	106	50	75	50	130	128.96	1.29	1.16	1.11
200	106	50	125	100	130	107.37	1.07	1.06	1.01
100	106	-	-	-	300	91.16	-	-	-
100	106	50	25	0	250	109.15	1.20	1.25	0.96
100	106	50	75	50	250	103.16	1.13	1.16	0.98
100	106	50	125	100	250	94.81	1.04	1.05	0.98
100	106	-	-	-	155	85.40	-	-	-
100	106	25	25	0	130	93.38	1.09	1.13	0.97
100	106	25	75	50	130	90.09	1.05	1.08	0.98
100	106	25	125	100	130	83.17	0.97	1.03	0.94
100	106	-	-	-	275	91.16	-	-	-
100	106	25	25	0	250	102.30	1.12	1.13	1.00
100	106	25	75	50	250	97.71	1.07	1.08	0.99
100	106	25	125	100	250	95.31	1.05	1.03	1.01
42	83	-	-	-	180	49.24	-	-	-
42	83	50	25	0	130	57.99	1.18	1.24	0.95
42	83	50	75	50	130	52.22	1.06	1.12	0.95
42	83	50	125	100	130	47.38	0.96	1.00	0.96
100	83	-	-	-	180	68.41	-	-	-
100	83	50	25	0	130	87.50	1.28	1.24	1.03
100	83	50	75	50	130	71.84	1.05	1.12	0.94
100	83	50	125	100	130	66.58	0.97	1.00	0.97
166	83	-	-	-	180	76.39	-	-	-
166	83	50	25	0	130	101.54	1.33	1.24	1.07
166	83	50	75	50	130	83.78	1.10	1.12	0.98
166	83	50	125	100	130	74.06	0.97	1.00	0.97
100	83	-	-	-	300	68.60	-	-	-
100	83	50	25	0	250	86.07	1.25	1.12	1.01
100	83	50	75	50	250	73.66	1.07	1.06	0.96
100	83	50	125	100	250	73.13	1.07	1.00	1.07
100	83	-	-	-	155	65.24	-	-	-
100	83	25	25	0	130	76.67	1.18	1.25	1.05
100	83	25	75	50	130	67.67	1.04	1.16	0.98
100	83	25	125	100	130	64.15	0.98	1.06	0.98
60	60	-	-	-	180	38.02	-	-	-
60	60	50	25	0	130	45.10	1.19	1.22	0.98
60	60	50	75	50	130	40.84	1.07	1.05	1.02
60	60	50	125	100	130	37.19	0.98	0.88	1.11
100	60	-	-	-	180	46.26	-	-	-
100	60	50	25	0	130	55.84	1.21	1.22	0.99
100	60	50	75	50	130	47.95	1.04	1.05	0.99
100	60	50	125	100	130	44.14	0.95	0.88	1.08

c_1 [mm]	h_{ef} [mm]	h_p [mm]	d_s [mm]	d_b [mm]	h [mm]	N_u [kN]	$N_u/N_{u,Ref}$ [-]	$\Psi_{p,N\ proposal}$ [-]	Simulation-to-proposal [-]
100	60	-	-	-	300	48.11	-	-	-
100	60	50	25	0	250	55.46	1.15	1.22	0.95
100	60	50	75	50	250	49.57	1.03	1.05	0.98
100	60	50	125	100	250	47.51	0.99	0.88	1.12
100	60	-	-	-	155	44.89	-	-	-
100	60	25	25	0	130	51.60	1.15	1.11	1.04
100	60	25	75	50	130	46.46	1.03	1.03	1.01
100	60	25	125	100	130	45.42	1.01	0.94	1.07
100	60	-	-	-	130	43.10	-	-	-
100	60	50	25	0	80	50.63	1.17	1.22	0.97
100	60	50	75	50	80	41.55	0.96	1.05	0.92
100	60	50	125	100	80	39.04	0.91	0.88	1.03
100	60	-	-	-	105	37.46	-	-	-
100	60	25	25	0	80	44.20	1.18	1.11	1.06
100	60	25	75	50	80	39.41	1.05	1.03	1.03
100	60	25	125	100	80	36.95	0.99	0.94	1.05

CURRICULUM VITAE

Anton Bogdanić was born on 30 December 1993. In 2015, he obtained his bachelor's degree *cum laude* from Faculty of Civil Engineering in Rijeka. Two years later, in 2017, he graduated *summa cum laude* from the same Faculty with a master's degree in civil engineering. In November 2017, he enrolled in Postgraduate Doctoral Study Programme at the Faculty of Civil Engineering in Rijeka, where he is currently working as a research assistant in the project: "Anchor channels in composite concrete structures: experimental and numerical investigation". Aforementioned project is being implemented in cooperation with Hilti Corporation, one of the global leaders in fastening technology. His supervisor is Prof. Dr.-Ing. habil. Joško Ožbolt, who is the author or co-author of numerous publications in the field of finite element analysis of concrete and reinforced concrete structures, fracture mechanics of concrete, transport processes, behaviour of concrete under high loading rates etc.

His main research interests include numerical modelling of structures (especially concrete structures), structural analysis and experimental investigation with emphasis on various fastening systems. In addition to these research areas, he is also interested in programming.

LIST OF RELEVANT JOURNAL ARTICLES:

[1] Bogdanić, A., Casucci, D., Ožbolt, J. (2021) Numerical and experimental investigation on concrete splitting failure of anchor channels. *CivilEng* **2(2)**, 502-522

[2] Bogdanić, A., Casucci, D., Ožbolt, J. (2021) Numerical and experimental investigation of anchor channels subjected to shear load in composite slabs with profiled steel decking. *Engineering Structures* **240**, 112347

[3] Bogdanić, A., Casucci, D., Ožbolt, J. (2021) Concrete edge breakout of anchor channels – on the influence of member thickness and installation in pockets. *Structural Concrete* (Early view - Online Version of Record before inclusion in an issue)

[4] Bogdanić, A., Casucci, D., Ožbolt, J. (2022) Numerical and experimental investigation of anchor channels subjected to tension load in composite slabs with profiled steel decking. *CivilEng* **3(2)**, 296-315

LIST OF OTHER PUBLICATIONS:

[1] Bogdanić, A., Ožbolt, J. (2019) Proračun prodora klorida u beton. *Zbornik radova (Građevinski fakultet Sveučilišta u Rijeci)*, **22(1)**, 27-42.

[2] Bogdanić, A., Ožbolt, J. (2019) 3D numerička parametarska analiza nosivosti sidrenih kanala. In : *Zbornik radova devetog susreta Hrvatskog društva za mehaniku*, Zagreb, Croatia.

[3] Bogdanić, A., Ožbolt, J. (2019) Crack band metoda – utjecaj oblika konačnih elemenata na numeričke rezultate. In : *Zajednički temelji 2019 - Sedmi skup mladih istraživača iz područja građevinarstva i srodnih tehničkih znanosti*, Rijeka, Croatia.

[4] Bogdanić, A., Ožbolt, J., Casucci, D. (2020) Concrete splitting failure of anchor channels: numerical and experimental investigation. In : *WCCM-ECCOMAS Congress 2020*, Paris, France.

[5] Kožar, I., Bede, N., Bogdanić, A., Mrakovčić, S. (2021) Inverse stohastic models for fiber reinforced concrete. In : *ECCOMAS 2021 5th International Conference on Multi-Scale Computational Methods for Solids and Fluids*, Sarajevo, B&H.